ROYAUME DU MAROC
Université Mohammed V - RABAT -
جامعة محمد الخامس – الرباط –
Faculté des sciences
كلية العلوم
CENTRE D'ETUDES DOCTORALES - SCIENCES ET TECHNOLOGIES

N° d'ordre : 3608

THÈSE

En vue de l'obtention du : ***DOCTORAT***

Structure de Recherche : Laboratoire de matière condensée et sciences interdisciplinaires (LaMCScI)
Discipline : Physique
Spécialité : Sciences des Matériaux et Energies Renouvelables

Présentée et soutenue le 26/03/2022 par :

Imane HAMIDEDDINE

DFT study of structural, electronic, optical and transport properties of Halide Perovskite ABX_3 and Halide Mixed Perovskite $ABI_{3-x}Br_x$ for photovoltaic applications.

JURY

BENAISSA Mohammed	PES, Université Mohammed V, Rabat, Faculté des sciences	Président
BENCHRIFA Rachid	PES, Université Mohammed V, Rabat, Faculté des sciences	Examinateur / Rapporteur
MASAIF Noureddine	PES, Université Ibn Toufail, Faculté des sciences de Kénitra,	Examinateur / Rapporteur
EL MANSOURI Abdelmajid	PH, Institut Supérieur des Métiers de l'Audiovisuel et du Cinéma	Examinateur / Rapporteur
EL MELLOUKI Sanae	PH. Université Mohammed V, Rabat, Faculté des sciences	Examinateur
TAHIRI Najim	PA, Université Mohammed V, Rabat, Faculté des sciences	Co-encadrant
EZ-ZAHRAOUY Hamid	PES, Université Mohammed V, Rabat, Faculté des sciences	Co-directeur de thèse
EL BOUNAGUI Omar	PH, Université Mohammed V, Rabat, Faculté des sciences	Directeur de thèse

Année Universitaire : 2021-2022

Faculté des Sciences, avenue Ibn Battouta, BP. 1014 RP, Rabat –Maroc
00212 (05) 37 77 18 76 00212(05) 37 77 42 61; http://www. fsr.um5.ac.ma

Dédicace

À mon très cher père Hassan HAMIDEDDINE, De tous les pères, tu es le meilleur. Tu as été et tu seras toujours un exemple pour moi par tes qualités humaines, ta persévérance et perfectionnisme. En témoignage de brut d'années de sacrifices, de sollicitudes, d'encouragement de prières. Pourriez-vous trouver dans ce travail le fruit de toutes vos peines et tous vos efforts. En ce jour, j'espère réaliser l'un de tes rêves. Aucune dédicace ne saurait exprimer mes respects, ma reconnaissance et mon profond amour. Puisse Dieu vous préserver et vous procurer santé et bonheur.

À ma très chère mère Najat BOUTAYEB, Source inépuisable de tendresse et de patience et de sacrifice. Ta prière et ta bénédiction m'ont été d'un grand secours tout au long de ma vie. Quoique je puisse dire et écrire, je ne pourrais exprimer ma grande affection et ma profonde reconnaissance. J'espère ne jamais te décevoir, ni traiter ta confiance et tes sacrifices. Puisse Dieu tout puissant, te préserver et t'accorder santé, longue vie et bonheur.

Je dédie également ce travail à ma sœur Oumayma HAMIDEDDINE, mon beau-frère Salaheddine SAGHIR et mon neveu Adam, qui ont toujours été à mes côtés. Je vous remercie infiniment pour le soutien et pour tout ce que vous avez fait pour moi, je vous remercie tous du fond du cœur.

À la mémoire de mes grands-parents, Que vous reposiez dans le paradis du seigneur.

À toutes ma famille maternelle et paternelle, Aucun langage ne saurait exprimer mon respect et ma considération pour votre soutien et encouragements.

Remerciements

Ce manuscrit présente un travail qui a été réalisée au sein du Laboratoire de Matière Condensé et Sciences Interdisciplinaire (LaMCScI), de la Faculté des Sciences de l'Université Mohammed V-Rabat, sous la direction de Monsieur le Professeur d'Enseignement Supérieur **ELBOUNAGUI Omar** et Co-encadrer par le Professeur **TAHIRI Najim** ainsi que le Professeur responsable du laboratoire de matière condensée et sciences interdisciplinaires (LaMCScI) Monsieur **Hamid EZ-ZAHRAOUY.**

J'exprime mes profonds remerciements à Monsieur **EL BOUNAGUI Omar** de m'avoir fait l'honneur d'être mon encadreur et je tien a le remercie pour la confiance qu'il m'a accordée et d'avoir mes a ma disposition tous les moyens nécessaires, sans quoi je n'aurais pu réaliser mon travail et mes calculs.

J'exprime toute ma gratitude et ma profonde reconnaissance à mon Co-directeur de thèse Monsieur **EZ-ZAHRAOUY Hamid** qui m'a dirigé durant ces quatre années ainsi que pour ses conseils avisés tant sur le traitement de mon sujet de thèse.

Je tiens à remercier le professeur **TAHIRI Najim** pour son Co-encadrement et son implication très active dans le travail de cette thèse, ainsi que pour ses conseils avisés tant sur le traitement de mon sujet de thèse.

Je remercie Monsieur **BENAISSA Mohammed**, Professeur de l'Enseignement Supérieur à la Faculté des Sciences de Rabat, président du jury, de m'avoir honoré par sa présence en présidant le jury de soutenance de mon doctorat. J'en suis honorée et je lui exprime toute ma profonde reconnaissance.

Je remercie également Monsieur **BENCHRIFA Rachid**, Professeur de l'Enseignement Supérieur à la Faculté des Sciences de Rabat, d'avoir accepté de rapporter et examiner cette thèse et de scruter de si près le contenu de ma thèse de doctorat.

Je remercie Monsieur **MASAIF Noureddine**, Professeur de l'Enseignement Supérieur à l'Université Ibn Toufail, Faculté des sciences de Kénitra, d'avoir accepté de juger mon travail en étant un rapporteur et examinateur, et pour l'intérêt qu'il a porté à mon travail.

J'adresse tous mes remerciements à Monsieur **EL MANSOURI Abdelmajid**, Professeur à l'Institut Supérieur des Métiers de l'Audiovisuel et du Cinéma, de l'honneur qu'il m'a fait en acceptant d'être rapporteur et examinateur cette thèse.

Je remercie Madame **EL MELLOUKI Sanae**, Professeur de l'Enseignement Supérieur à la Faculté des Sciences de Rabat, pour faire partie de ce jury en étant un examinateur.

Résumé

Nous avons étudié dans le présent projet de thèse, les propriétés structurelles, électroniques, et optiques du $CuInGaSe_2$ en structure cristalline chalcopyrite, en utilisant la méthode des ondes planes augmentées linéarisées avec un potentiel total (FP-LAPW) dans le cadre de la théorie de la fonctionnelle de la densité (DFT) implémentée dans le code Wien2k. Le potentiel d'échange et de corrélation est traité avec les approximations GGA-PBE, et MBJ-GGA. Une étude qui s'est basée sur la substitution entre les atomes de gallium et celle d'indium, afin d'obtenir de meilleures performances photovoltaïques. Dans la deuxième partie nous avons étudié les composés halides pérovskites KBX_3 (B = Ge ; Sn et X= Cl ; Br ; I) en utilisant la méthode ab-initio, dans le but d'élargir notre compréhension des caractéristiques électroniques, et optique des composés pérovskites. Pour les propriétés électroniques, les résultats indiquent que tous ces composés étudiés possèdent un caractère semi-conducteur avec un gap direct. Les propriétés optiques montrent une large gamme d'absorption dans le visible ce qui ouvrent le domaine pour des applications dans l'optoélectronique comme des cellules solaires ou photovoltaïques. Enfin, et dans une troisième partie, nous avons étudié les propriétés structurelles, électroniques et optiques des composés pérovskites halides mixtes $ABI_{3-x}Br_x$ avec (A = K; Rb; Cs / B = Ge; Pb). Afin d'envisager une potentielle application en photovoltaïque. Les résultats montrent un aspect semi-conducteur avec une bonne ouverture du gap qui a mené à d'autres applications potentielles comme la photocatalyse.

Mots clés : Halides perovskites ; DFT ; mBJ-GGA ; Photovoltaique ; Perovskites halides mixtes ; Propriétés optiques.

Abstract

In the present thesis project, we have studied the structural, electronic, and optical properties of CuInGaSe2 in chalcopyrite crystal structure, using the linearized augmented plane wave method with a total potential (FP-LAPW) in the framework of the density functional theory (DFT) implemented in the Wien2k code. The exchange and correlation potential is treated with the GGA-PBE, and mBJ-GGA approximations. A study based on the substitution between gallium and indium atoms, in order to obtain better photovoltaic performances. In the second part we studied the halide perovskite compounds ABX3 (A=K / B = Ge ; Sn and X= Cl ; Br ; I) using the ab-initio method, with the aim of broadening our understanding of the electronic, and optical characteristics of perovskite compounds. For the electronic properties the results indicate that all these studied compounds possess a semiconducting character with a direct gap. The optical properties show a wide range of absorption in the visible range which opens the field for applications in optoelectronics such as solar cells or photovoltaics. Finally, and in a third part, we studied the structural, electronic and optical properties of the mixed halide perovskite compounds ABI3-xBrx with (A = K; Rb; Cs / B = Ge; Pb). In order to consider a potential application in photovoltaic. The results show a semiconducting aspect with a good gap opening which led to other potential applications like photocatalysis.

Keywords: Perovskite halides; DFT; mBJ-GGA; Photovoltaics; Mixed perovskite halides; Optical properties.

Résumé étendu

De nos jours, l'intérêt porté au changement climatique, aux transitions énergétiques ainsi que les énergies renouvelables a pris de grande ampleur. Une infinité de recherche, étude et de projet sont en cours. Dans le domaine énergétique, plus précisément en photovoltaïque, les chercheurs tante l'infinité de combinaison possible afin de trouver le matériau qui fera la moindre différance. C'est dans cette optique que vient ce projet de thèse, ou nous avons étudié les propriétés structurelles, électroniques, et optiques du $CuInGaSe_2$ en structure cristalline chalcopyrite, en utilisant la méthode des ondes planes augmentées linéarisées avec un potentiel total (FP-LAPW) dans le cadre de la théorie de la fonctionnelle de la densité (DFT) implémentée dans le code Wien2k. Le potentiel d'échange et de corrélation est traité avec les approximations GGA-PBE, et MBJ-GGA. Une étude qui s'est basée sur la substitution entre les atomes de gallium et celle d'indium, afin d'obtenir de meilleures performances photovoltaïques. Dans une deuxième partie nous avons étudié les pérovskites halides de type ABX_3 (A=K, B = Ge ; Sn et X = Cl; Br; I) en utilisant la méthode ab-initio, dans le but d'élargir notre compréhension des caractéristiques électroniques, et optiques des composés pérovskites. Pour les propriétés électroniques les résultats indiquent que tous ces composés étudiés possèdent un caractère semi-conducteur avec un gap direct. Les propriétés optiques montrent une large gamme d'absorption dans le visible, avec un petit avantage aux composé basé gallium, ce qui ouvrent le domaine pour des applications dans l'optoélectronique comme des cellules solaires ou photovoltaïques. En addition, nous avons étudié les propriétés structurelles, électroniques et optiques des composés pérovskites halides mixtes $ABI_{3-x}Br_x$ avec (A = K; Rb; Cs / B = Ge; Pb). Afin d'envisager une potentielle application en photovoltaïque. Les résultats montrent un aspect semi-conducteur avec une bonne ouverture du gap qui a mené à d'autres applications potentielles comme la photocatalyse.

Table of Contents

List of Abbreviations

PV: Photovoltaic.

E : Energy.

h : Plank's constant.

λ : The wavelength.

n : The index of refraction.

R: The reflection coefficient.

eV : electron volt.

k : Boltzmann constant.

T : Temperature.

°K : Degree kelvin.

Ab-initio: Calculation of the first principle.

DFT: Density Functional Theory.

H: Total Hamiltonian of the system.

Ψ: Wave function.

ρ(r) : The electronic density.

LDA: The local density approximation.

GGA: generalized gradient approximation.

PCE : Highest power conversion efficiency.

mBJ : The modified Becke-Johnson.

DOS : The density of states.

PF : Power factor.

FP LAPW: Full Potential Linearized Augmented Plane Waves.

CBM: The minimum of the valence band.

VBM: The maximum of the conduction band.

CIGS : CuInGeSe2 copper, indium, gallium and selenide respectively

$\mathbf{I_{sat}}$: The saturation current.

U : The voltage across the diode.

$\mathbf{U_T}$: The thermal voltage,

q : The elementary charge.

ZnO : Zinc oxide.

a-Si :Amorphous silicon.

CdTe : Cadmium tellurium/

CdS : Cadmium Sulfide.

CaTiO : Calcium titanate.

CZTS : Zinc tin copper sulfide.

δ : The ionic character.

χ_{A-O} : The differences in electronegativity

$\varepsilon_{XC}[\rho(\vec{r})]$::The exchange-correlation energy for a uniform gas of electrons.

t : The Goldschmidt factor (t),

R_O : The ionic radii

$CsPbX_3$: Lead halide and cesium

SOC : The spin–orbit coupling

χ : Pauli Magnetic.

S : Seebeck Coiffecients.

σ: Electrical Conductivity.

PF : Power Factor.

κ : Thermal Conductivity.

n : Number of Carriers.

RH : Hall Coefficient.

c : Electronic Specific Heat.

HSE : Hybrid functionals

SCF : Self-Consistent Field.

Z.B : Brillouin zone.

Fig : Figure

List of Figures

List of Tables

Introduction

Over the last years, research has been aimed at developing renewable energies in order to offer a reliable alternative to fossil fuels and nuclear energy with the aim of reducing greenhouse gas emissions and ensuring energy sustainability in the context of sustainable development. Faced with the predicted inevitable depletion of the world's fossil energy resources (oil, gas, coal...), the consumption of fossil fuels leads to multiple oil and economic crises besides climate change due to the greenhouse effect. The increase in population and the growing demand for energy supply have allowed us to explore more sustainable energy resources. For this, scientists and industrialists are turning to other sources of renewable energy that are non-polluting but above all based on an inexhaustible source, also referred to as green or clean energy. On Earth, solar energy is at the origin of the water cycle, wind and photosynthesis of the plant kingdom. The animal kingdom, including humanity, depends on plants on which all food chains are based. Solar energy is thus at the origin of all forms of energy production used on Earth today, except for nuclear energy, geothermal energy and tidal energy. Several technologies exist to capture and convert solar energy. They are based on the capture of the energy of photons, energetic particles that make up light. The technologies developed allow them to convert their energy into heat or electricity. Solar energy is a renewable energy whose use does not produce CO_2. Therefore, it appears as a possible solution to the problems posed by the scarcity of certain energy sources, their cost and impact on the environment. Currently, there are two main ways of exploiting solar energy thanks to semiconductor materials that capture light radiation and transform it directly into electricity by photovoltaic effect, or after conversion into heat and mechanical energy by thermodynamic effect. Photovoltaic technology is a promising technology that so far has attracted the attention of researchers and currently many efforts are being undertaken to maximize the efficiency of this technology, which goes to study the infinite possible materials.

In this perspective, we have started the research of possible materials for photovoltaic application using the first principles called "ab-initio", which are among the most accredited methods of modeling and simulation, which allows us to obtain a wide range of information on the microscopic origin of material properties. Our work is a first-principles calculation, it was carried out by the Full-Potential Linearized Augmented Plane Wave (FP-LAPW) method, implemented in the Wien2k calculation code. In the first chapter we present the general introduction of our thesis work, followed by a bibliographical study concerning the principle of photovoltaic conversion and photovoltaic solar cell technologies. Then, in the second chapter, we are interested in the foundations of the Density Functional Theory (DFT), as well as in the new methods of simulation and numerical modeling very advanced such as the ab-initio or first principal methods. In the first step, we studied a second-generation PV cell material, CIGS has many advantages, such as large optical absorption coefficient, long term stability, low cost and high efficiency. And we present all the theoretical results obtained concerning the ab initio study of the structural, electronic, optical and thermoelectric properties of CIGS as well as their interpretations. On the other side of these work, In the fourth chapter, we studied perovskite materials from the third PV generation, more precisely the simple halide perovskites of general formula ABX_3 with (A = K; B= Sn, Ge, Pb; X = Cl, Br, I), we try to see the effect of the change of the cation B as well as the halogen X, on the physical properties of these compounds. In a perspective of improving properties, we investigate in the fifth chapter, the perovskite halides mixte with general formula $ABI_{3-x}Br_x$ with (A = Cs,K and B = Pb, Sn, Ge), we explored the effect of mixed halides on the electronic and optical properties of the studied materials. In the last chapter. We inestigate the perovskite halides mixte with general formula $AGeI_2Br$ with (A = Cs,K and Rb) with strain effect study and other perspective of application for this compounds. This work ends with a general conclusion, summarizing the main results obtained with the associated physical interpretations, while proposing the envisaged perspectives.

Chapter I : Overview

I. Introduction

The Sun is an extremely powerful energy source, and sunlight is by far the largest source of energy received by Earth. Abundant and free primary energy, it is at the origin of the water cycle, wind and also photosynthesis [1]. Solar energy is thus at the origin of all forms of energy production used nowadays, with the exception of nuclear energy, geothermal energy and tidal energy. Solar radiation is partly reflected, partly diffused within the atmosphere, so that, at ground level, there are two components: direct radiation, from the portion of the sky occupied by the sun, and diffuse radiation, from the rest of the sky [2]. The diffuse radiation is the result of several phenomena: scattering by molecules (Rayleigh scattering, which is the origin of the blue color of the atmosphere) [3] or by aerosols (Mie scattering, independent of the wavelength of radiation), reflection on clouds or dust [4]. **Figure I.1** illustrates these phenomena schematically. Solar radiation can be converted either into thermal energy (heat) or into electrical energy [5]. Today technologies are at the base of this conversion, the photovoltaic (PV) modules are the primary elements of photovoltaic systems, which allow the conversion of solar radiation into electricity and it concerns both components of the illumination, which makes possible the production of solar electricity even during cloudy days [6].

In the 21st century solar energy is expected to become increasingly attractive as a renewable energy source because of its inexhaustible supply and its nonpolluting character, there is a hope that photovoltaic systems can make us independent of fossil fuels, addressing the current environmental problems.

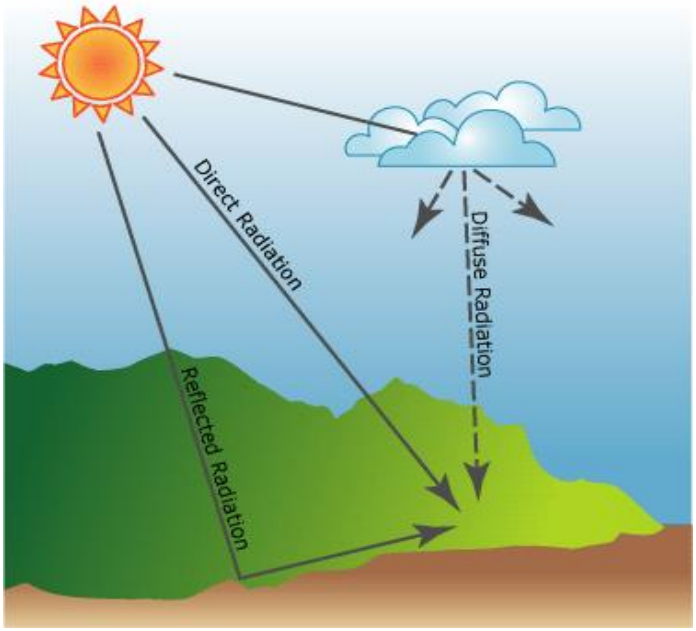

Figure I. 1: *Solar radiation*

I.1. Photovoltaic / solar cell

The word photovoltaics (PV) was first mentioned around 1890, and it comes from the Greek words: photo, ‘phos,’ meaning light, and ‘volt,’ which refers to electricity. Photovoltaic, therefore, means light-electricity, describing exactly the photovoltaic phenomenon where we can directly convert light into electricity using semiconducting materials. Observed by Henri Becquerel in 1939 [7]. It is quite generally defined as the emergence of an electric voltage between two electrodes attached to a solid or liquid system upon shining onto this system. In most cases, semiconductors are used for the solar conversion in solar cell material. The energy conversion consists of absorption of light (photon) energy producing electron–hole pairs in a semiconductor and charge carrier separation [8]. For a charge carrier separation, a p–n junction is used. It is important to learn the basic properties of semiconductors and the principle of conventional p–n junction solar cells to understand how the conventional solar cell works. In a crystalline semiconductor, the crystal structure determines the different energy levels available to electrons. These energy levels constitute two sets that can be considered continuous: the valence and

conduction bands, separated by a band-gap (of the order of one electron-Volt), depend on the material **Fig I.2**.

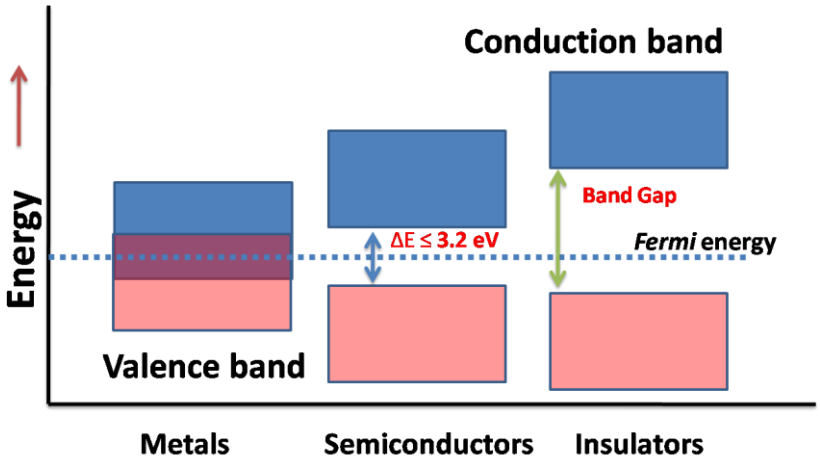

Figure I. 2:Energy levels

An impurity can be introduced into the crystal lattice: it is a dopant atom. The atom is an electron acceptor if it is located on the previous column of the constituent element of the network in the periodic classification of elements, it is a donor if it is on the next column. For example, silicon can be doped with boron (P doping: there is an excess of holes) or with phosphorus (N doping: excess of electrons). When an N-doped semiconductor and a P-doped semiconductor are brought into contact, a p-n junction is obtained. That's why the photovoltaic cells are p-n junctions [9].

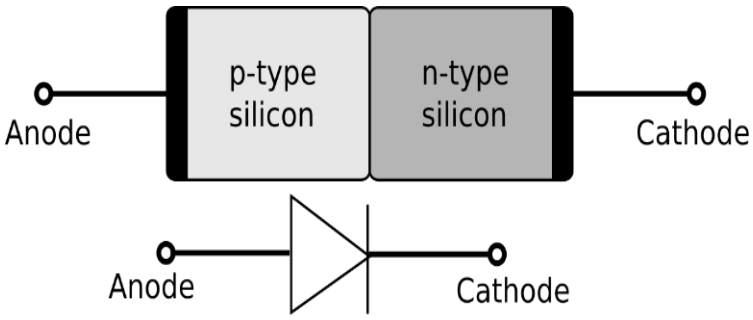

Figure I. 3:A p-n junction

When the p-doped region and the n-region are brought into contact with, electrons and holes spontaneously diffuse on both sides of the junction, creating a depletion zone. While a doped semiconductor is a good conductor. The width of the depletion zone varies with the voltage applied on both sides of the junction. The smaller the width of the depletion zone is, the lower is the value of the resistance of the junction. This allows electrical current to pass through the junction only in one direction, the main characteristic of a diode **Fig.I.3**. The electrical characteristic U-I (current - voltage) **Figure I.4** of a p-n junction under illumination is that of a p-n diode and it is called the Shockley equation [10]:

$$I_D = I_{sat}.\left(e^{\frac{U}{U_T}} - 1\right) = I_{sat}.(e^{\frac{qU}{kT}} - 1) \qquad (1.1)$$

With :

I_{sat} : the saturation current.
U : is the voltage across the diode.
U_T : is the thermal voltage, equal to $\frac{kT}{q} = 26mV \ at \ T = 300K$.
q : is the elementary charge.
T : absolute temperature of the junction.
k : the Boltzmann constant.

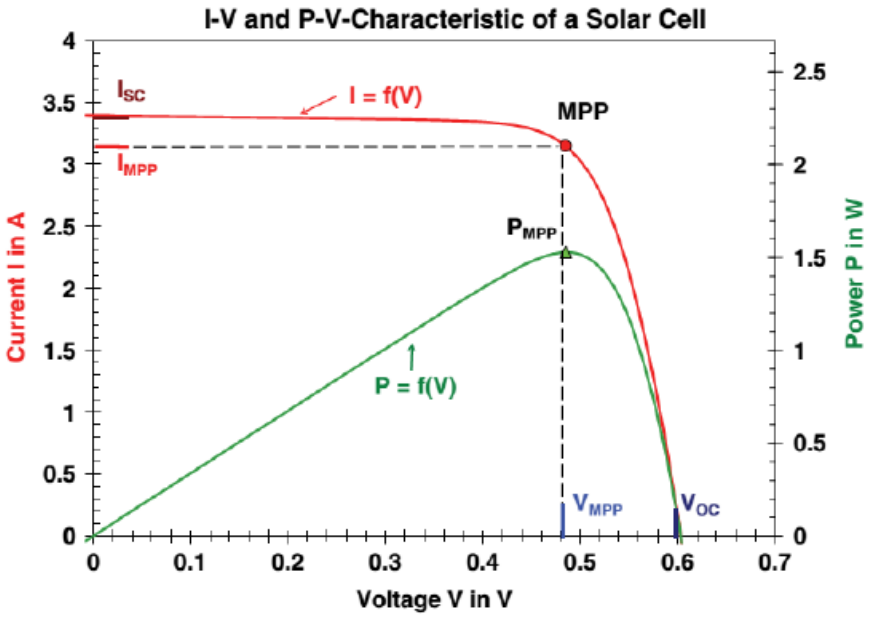

Figure I. 4:I-V cararcteristic of a solar cell.

The p-n junction is an essential component of a solar cell, which is used to generate solar energy. Its purpose is to capture the sun's radiation in order to transform it into electricity. The solar cell, or photovoltaic, can work alone, when the needs are lesser, for a solar calculator for example. For larger needs, it is assembled into photovoltaic solar modules, which we commonly call solar panels. For a solar cell we have five main Component **Fig I.5**.

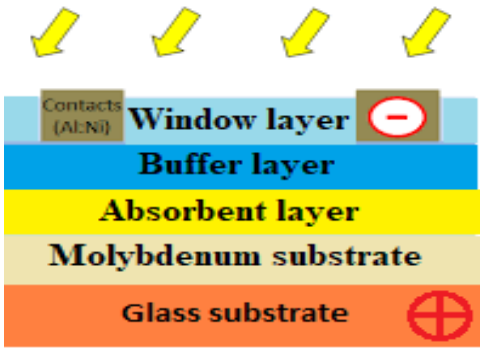

Figure I. 5: Solar cell Component

- **Glass substrate**

The substrate generally used for the realization of solar cells is a soda-lime glass substrate chosen for its thermal expansion close to that of the absorber and its low cost.

- **Molybdenum substrate**

On the glass substrate, a layer of molybdenum is deposited as the back contact. This layer of 500 to 1000 nm is deposited by sputtering and has a fundamental role in the performance of the solar cell [11]. Initially, molybdenum was chosen for its good conductivity and its resistance under selenium atmosphere but it also presents electronic properties adapted to the solar cell.

- **Absorbent layer**

For the absorption of light, an important characteristic of the material is its gap. This is the gap between the maximum of the valence band and the minimum of the conduction band of a material. The valence band is assumed to be entirely occupied by electrons and the conduction band entirely empty. There are two types of gaps: the direct gap and the indirect gap. The direct

gap: When the minimum of the conduction band and the maximum of the valence band correspond to the same value of the wave vector (k), the gap is direct. The transitions between bands are vertical, and are therefore radiative. The indirect gap: the transition of the extrema of the bands does not occur vertically but obliquely: the electronic transitions are non-radiative.

- **Buffer layer**

As a buffer layer we can use a thin layer of cadmium sulfide (CdS) deposited by chemical bath on the absorbent layer [12]. This thin 50-80 nm layer participates in the formation of the pn junction but also passivates the surface states and protects the absorbent surface from the high-energy ions used for the window layer sputtering. In order to deposit the CdS layer, the layer is immersed in a solution that includes a cadmium salt, an ammonia NH_3 complexing agent and a thiourea $SC(NH_2)_2$ precursor. In the laboratory, the absorbent layer is immersed in the solution at a temperature of 60◦C for 7 minutes. The CdS layer has a much higher doping than the absorbent layer allowing the formation of the p-n junction in the absorber layer. In addition, the buffer layer has a larger band gap than the absorber (Eg(CdS) = 2.4 eV) [13].

- **Window layer**

Finally, two layers of zinc oxide (ZnO) are deposited by sputtering. The first layer consists of highly resistive ZnO. The second layer is the transparent and conductive contact. Its role is to constitute the front electrode while ensuring the optimal transmission of photons of the solar spectrum. It is therefore a large gap material whose conductivity is promoted by doping with aluminum.

The standard manufacturing process for photovoltaic systems has several steps. The following explanations apply to the crystalline silicon sector. Currently, most solar panels are made of silicon. The first step in manufacturing a solar panel is to produce silicon ingots, which are large blocks of ultra-pure silicon (99.999999%).

The silicon is taken out of the furnace in the form of bars called "ingots". The ingots are cut into thin plates called "wafers" using wire saws. The thickness of the wafers is less than 200 microns, the equivalent of a sheet of paper. The next step is to chemically treat the wafer to make it less reflective. At the end of this treatment, the surface of the wafers, smooth at the beginning, is made up of tiny pyramids. This relief texture increases the conversion of light into electricity.

In order for the wafer to become a photovoltaic cell, phosphorus, a simple non-metallic body that is luminous in the dark, is deposited at very high temperature on its front surface. This addition of phosphorus gives a negative polarity to this front face. The wafer is now a photovoltaic cell, with a negative polarity front side and a positive polarity back side. It remains to deposit metal contacts on the front and back of the cell to collect the electrons released in the silicon. Each photovoltaic cell works like an electric battery, with a positive and a negative pole. The most common panels are composed of 60 cells. The next step is to place a tempered glass, whose thickness is 3 to 4 mm, in front. The panel is then equipped with its aluminum frame whose composition and profile have been studied to offer the best qualities of mechanical resistance. Finally, a junction box is attached to the back of the solar panel: it is the solar electricity output terminal. Each terminal has a "plus" and a "minus" cable equipped with special connectors to ensure the best electrical connection and a perfect seal.

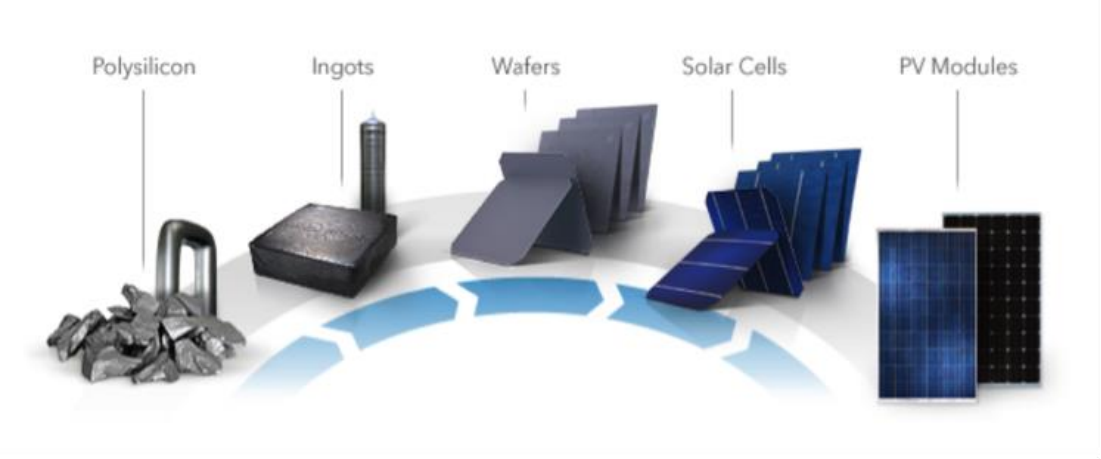

Figure I. 6: Manufacture of photovoltaic panels

So, by using the photovoltaic phenomenon, we can easily convert solar energy into electricity and use it as an alternative to traditional means of energy generation. Generally, we distinguish photovoltaic cells according to the technological developments and untill now there is three generation of solar cells:

I.1.1 The 1st generation cells:

First generation cells are based on a single P-N junction and generally use silicon in crystalline form as the semiconductor material. The silicon is melted and then cooled to obtain a crystal that is cut into thin wafers to obtain the photovoltaic cell. This production method is very energy intensive and therefore very expensive. It also requires high-purity silicon. We differentiate between monocrystalline and polycrystalline silicon cells.

I.1.2 The 2nd generation cells:

Thin films are the second generation of photovoltaic technology. In this generation, we distinguish amorphous silicon (a-Si), Copper Indium Gallium Selenide (CIGS) solar cells, cadmium tellurium /Cadmium Sulfide (CdTe/CdS) solar cells. In the case of thin films, the semiconductor layer is directly deposited on a substrate (e.g. glass, plastic ,..). The production of this type of cells is less expensive than that of the 1st generation because they consume less semiconductor material and do not require the stage of transformation into "wafers".

I.1.3 The 3rd generation cells:

The 3rd generation cells are more flexible, ultra-thin, and therefore more "agile" than silicon panels, based on macromolecules and nanoparticles, whose manufacturing processes are much less energy intensive and, potentially, lower cost. These third-generation photovoltaic cells are solar cells potentially capable of exceeding the Shockley limit - Queisser's 31-41% energy efficiency for single band gap solar cells [14]. This includes a range of alternatives to cells made of semiconductor p-n junctions ("first generation") and thin film cells ("second generation").

Unfortunately for the PV industry, these cells lack stability over time, resulting in a lifetime when exposed to sunlight that is too short for PV applications. Current third generation systems include :

- Zinc tin copper sulfide (CZTS) solar cell and derivatives CZTSe and CZTSSe
- Dye-sensitized solar cell, also called "Grätzel cell
- Organic solar cell
- Perovskite solar cell
- Quantum dot solar cell

In particular, the results obtained in perovskite cell research have received considerable public attention, with their research efficiency recently exceeding 20% [15].

I.2. Perovskite

I.2.1 introduction

Perovskite solar cells have shown remarkable progress in recent years with rapid increases in conversion efficiency, from reports of about 3% in 2006 to over 25% today. While perovskite solar cells have become highly efficient in a very short time, a number of challenges remain before they can become a competitive commercial technology. The word perovskite was first used by the German mineralogist Gustav Rose [16] in 1839, to designate calcium titanate of formula $CaTiO_3$. The choice of this name was to commemorate the name of the Russian mineralogist L. A. Perovskite (1792-1858). Then this word was extended to designate all the oxides of general formula ABO_3, which have the same structure as $CaTiO_3$. The ideal perovskite structure is cubic, with a Pm3m space group. Perovskite oxides have been widely studied since then, due to the wide variety of properties that these materials present. For example, ferroelectricity [17-18], piezoelectric [19], semi-metallicity [20] and dielectric [21]. However, these oxide perovskites do not have good semiconducting properties that would make them suitable for photovoltaic (PV) applications. For this reason, research has been directed towards another class of perovskite-like

materials, halide perovskites, which differ from oxide perovskites by the fact that halide anions replace oxide anions (ABX_3; A = cation, B = divalent metal cation, X = halogen anion) **Fig I.7**. These compounds have shown desirable semiconducting properties for photovoltaic (PV) applications.

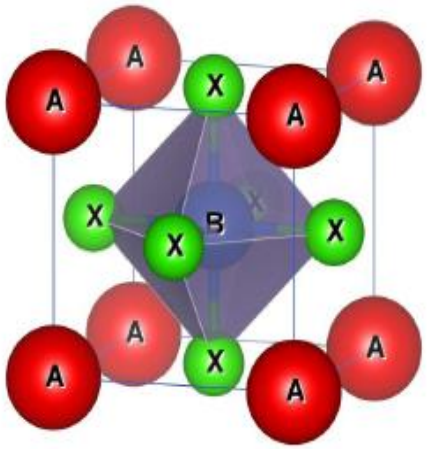

Figure I. 7: Elementary structure of perovskite type ABX_3.

According to the occupation of the A and B sites, we can define two types of perovskites:

- Simple perovskites: these are perovskites for which the A and B sites are occupied by a single type of atom, for example the compounds: $CaTiO_3$, $BaTiO_3$, $NaTaO_3$, $PbTiO_3$....
- Complex perovskites: these are perovskites in which one of the two sites A or B is occupied by two types of atoms, the distribution of cations can be random or ordered, for example the compounds used in the manufacture of capacitors: $PbMg_{0.33}Nb_{0.66}O_3$, $PbSc_{0.5}Ta_{0.5}O_3$, $Na_{0.5}Bi_{0.5}TiO_3$.

The choice of the atoms positioned on the sites of the cations A and B in the crystal structure of the perovskites is primordial and essential in the stability of these compounds, particularly the relation linking the lengths of the ionic radius of the cations A, B and the anion X by the ionicity of the bonds as well as the difference of electronegativity between the cations and the anions playing a decisive role in the determination of the properties of these materials. So we can conclude

that there are two factors that mainly influence the stability of the perovskite structure the ionicity of the anion-cation bonds and the Goldschmidt tolerance factor [22].

I.2.2. Stability factors of the perovskite structure

a . **Ionicity of anion-cation bonds**

The difference in electronegativity between the different ions plays a major role in the stability of the perovskite structure. The ionic character of this structure can be determined from the average electronegativity difference, according to the Pauling scale [23].

$$\delta = \frac{(\chi_{A-O}+\chi_{B-O})}{2} \qquad (1.2)$$

Where: χ_{A-O} and χ_{B-O}represent the differences in electronegativity between A and O and B and O respectively.

b. Goldschmidt tolerance factor (t)

The Goldschmidt factor (t), allows to quantify and explain in a global way the compactness, the stability and the existence of distortions in the perovskite structure as well as the stability of the crystalline structure for different relative values of ionic radii. Thanks to Goldschmidt we can define a relationship between the ionic radii of the elements that constitute the simple perovskite structure.This tolerance factor (t) is expressed by the following relation:

$$(R_A+R_O) = t\sqrt{2}\,(R_B+R_O) \qquad (1.3)$$

R_A, R_B and R_O represent, respectively, the ionic radii of cations A, B and oxygen ion. The value of $\boldsymbol{t}$, which approaches 1, favors the ideal cubic structure for simple perovskites. When the value of "t" moves away from 1, the elementary mesh is distorted. For low values and in a certain limit, the structure goes through phase transitions trying to compensate the imbalance of the size of the cations. This compensation is done, in general, by a tilt of octahedra BX6 perovskite giving place to different crystal structures

c . Formation Energie

One of the most useful quantities calculations is its formation energy, it's the energy required to the compound formation from its constituent elements. Compound-formation energies are required to predict compound stability, generate phase diagrams, calculate reaction enthalpies and voltages and determine many other material properties. Because this quantity is so ubiquitous, it is important to determine the trustworthiness of our predictions. The DFT calculations are performed at 0 K and experimental formation energies are typically measured at room temperature, we must consider how much we can expect the formation energy to change between 0 and 300 K. The largest source of differences between 0 and 300 K formation energies is the existence of phase transformations in this temperature range. These phase transformations can take the form of solid–liquid, solid–gas or solid–solid transformations and lead to significant changes in energetics. In general, the formation energy for a compound is given by [24] :

$$E_{form}^{ABX3} = \frac{1}{x+y+z}\left[E_{total}^{ABX3} - \left(xE_{solid}^{A} + yE_{solid}^{B} + zE_{solid}^{X}\right)\right] \qquad (1.4)$$

Where E_{total}^{ABX3}, E_{solid}^{A}, E_{solid}^{B} and E_{solid}^{X} are the calculated total energies of ABX_3 compounds, and the energy of A, B and X, respectively. x, y and z are the numbers of the atoms A, B and X in the unit cell respectively.

I.3. Halide pérovskite

1.3.1 Introduction

The discovery of such halide perovskites dates back to the 1890s. Indeed, in the year 1893, Wells et al conducted an extensive study on the synthesis of lead halide compounds from solutions comprising lead halide and cesium, $CsPbX_3$ (X = Cl, Br, I) [25], ammonium (NH_4) or rubidium, $RbPbX_3$ [26]. Much later, in 1957, the Danish researcher CK. Moller discovered that the structures CsPbCl3 and CsPbBr3 had a perovskite structure [27]. In 1978 Weber presented the first

crystallographic study of lead perovskites. The year 1995 is marked by the work of David Mitzi who succeeded in synthesizing a large variety of halide perovskites based on organic cations [28]. These and other researches have shown the possibility of using halide perovskites in optics and electroluminescence. The work of Kojima Akihiro, et al started in 2005 showed the possibility of using perovskite halides in the field of solar cells with an acceptable efficiency [29]. Based on the information provided by "Clarivate Analytics" in 2018, researchers from more than 1000 institutes around the world are currently working on photovoltaic and optoelectronic technologies related to halide perovskite, resulting in more than 9000 scientific papers in this field. The simple perovskite halide structure has a general formula ABX_3 where 'A' and 'B' are two cations and 'X' is a halogen. The ideal structure of a perovskite is a face-centered cubic structure of high symmetry, with a space group (#221) [30]. Its structure can be described as a cubic lattice of A cations at the vertices, with X anions placed at the center of the faces and a B cation occupying the octahedral site at the center of the cube. This structure can also be described as a cubic network of BX6 octahedra connected by the vertices, and between which the A cations occupying the centers of the cuboctahedral are intercalated.

I.3.2 Fields of application of perovskites

Single and double halogen-based perovskites have the potential to become new materials with multifunctional properties, due to the different possibilities of chemical combinations. With general formula ABX_3, halide perovskites present a variety of physico-chemical properties; starting with large gap insulating compounds, passing by semiconductors or ferroelectric, or even superconductors compounds [31-33]. Therefore, the study of the properties of these compounds becomes a necessity to predict possible uses depending entirely on these properties.

In recent years, halide perovskites have emerged as leading materials for many optoelectronic applications. However, oxide perovskites have a much longer history and perform a critical role in many technological applications. Applications based on perovskites are finding their way into

industrial use, whether in innovative projects such as the superconducting properties already used in magnetic levitation trains in Japan and in electric cables for urban distribution networks, or in the health field, such as fluoro perovskites which can be used in the medical field to measure the dose during radiotherapy, and which can also be used in the manufacture of X-ray imaging plates, sensors also have their share of perovskites [34], magnetoresistance, transistor, solar cells [35]. Perovskites are intensively studied in recent years, due to their optoelectronic properties such as semi conductivity, dielectric permittivity, ferroelectricity, thermoelectricity, further characterized by their abundance and low cost. Thanks to their extraordinary properties, these materials are becoming very promising and play an important role in modern electronics. Perovskites are therefore promising candidates in the development of new materials to meet the needs of new markets in modern electronics.

Also, perovskites can be tuned to respond to different colors in the solar spectrum by changing the material composition, and a variety of formulations have demonstrated high performance. This bandgap flexibility opens up another useful application for perovskite solar cells in high-performance tandem device architectures, with potential power conversion efficiencies over 30%. In these structures, perovskites are combined with another, differently tuned absorber material to deliver more power. Perovskite solar cells of certain compositions can convert ultraviolet and visible light into electricity very efficiently, meaning they might be excellent hybrid-tandem partners for absorber materials such as crystalline silicon that efficiently convert infrared light. It is also possible to combine two perovskite solar cells of different composition together to produce a perovskite-only tandem. Doing so could lead to even higher efficiency and more cost-effective tandem photovoltaic (PV) applications. Perovskite-only tandems could be particularly competitive in the mobile, disaster response, and defense operational energy areas, as they can be produced on flexible substrates with high power-to-weight ratios. The perovskite PV R&D community is heavily focused on operational lifetime and is considering multiple approaches to understand and improve intrinsic and extrinsic stability and degradation. Efforts include improved surface

passivation of absorber layers; alternative materials and formulations for absorber layers, charge transport layers, and electrodes; and advanced encapsulation materials and approaches that mitigate degradation sources during fabrication and operation.

I.4 Conclusion

Actually, some perovskite researchers continue to push conversion efficiencies by characterizing defects in the perovskite. While perovskite semiconductors are remarkably defect-tolerant, defects still –negatively affect performance — especially those occurring at the surface of the active layer. Other researchers are exploring new perovskite chemical formulations, both to tune their electronic properties for specific applications (like tandem cell stacks), or further improve their stability and lifetime. Researchers are also working on new cell designs, new encapsulation strategies to protect perovskites from the environment, and to understand basic degradation pathways so they can use accelerated aging studies to predict how perovskite solar cells will last on rooftops. Others are rapidly exploring a variety of manufacturing processes, including how to adapt perovskite “inks” to established large-scale solution printing methods. Finally, while the best-performing perovskites are today made with a small amount of lead, researchers are also exploring alternative compositions and new encapsulation strategies, in order to mitigate concerns associated with lead toxicity.

Chapter II : Density Functional Theory (DFT)

II.1. History

Many mechanical or electronic properties of materials are routinely calculated in laboratories. Moreover, these methods are continuously updated to adapt to the speed and memory capacity of computers. They are all based on the density functional theory (DFT) [36]. The full-potential linearized augmented plane wave (FP-LAPW) [37] method is one of the most powerful and accurate methods for electronic structure calculations of condensed matter in a ground state, transition state or excited state. These computational methods use approaches from the fundamental laws of quantum mechanics, electromagnetism, and statistical physics to solve the Schrödinger equation [38], which provides a formal link between atomic-scale structure and macroscopic properties. However, the key problem to study, analyze the structure of matter, and understand the different physical properties of a system of interacting particles (or N-body problem) is to solve Schrödinger's equation (2.1).

$$H\Phi(r,t) = i\hbar\frac{\partial}{\partial t}\,\Phi(r,t) \qquad (2.1)$$

Indeed, the N-body problem does not admit any analytical solution, so incessant research, which is of extreme importance, has been carried out. Several methods have been proposed to solve equation (2.1). The stationary form for time independent potentials [39] is:

$$H\Psi(r_i,R_i) = E\Psi(r_i,R_i) \qquad (2.2)$$

Where:

E: Total energy of the system in its ground state described by the wave function $\Psi(r_i,R_i)$.

$\Psi(r_i,R_i)$: Wave function with several particles, where the set (r_i),, contains the variables describing the electrons and (R_i), those describing the nuclei.

H: The operator corresponding to the Hamiltonian of the system.

The Hamiltonian operator is written:

$$H = T_e(r) + T_{ions}(R) + V_{int}(r) + V_{ions}(R) + V_{ext}(r, R) \qquad (2.3)$$

Where:

$T_e \; et \; T_{ions}$: The kinetic energy operators of electrons and ions,

$V_{int} \; et \; V_{ions}$: The interaction potentials between electrons and between ions,

V_{ext} : The external potential experienced by the electrons which contains the external fields imposed by the ions.

The calculation of the energy of the ground state of the system is based on the solution of the time-independent Schrödinger equation (2.2) with the Hamiltonian (2.3) for an atomic or molecular system, and it is called an electronic structure calculation. Quantum computational methods can be classified as ab initio (first principles) or semi-empirical. Semi-empirical methods use approximate Hamiltonians instead of the exact Hamiltonian and parameters whose values are adjusted to experimental data or to the results of ab initio calculations. These methods require relatively short computation times and are appropriate for the study of large systems. On the other hand, ab initio calculations use the exact Hamiltonian and the values of the fundamental physical constants. As we will see, there are several levels of approximation in ab initio calculations and, in general, depending on the physical and chemical characteristics of the system under study, one can choose the most appropriate level of calculation to obtain the desired results. In this chapter, we will develop the theoretical tools that allow us to conduct the structural, electronic and elastic study. We start by briefly describing the Born-Oppenheimer approximation [40], the Hartree theory [41] and the Hartree-Fock theory [42], then we present the density functional theory [43,44] as the modern method of electronic structure calculation whose main argument is not the wave function but the electronic density.

II.2 Born-Oppenheimer approximation

The Born-Oppenheimer approximation or the adiabatic approximation [40]. First approximation historically presented by Max Born (1882-1970) and Robert Oppenheimer (1904-1967). This approximation is based on the separation of the motion of the electrons from that of the nuclei because the mass of the nucleus is much greater than that of the electrons [45]. It consists in supposing that the atomic nuclei are fixed in relation to the electrons, which allows us to separate the study of the motion of the electrons from that of the nuclei. And because the nuclei are heavier than the electrons and therefore slower, we begin by neglecting their motion in relation to that of the electrons and we take into account only that of the electrons in the rigid periodic network of nuclear potentials. Thus, the kinetic energy of the nuclei is neglected and the nucleus-nucleus potential energy becomes a constant that can be chosen as the new origin of energies. The Hamiltonian described in equation (2.3) can be simplified, since the kinetic energy of the nuclei becomes zero ($T_{ions}(R) \sim 0$), the interaction energy of the nuclei becomes constant ($V_{ions}(R) \sim cste$) but can be made zero by a suitable choice of the origin [42].

The Hamiltonian becomes:

$$H = T_e(r) + V_{ext}(r) + U \qquad (2.4)$$

With:

T_e : The kinetic energy operator, $T_e = -\sum_i \frac{\hbar}{2m_e} \nabla_i^2$

V_{ext} : The external potential felt by the electrons, $V_{ext} = -\sum_{i,I} \frac{Z_I e^2}{|\vec{r}_i - \vec{R}_I}$

U : the interaction potential e-e, $U = -\frac{1}{2}\sum_{i,I} \frac{e^2}{|\vec{r}_i - \vec{R}_I}$

The equation is written in the condensed form :

$$H_e \Psi = [T + V_{ext} + U]\Psi = E_e \Psi \qquad (2.5)$$

The problem is now purely electronic and neglects lattice vibrations, which gives this approximation the name adiabatic. However, the problem is simpler than the original one, but still difficult to solve and does not admit any analytical solution except in very simple cases like the hydrogen atom [46]. Therefore, other approximations are necessary.

II.3 Hartree approach

Proposed in 1928, it is an approximation that consists in assuming that each electron moves independently in the mean field created by the other electrons and nuclei [41]. It consists in replacing the poly-electron function by a product of mono electron functions. Thus, the problem passes from a system of electron-electron pair repulsion to a problem of a particle immersed in an average electrostatic field created by the charge distribution of all the other electrons and nuclei. This approximation is based on the assumption of free electrons which means that the interactions between electrons and spin states are not taken into account. This has two important consequences: the first is that the total coulombic repulsion of the electronic system is overestimated, the second is that the Hartree description does not take into account the Pauli exclusion principle, which requires the wave function to be antisymmetric with respect to the exchange of the coordinates of two electrons [47]. This approximation reduces the N-body problem to that of an independent electron problem. The treatment consists in reducing the body problem to that of a single particle, which allows us to consider the wave function of the system as the direct product of the one-particle wave functions as presented on (2.6).

$$\psi(r_1, r_2 \dots\dots\dots r_N) = \psi(r_1).\psi(r_2) \dots\dots \psi(r_N) \qquad (2.6)$$

It is a self-consistent equation of a singular particle to describe the electronic structure of the atom approximately. Each atom is considered in motion in an effective potential. The mono-electronic Schrödinger equations, called Hartree equations, are written in the form [48]:

$$-\frac{\hbar^2}{2m}\nabla^2\psi_i(\vec{r}) + V_{eff}(\vec{r})\psi_i(\vec{r}) = E\psi_i(\vec{r}) \qquad (2.7)$$

The first term corresponds to the kinetic energy of the electron i and the second term $V_{eff}(\vec{r})$ corresponds to the potential that the electron experiences.

The potential $V_{eff}(\vec{r})$ must take into account the electron-nucleus interaction and the action of other electrons. The electron-nucleus interaction is denoted by $V_N(r)$ given by:

$$V_N(r) = -Ze^2 \sum_R \frac{1}{|r-R|} \qquad (2.8)$$

As well as the action of the other electrons. This last effect is more difficult to take into account and in the Hartree approximation we consider that the other electrons form a negative charge distribution ρ(r'). Moreover, the electron moves in an average electrostatic potential V_H(r) coming from the set of neighboring electrons expressed by :

$$V_H(r) = -e \int d^3r' \rho(r') \frac{1}{|r-r'|} \qquad (2.9)$$

Finally, we express the effective potential as the sum of these two contributions:

$$V_{eff}(r) = V_N(r) + V_H(r) \qquad (2.10)$$

This approach gave a self-consistent solution to the problem of the physical system (the wave function and the electron density are interdependent). The equation is now simple to solve, but does not give very good results. Because of the neglect of the Pauli exclusion principle and the spin of the electrons. This requires the use of other approximations to better describe the term responsible for this contribution.

II.4 The self-consistent Hartree-Fock method

The electronic system in the Hartree approximation is not completely described. In 1930, Fock [42][49] showed that the Hartree wave function violates Pauli's exclusion principle because one of the missing interactions is the exchange interaction. This is the effect that expresses the antisymmetric of the wave function with respect to the exchange of the coordinates of any two electrons leading to the description of the N-body system (electrons) by the equality:

$$\psi(r_1, r_2, \ldots\ldots\ldots, r_i, \ldots\ldots, r_j, \ldots\ldots, r_N) = -\psi(r_1, r_2, \ldots\ldots\ldots, r_j, \ldots\ldots, r_i, \ldots\ldots, r_N) \qquad (2.11)$$

The Hartree-Fock approximation [50] is the basis of almost all ab initio and semi-empirical methods, hence its confirmed success in this field for several decades. The Hartree-Fock method is the starting point of many quantum calculations. Indeed, most of the methods allowing the treatment of electronic correlation are based on the use of the wave function obtained after a Hartree-Fock calculation. The fundamental principle is the consideration of the independence of the motion of an electron with respect to the motion of its neighbors. Thus, in this approximation, no account is taken of the dynamic electron correlation resulting from the influence of the motion of the surrounding electrons on the reference electron. As in the Hartree approach, the wave function of an N electron system is described by a linear combination of mono-electron functions with the addition of the antisymmetric of the ensemble. This first approximation allows us to write the wave function of the system as a Slater determinant [51].

$$\Psi_e = \phi_{sd} = \frac{1}{\sqrt{N!}} \begin{pmatrix} \phi_1(r_1) & \cdots & \phi_n(r_n) \\ \vdots & \ddots & \vdots \\ \phi_1(r_n) & \cdots & \phi_n(r_n) \end{pmatrix} \qquad (2.12)$$

$\frac{1}{\sqrt{N!}}$: is the factor of the valid normalization of orthonormal spin-orbitals.

The permutation of the coordinates of two electrons corresponds to the permutation of two rows or two columns where the determinant changes sign. The Pauli principle is the direct cause of this antisymmetry. This means that the motion of pairs of electrons of the same spin is correlated. The antisymmetry of the wave function can be shown by a spatial separation between the electrons of the same spin of a system with N electrons and this wave function described by a linear combination of mono-electron functions with in addition the consideration of the antisymmetry of the set. This cannot be obtained with a product of functions like the one given in equation (2.6). For the treatment of extended systems such as solids, because of the very rapid increase in the number of configurations with the number of electrons involved, the correlations due to short range coulomb interactions are neglected. This can have a significant influence on the accuracy of the

calculations in periodic solids. Therefore, this method does not allow us to find the exact energy of the real system. A more powerful theory for solids, which allows to circumvent these limitations, is the Density Functional Theory (DFT).

II.5 Density Functional Theory (DFT)

The Density Functional Theory (DFT) is an approach to the study of N-particle systems in which the development of the equations is done in terms of the exact electron density of the system. Its fundamental concept $\rho(r)$ is that the energy of an electronic system can be expressed in terms of its density. This is in fact an old idea dating mainly from the work of Thomas (1927) [52] and Fermi [53] Many works have been devoted to explaining the theory of the density functional [54,55] This theory is based on two fundamental theorems, proved in 1964 by Hohenberg and Kohn (1964) [56] which establish that the energy of a system in its fundamental state is a functional of the electron density $\rho(r)$ of this system, therefore, contrary to the methods described above, the theory of the density functional does not consist in searching for a complex wave function ψ in 3N , dimensions for the system to be studied, but rather a simple function in three dimensions which is the total electron density. This theory has obtained a formal proof only after the statement of the two theorems of Kohn and Sham (1965) [57], They treated the N-body problem with the help of Schrödinger type equations with one particle named the Kohn-Sham equations. Thanks to the Kohn-Sham approach, the DFT has been very successful since the beginning of the 60's in the calculation of the electronic structure of atoms, taken in their fundamental states. The resolution of these equations leads to the total energy, and to the electronic density $\rho(r)$ of the fundamental state [58]. Its simplest version, namely the (LDA) (Local Density Approximation), gives results often as good as those of the Hartree-Fock type methods, for less computing time.

II.5.1 Hohenberg and Kohn approximation

DFT really started in 1964 with the two fundamental theorems of Hohenberg and Kohn [56]. This approach applies to any system with several interacting particles evolving in an external potential. The formalism of the density functional theory (DFT) is based on two fundamental theorems that were proved by Hohenberg and Kohn:

Theorem 1 (Density as a basic variable) : The total ground state energy E is a unique functional of the particle density ρ (r) for an exterior potential V_ext(r) gives by [56] :

$$E=E,\rho(r) \qquad (2.13)$$

Theorem 2. (The variational principle) : The total energy functional of any multi-particle system has a minimum that corresponds to the ground state and the density of ground state particles.

$$E(\rho_0) = \min E(\rho) \qquad (2.14)$$

With ρ_0: Density of the ground state.

This is valid for a non-polarized spin system, but for a spin-polarized system the total energy and other properties of the ground state become a functional of the two high and low spin densities:

$$E = E(\rho\uparrow, \rho\downarrow) \qquad (2.15)$$

The expression for the function E(ρ) for a set of electrons in an external potential is:

$$E(\rho) = \langle \Psi(\rho)|T + V_{e-e} + V_{ext}|E(\rho)\rangle \qquad (2.16)$$

Where: T represents the kinetic energy of the electrons and $V_{e\text{-}e}$ the interaction term between the electrons.

According to Hohenberg and Kohn E(ρ) the total energy functional of the ground (fundamental) state is written as follows:

$$E[\rho(r)] = F[\rho(r)] + \int V_{ext}(r)\rho(r)dr \qquad (2.17)$$

where:

$$F[\rho(r)] = T(\rho) + \int \frac{\rho(r)\,\rho\prime(r\prime)}{|r-r'|} dr\, dr' + E_{ex}(\rho) \qquad (2.18)$$

T (ρ) is the mean value of the kinetic energy; the second term corresponds to the Hartree coulombic interaction and are both exactly calculable. The term E_ex (ρ) is called the unknown exchange-correlation energy in the general case. The Hohenberg-Kohn theorem is a real revolution in the theory of interacting particle systems. The solution proposed by Hohenberg-Kohn is the determination of the electron density (3 variables) instead of the wave function (3N variables). The knowledge of the electron density implies the knowledge of the wave function and the potential and thus of all the other observables. So, these two theorems provide a theoretical framework for perceiving the solution of the Schrödinger equation using the electron density ρ(r) as the main variable. However, the Hohenberg and kohn functional F[ρ(r)] still remain unknown. To solve this problem Kohn and Sham proposed to replace the (real) interacting system by a (fictitious) non-reacting system.

II.5.2 The Kohn-Sham equations

The goal of the Kohn and sham equations is to determine electronic wave functions that minimize the total energy. From equations similar to Schrödinger's:

$$E\varphi_i = H\varphi_i \qquad (2.19)$$

With:

$$H = -\frac{\hbar}{2m}\Delta + V_{ks}(r) \qquad (2.20)$$

The first equation of Kohn-Sham gives the definition of the effective potential in which the electrons bathe ($V_{eff} = V_{ks}$) which is the sum of three contributions:

$$V_{ks} = V_{ext}(r) + V_H(r) + V_{xc}(r) \qquad (2.21)$$

With:

V_{ext}: The coulombic electron-nucleus interaction $V_{ext}(r) = -\frac{z}{r}$

V_H: The coulombic interaction e-e $V_H(r) = \int \frac{\rho(r')}{|r-r'|}\, d^3r'$

V_{xc}: The exchange and correlation interaction $V_{xc}(r) = \frac{\partial E_{xc}[\rho(r)]}{\partial \rho(r)}$

The second Kohn-Sham equation is used to use V_ks in the N single-electron Schrödinger equation to obtain φ_i (r). It is written in the form:

$$H\varphi(r) = \left(-\frac{\hbar^2}{2m}\nabla^2 + V_{ks}(r)\right)\varphi_i(r) = \varepsilon_i\varphi_i(r) \quad ; i = 1,2,3, \ldots \ldots, N \qquad (2.22)$$

Where each electron undergoes the effect of the effective potential created by all the nuclei and the other electrons.

The third Kohn-Sham equation provided access to the electron density from the N single-electron functions $\varphi_i(r)$.

$$\rho(r) = \sum_{i=1}^{N} |\varphi_i(r)|^2 \qquad (2.23)$$

The wave functions $\varphi_i(r)$known as Kohn-Sham orbitals, can be written in any complete basis of wave functions. These bases can be atomic orbitals, plane waves or Gaussian wave functions, ... etc.

So far, the only problem that remains to be solved is the formula of $E_{xc}[\rho(r)]$ so that the DFT and the Kohn-Sham equations can be used in practice. For this, we will use approximations.

II.5.3 Approximations used in the DFT

II.5.3.1 The local density approximation LDA

The Local Density Approximation is the simplest approximation of the potential V_xc (r), proposed in 1965 by Kohn-Sham [57]. It consists in assuming an inhomogeneous gas (real) similar to a homogeneous gas of the same density ρ(r), for the calculation of the exchange-correlation energy. This approximation is based on the following two assomptions :

- The exchange-correlation effects are dominated by the density located at r point.
- The density ρ(r) is a slowly varying function of r.

it is then possible to write [59]:

$$E_{xc}[\rho(r)] = \int \varepsilon_{xc}(r)\rho(r)d^3r \quad (2.24)$$

with:

$$\varepsilon_{xc}(r) = \varepsilon_{xc}^{hom}\rho(r) \quad (2.25)$$

where: $\varepsilon_{xc}^{hom}\rho(r)$ is the homogeneous density of an electron gas.

In the case of magnetic materials, the electron spin provides an additional degree of freedom and the LDA must then be extended to the local spin density approximation (LSDA) [60], The introduction of the latter consists in considering two populations ρ (↑) and ρ (↓) in the density matrix and formulating the spin-dependent potential. Thus, we define the LSDA approximation to the exchange-correlation energy as follows:

$$E_{xc}^{LSDA}[\rho(r)\uparrow, \rho(r)\downarrow] = \int \varepsilon_{xc}^{hom}(\rho(r)\uparrow, \rho(r)\downarrow)\rho(r)d^3r \quad (2.26)$$

The (LSDA) correctly describes physical systems with small variations in electron density, as in the case of alkaline metals, but gives less convincing results for insulators and semiconductors. The application of (LDA) to these systems leads to an underestimation of the value of the band gap, which is a well-known defect of DFT [61]. The (LDA) is particularly insufficient to describe strongly correlated systems. For these systems, approximations have been developed.

II.5.3.2 The generalized gradient approximation GGA

In many cases, the (LDA) gave reliable results, but in others, it was less accurate with the experimental results. Most of the corrections that have been introduced to the (LDA) are based on the idea of taking into account the local variations of the density. For this reason, the gradient of the electron density has been introduced leading to the Generalized Gradient Approximation (GGA) [62], in which the exchange and correlation energy is a function of the electron density and its gradient:

$$E_{xc}^{GGA}[\rho(r)] = \int \varepsilon_{xc}[\rho(r)|\nabla\rho(r)|]\rho(r)d^3r \quad (2.27)$$

where: $\varepsilon_{xc}[\rho(r)|\nabla\rho(r)|]$ the exchange and correlation function depending on the electronic density and its gradient.

GGA gives better results for energy gaps and band gaps in oxides or fluorides of transition metals. In the case where spin polarization is considered, the exchange and correlation energy is described as follows :

$$E_{xc}^{GGA}[\rho(r)\uparrow,\rho(r)\downarrow] = \int \varepsilon_{xc}^{GGA}(\rho\uparrow(r),\rho\downarrow(r),\nabla\rho(r),\nabla\rho\uparrow(r),\rho\downarrow(r))\rho(r)\,d^3r \quad (2.28)$$

The GGA is an improvement of the LDA in the treatment of the exchange-correlation energy which consists in making it dependent not only on the electron density but also on its gradient. There are several versions of the GGA, the most frequently used are those introduced by Perdew and Wang (GGA-PW91) [63], Perdew, Burke and Ernzerhof (GGA-PBE) [64], Engel and Vosko (EV-GGA) [65].

II.5.3.3 Modified Becke and Johnson potential (mBJ)

For semiconductors are insulators, in order to improve the results obtained concerning the gap energy, where they underestimate by the previous methods (LDA and GGA). In 2006 Becke and Johnson [66] proposed a version of the exchange potential (BJ), then it was corrected and published by Tran-Blaha in 2009 [67]. Known as the modified potential of Becke and Johnson (Modified Becke Johnson potential), it is expressed as:

$$V_{x,\sigma}^{TB-mbj}(r) = cV_{x,\sigma}^{BR}(r) + (3c-2)\frac{1}{\pi}\sqrt{\frac{5}{6}}\sqrt{\frac{t_\sigma(r)}{\rho_\sigma(r)}} \quad (2.29)$$

with:

$\rho_\sigma(r) = \sum_{i=1}^{N_\sigma}|\phi_{i,\sigma}(r)|^2$: Represents the density of electrons.

$t_\sigma(r) = \frac{1}{2}\sum_{i=1}^{N_\sigma}\nabla\,\phi_{i,\sigma}^*(r)\nabla\phi_{i,\sigma}(r)$: Represents the density of the kinetic energy.

$V_{x,\sigma}^{BR}(r)$: Represents the Becke-Roussel potential (BR).

The c stands for

$$c = \alpha + \beta\left(\frac{1}{V_{cell}}\int\frac{\nabla\rho(r)}{\rho(r)}d^3r\right)^{\frac{1}{2}} \quad (2.30)$$

α and β are free parameters. Within the Wien2k code [68] α = -0.012 and β = 1.023 $Bohr^{1/2}$.

II.5.3.4 Hybrid functionals

The term hybrid refers to the combined use of the exact exchange energy of the H-F model and the exchange-correlation energy at the DFT level. The advent of these GGA-like functionals was

responsible for the massive use of DFT within the chemical community in the 1990s. The construction of hybrid functionals was an important advance in the treatment of exchange-correlation energy by allowing an explicit incorporation of the non-local character through the use of the exact exchange energy term. The observation that the LDA and the GGA are opposed to the Hratree-Fock method motivates a development of approximations that combine the advantages of both approaches [69]. This implies a combination of the correlation and exchange of the DFT with the Hratree-Fock exchange: the exchange and correlation energy can then be written:

$$E_{xc}^{Hyb} = \alpha E_{xc}^{HF} + (1-\alpha)E_x^{LDA} + bE_x^{GGA} + E_c^{LDA} + cE_c^{GGA} \quad (2.31)$$

II.5.3.5 Spin orbit coupling

Spin–orbit coupling is the relativistic interaction between electrons' spin and momentum degrees of freedom. When an electron moves in the finite electric field of the nucleus, the spin–orbit coupling causes a shift in the electron's atomic energy levels due to the electromagnetic interaction between the spin of the electron and the electric field. In the rest frame of the electron, there exists a magnetic field created by the interaction of the angular momentum of the electron and the electric field of the nucleus. The electrical field in this case can have various physical origins, such as the electric field of an atomic nucleus or the band structure of a solid [70]. The spin–orbit coupling of a free electron in an electric field **E** can be derived from the Dirac equation in the nonrelativistic approximation:

$$H_{so} = \frac{e\hbar}{4m^2c^2}\sigma(E \times P) \quad (2.32)$$

where **p** is the momentum. The spin–orbit coupling can be interpreted as an effective Zeeman term in the rest frame of a moving electron, where the electric field acts as an effective magnetic field $B_{\text{eff}} = (1/2mc^2)\ \mathbf{E} \times \mathbf{p}$. In a crystal, the potential gradient is dominated by the spherical atomic potential, $\mathbf{E} = -\nabla V(r)$, so that the largest contribution to spin–orbit coupling comes from the nuclei. The spin–orbit coupling is responsible for a variety of transport phenomena in solids.

Spin–orbit coupling is the relativistic interaction between electrons' spin and momentum degrees of freedom. When an electron moves in the finite electric field of the nucleus, the spin–orbit coupling causes a shift in the electron's atomic energy levels due to the electromagnetic interaction between the spin of the electron and the electric field. In the rest frame of the electron, there exists a magnetic field created by the interaction of the angular momentum of the electron and the electric field of the nucleus. The electrical field in this case can have various physical origins, such as the electric field of an atomic nucleus or the band structure of a solid. The spin–orbit coupling of a free electron in an electric field **E** can be derived from the Dirac equation in the nonrelativistic approximation :

$$H_{so} = \frac{e\hbar}{4m^2c^2}\sigma(E \times P) \qquad (2.33)$$

where **p** is the momentum. The spin–orbit coupling can be interpreted as an effective Zeeman term in the rest frame of a moving electron, where the electric field acts as an effective magnetic field $B_{\text{eff}} = (1/2mc^2)\ \mathbf{E} \times \mathbf{p}$. In a crystal, the potential gradient is dominated by the spherical atomic potential, $\mathbf{E} = -\nabla V\ (r)$, so that the largest contribution to spin–orbit coupling comes from the nuclei. The spin–orbit coupling is responsible for a variety of transport phenomena in solids.

II.5.3.6 Boltztrap calculation

BoltzTraP_Tools is an interface written using Python 2 language. It allows to parse and plot BoltzTraP output DATA (.trace, .condtens,.trace_fixdoping, and .condtens_fixdoping) in greater detail. BoltzTraP_Tools includes four folders:

• src : includes source files.

• doc : includes the user guide and some tutorials.

• tests : includes two BoltzTraP examples (output data).

• scripts : includes some scripts using BoltzTraP_Tools.

The program allows us to calculate the semi-classic transport coefficients of materials using First Principles electronic band structures. The code uses a mesh of self-consistent band energies and is interfaced to the WIEN2k code [71].

For the input file and after the we run the program with a file describing the parameters for BoltzTraP named case.intrans. Furthermore, we need a file with the band-structure and the crystal structure, case.energy(so) and case.struct, where case is the name of the directory. Presently case.energy(so) and case.struct have to be in the format of the WIEN2k code [72].

As an output file, it will be possible to plot the following quantities:

• Energy level : E

• Temperature : T

• Seebeck Coiffecients : S, Sxx, Syy, and Szz

• Electrical Conductivity : σ, σxx, σyy, and σzz

• Power Factor : PF, PFxx, PFyy, and PFzz

• Thermal Conductivity : κ, κxx, κyy, and κzz

• Number of Carriers : n

• Hall Coefficient : RH

• Electronic Specific Heat : c

• Pauli Magnetic : χ

II.6 The WIEN2k Code

The method used in this work is the FP-LAPW (Linearized Augmented Plane Wave) implemented in the calculation code "Wien2k" which is developed by Blaha, Schwartz and their collaborators [73] at the Institute of Material Chemistry of the Technical University of Vienna (Austria). This code was first distributed in 1990, it has been continuously revised since then and has undergone several updates to add computational properties or to solve some problems concerning the calculations. This numerical computation code is based on the "fortran" programming language and runs under the UNIX operating system, based on the density functional theory (DFT). It

gathers several packages of "independent programs" which are linked by a script allowing to perform self-consistent calculations.

II.6.1 Initialisation

In this step we have to insert the important parameters, we fill an input file named case.struct (Meaning: material name. Struct) with the following atomic parameters :

- The bravais lattice.
- The space group.
- The mesh parameters of the temporary lattices (a, b, and c in Bohr or Å).
- The angles (α, β and γ).
- The positions of the atoms {inside the cell (x, y and z)}.
- The muffin-tin radii (Rmt), given in atomic units (Bohr radius).

After having generated the "case.struct" file, we carry out the initialization by the command init_lapw to engage several programs which will be executed in a successive way; these programs are the following :

- **NN:** This is a program that gives for each atom, the list of its first neighbors and the distances between the nearest neighbors. Thus it allows to determine the atomic radius of the sphere and checks the overlap of the muffin tin spheres; the output file of this program is named case.output nn.
- **LSTART:** it allows to generate the atomic densities; it also determines how the different atomic orbitals are treated in the calculation of the band structure, where we have to choose the exchange-correlation potential (LSDA or GGA....), also this program asks for the value of the cut-off energy that separates the core states from the valence ones, usually taken in Rydberg (Ry).
- **DSTART:** it generates a starting density for the self-consistent cycle (the SCF cycle) by superimposing atomic densities generated in LSTART.The information will be written in

the file "case.clmsum".For the case of spin-polarized systems, "DSTART" must be specified with the command -up (-dn) to generate the files "case.clmup (dn).

- **SGROUP:** This program allows you to determine the space group of the structure that is defined in the case.struct file, and all the point groups of the non-equivalent sites, thus producing a new structural file with the appropriate network type named case.struct-sgroup.
- **SYMMETRY:** is a program that enumerates the symmetry operations of the space group and saves them in the file named "case.struct_st", the latter determines the point group of the different atomic locations and highlights the quantum numbers (l, m) for the spherical harmonics materialized in file "case.in2_st".
- **KGEN:** generates a k-mesh in the irreducible part of the first Brillouin zone (Z.B). We specify the number of points K in the whole 1st ZB and where this mesh is written in the file "case.klist".

The initialization is the most important step, because a good calculation which gives good results, requires a judicious choice of the calculation parameters.

II.6.2 Self-Consistent Field (SCF) calculation

In this step, the SCF (Self Consistent Field) cycle process is then started and iterated until the solution converges. This cycle can be invoked by the command "run_lapw", and for spin polarized systems the command used is "runsp_lapw". The subroutines used are :

- **LAPW0:** Generates the poison potential to have the Coulomb potential VC and the exchange-correlation potential Vxc , which are used in the calculation of the total electron density as input.
- **LAPW1:** Calculates the matrix coefficients of the Hamiltonian in the LAPW wavebase and finds by diagonalization the valence band, the eigenvalues and the eigenvectors.

- **LAPW2:** Determines the Fermi level, the expansions of the valence electron densities consisting of electron densities inside each MT sphere (expressed by spherical harmonics) and in the interstitial region (expressed by a Fourier series).
- **LCORE:** Calculates the core states inside the MT spheres, keeping only the spherical part of the potential.
- **MIXER:** calculates the new electron density by mixing the electron densities of the core, half-core and valence states to generate the input density for the next iteration.

a. Calculations and determination of properties

Once the self-consistent calculation is completed, it is possible to access the properties of the ground state (charge density, band structure, thermodynamic properties, thermoelectric properties...etc). Each of these properties is calculated separately with a "package" program which is launched with consecutive steps.

II.7 Computational Methods

The basis of this theses is the first principl calculations, completed with the density functional theory (DFT), implemented on the Wien2k code which uses the full potential linearized augmented plane wave method (FP-LAPW). It enables the calculation of optical and electronic properties of our compounds. We applied the modified Becke-Johnson with Generalized Gradient Approximation (GGA- mBJ). We fix the convergence criterion to 0.0001Ry and the convergence force to 1 mRy/a.u. The electrical properties as electrical conductivity, carrier concentrations and motilities, were estimated with the Boltzmann theory, implemented on the BoltzTraP Code.

II.8 Conclusion

In this chapter we have analyzed the different approach existing to solve the Schrödinger's equation. They are all based on the density functional theory (DFT). And until now, the full-potential linearized augmented plane wave (FP-LAPW) method is one of the most powerful and

accurate methods for electronic structure calculations of condensed matter in a ground state, transition state or excited state. These computational methods use approaches from the fundamental laws of quantum mechanics, electromagnetism, and statistical physics to solve the Schrödinger equation, which provides a formal link between atomic-scale structure and macroscopic properties. We also elaborated the methods of calculation to use as well as the approximations by defining each of them with the appropriate equation

Chapter III: Investigation of the Electronic, optical and thermal properties of the $CuIn_{1-x}Ga_xSe_2$ Compound.

III.1 Introduction

The second generation of solar cells was developed in the 1980s with the objective of reducing costs by using thin films. Using only a few microns of material. Researchers have succeeded in finding an alternative to the very expensive manufacture of silicon ingots inherent in the manufacture of first-generation solar panels. Technologies based on this approach use Cu(In,Ga)Se2, CdTe and a-Si semiconductors with a very high absorption coefficient. Cu(In,Ga)Se2 (CIGSe) based solar cells are the most efficient thin film solar cells with a record of 22.6% in the laboratory [74]. The first CIGSe cells were fabricated at Bell Laboratory in the early 1970s [75]. Intended for the manufacture of photodetectors, the cells consisted of CuInSe2 (CISe) single crystals evaporated on an alumina/molybdenum substrate. From 1975, in view of the difficulties in growing CISe single crystals, Kazmerski et al. considered the production of CISe thin films [76]. The interest for photovoltaic applications grew very quickly due to the good yields of around 9% obtained by BOEING in 1981 [77]. In 1987, Chen et al. attempted to incorporate gallium atoms into the CISe structure [78]. The partial substitution of indium by gallium allowed to improve the electrical performance of the solar cell. In the previous years, the Copper Indium Gallium di-Selenide thin films CIGS solar cells have never ceased to surprise researchers. Among its strengths are a high-performance ratio, a good stability over organic solar cells, a direct band gap, a large optical absorption coefficient and long-term stability [79,80]. Its chemical formula is $CuIn_{1-x}Ga_xSe_2$. with the gap energies fluctuating from 1 eV (for x=0) to 1.7 eV (for x=1), with the increasing of the gallium proportion in the film. Devaney et al. [81] reported high efficient production when the value of x=0.3 of Ga, with a band gap value of 1.21 eV [82]. It has the advantage of being deposited with various techniques such as: physical evaporation [83], selenization of sequentially stacked precursors [84], rapid thermal process [85]. But these vacuum deposition techniques are too expensive. It is proved that chemical bath deposition technique is

low cost, and gives a good quality [86]. Zweibel et al. [87] and Wettling et al. [88] had reported that the CIGS solar cells are interesting because of their high efficiency performance without any degradation problems. Up to now, CIGS is used as the most promising absorber layer for thin-films solar cells, and much theoretical and experimental research was performed to investigate the various properties. As Hadjab et al.[89], Fu-Ling et al. [90], Cheng Wan et al.[91], whom explore the optical and the electronic properties of CIGS adopting the Density Functional Theory (DFT).The aim of this work is to investigate the electronic and optical properties of $CuIn_{1-x}Ga_xSe_2$, as reflectivity, absorption coefficient, optical band gap, refractive index, dielectric function, lattice structure, density of states (DOS) band gaps and electrical conductivity, the concentration (x) was selected from 0 to 1, looking for application of these materials in advanced optoelectronic devices, this study in this theses was my first try of the Wien2k code, so we can consider it as a test and a metrics of the code than a study.

III.2 Computational Methods

We applied the modified Becke-Johnson with Generalized Gradient Approximation (GGA- mBJ) [94]. We fix the convergence criterion to 0.0001Ry and the convergence force to 1 mRy/a.u. The RMT was generated for each element, 2.35, 2.45, 2.39 and 2.23 a.u for Cu, In, Ga, and Se respectively for chalcopyrite structure. We have used 300 k-point in the irreducible wedge of the Brillouin zone for optimization. The simulations were done with the I-42d space group (No.122) in chalcopyrite structure [95,97] as shown in **Fig III.1**. The electrical properties as electrical conductivity, carrier concentrations and motilities, were estimated with the Boltzmann theory, implemented on the BoltzTraP Code [98].

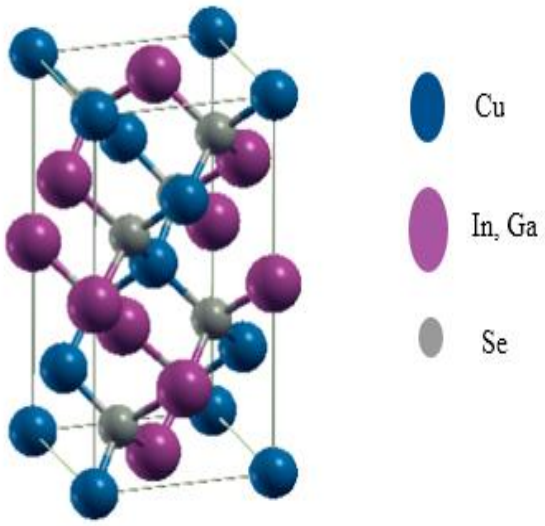

Figure III. 1:Crystal structures of CuIn1-x GaxSe2.

III.3 Results and discussion

III.3.1 Electronic properties

The density of states (DOS) figure III.3 and band structures show a semi-conducting behavior, which coincides with literature. The band structures are plotted in **Fig III.2**. For both materials the maximum of the valence band (VBM), and the minimum of the conduction band (CBM) are at the same point Γ, it results in a direct gap. The calculations give us values of band gaps too close to experimental results, the theoretical and experimental values of band gaps are represented in **Table III. 1.** The results obtained by the GGA+mBJ functional are close to the experimental results.

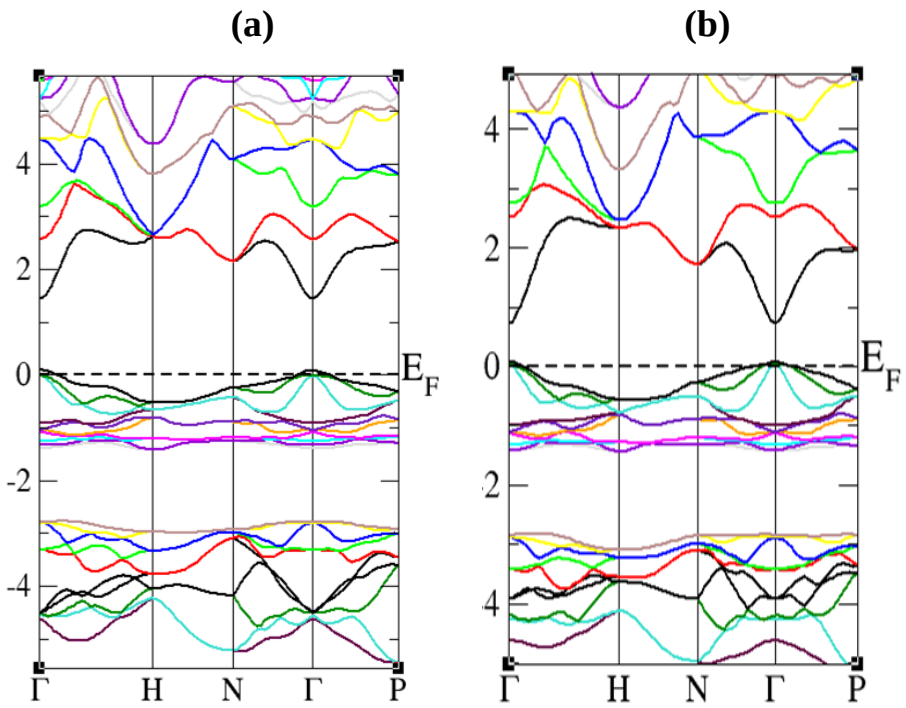

Figure III. 2: Band structure of for the tetragonal chalcopyrite: (a) CGS, (b) CIS.

Table III. 1 : Present work c ompared with experimental and other theoretical works.

	Present work	**Other theoretical**	**Experimental studies**
Eg (eV) (CIS)	0.904	1.205 [99] 0.550 [89]	1.04 [100]
Eg (eV) (CGS)	1.640	1.568 [99] 1.270 [89]	1.67 [101]

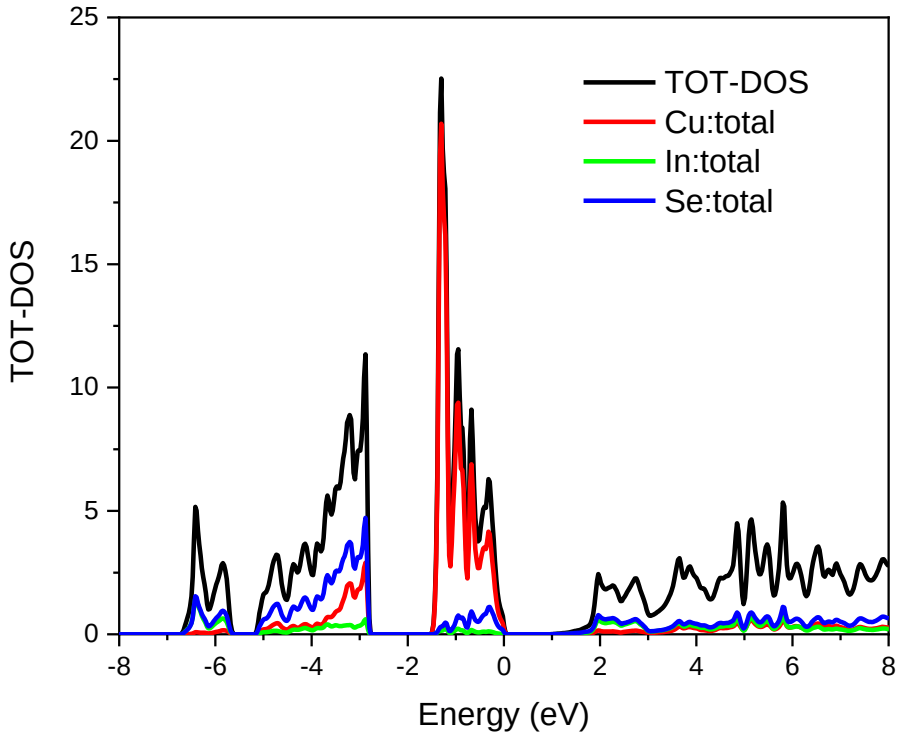

Figure III. 3:Total and partial state density of the compound $CuInSe_2$.

However, **Figs III.3 and III.4** presents the total and partial densities of states of both compounds using GGA+mBJ approximation. For $CuInSe_2$, the valence bands are dominated by the "p" states of the Selenium and the "d" states of copper with strong p-d hybridization. This indicates the strong covalent behavior between the Selenium atoms and the Copper, the conductivity bands are mainly dominated by the states ‘s’and 'p' of copper and Selenium. For CuGaSe2, the valence bands are dominated by the "p" states of Gallium and the "d" states of copper. This indicates the strong covalent behavior between the Gallium atoms and copper, and the conductivity bands are mainly dominated by the states of Gallium and Selenium.

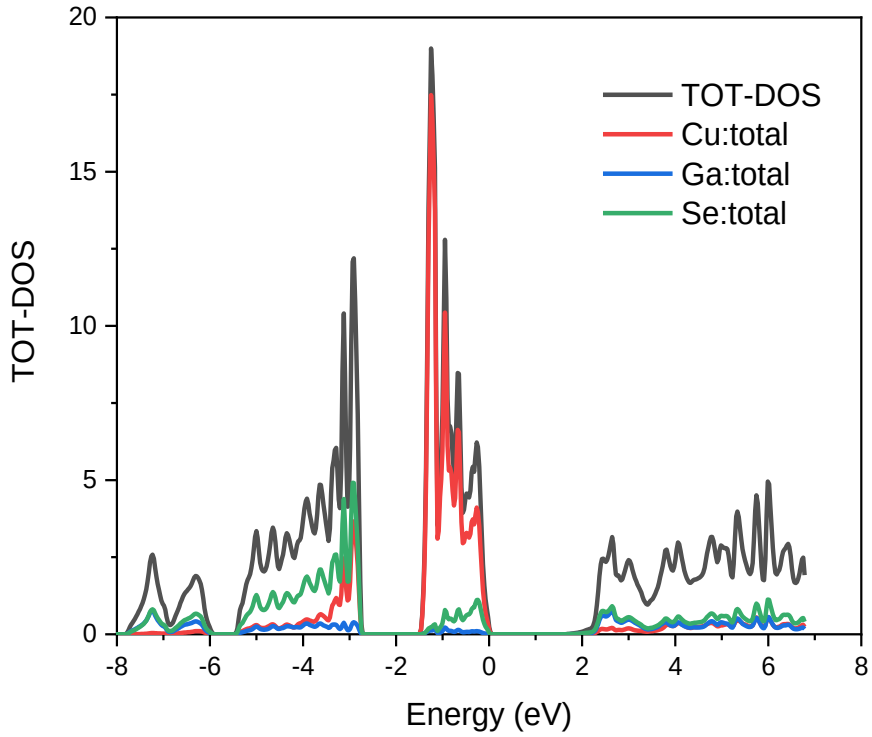

Figure III. 4: Total and partial state density of the compound $CuGaSe_2$.

For the following result we have varied the concentration (x) from 0 to 1. The **Table III. 2** shows the value of the band gap. The optical and electrical properties for the x = 0,25 confirm that the $CuIn_{0.75}Ga_{0.25}Se_2$ is more attractive because it's much more absorptive and can be more productive for photovoltaic applications.

Table III. 2: The band gap variation for x from 0 to 1.

Compound	Band gap (eV)	Optical Gap (eV)
CuInSe2	0.934	1.002
$CuIn_{0.75}Ga_{0.25}Se_2$	1.103	1.070
$CuIn_{0.50}Ga_{0.50}Se_2$	1.313	1.265
$CuIn_{0.25}Ga_{0.75}Se_2$	1.535	1.421
$CuGaSe_2$	1.640	1.671

III.3.2. Optical and Thermal properties

The optical and electrical properties as absorption coefficient α(ω), reflectivity R(ω), refractive index n(ω) of a material, can be described by the complex dielectric function ε (ω) [102,107]. **Fig III.5**, represents the optical absorption spectrums as function of wavelength (λ) in the range 300-900 nm, studied by GGA+mBJ approximation. A gradual decrease of all compounds between 300 and 350 nm can be noted. For CGS, we can see peaks of absorption noticed at 373 nm and 433 nm. For $CI_{0,75}G_{0,25}S_2$ the first peak was at 405 nm and the second one was at 463 nm. For CIS at 434 nm. for all λ>505 the curves begin decreasing until it reaches zero. In the visible range, we can conclude that the $CI_{0,75}G_{0,25}S_2$ have the best optical absorption. The absorbance of the quaternary CIGS has higher absorbance than that of the ternary CIS and CGS at visible range.

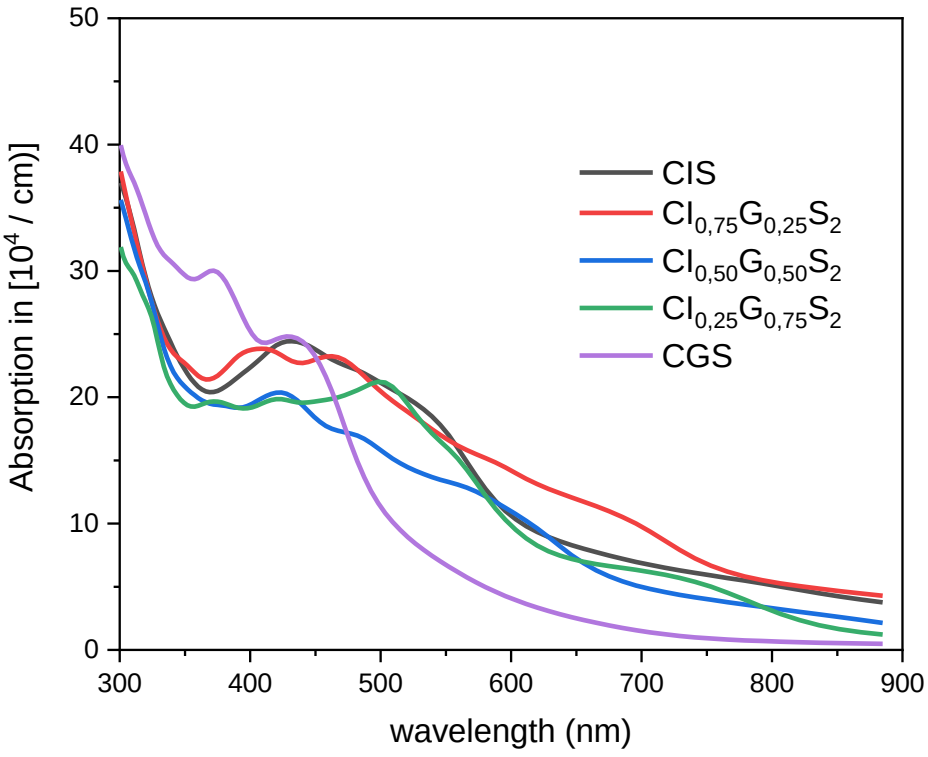

Figure III. 5:The optical absorption spectrums as a function of wavelength.

The reflectivity curves of the five compounds are shown in **Fig III.6,** the coefficient varies randomly between 0.2 and 0.3 at 300-900 nm wavelength range. We are interested in the visible range, a minimum value is seen for $CuIn_{0.25}Ga_{0.75}Se_2$ which is 0.2 at 400 nm, and a maximum of

0.29 for CGS at 465 nm. Between 537nm and 600 nm, CIS reached 0.27, for λ> 600 nm $CuIn_{0.75}Ga_{0.25}Se_2$ is the more reflective compared to others compounds. The **Fig III.7** represents the refractivity index, in the visible range it can clearly note that the CGS stands out with a high coefficient that reached a maximum of 3.2 at 480 nm, after the peak, the curve starts decreasing until stabilization. At 650 nm $CuIn_{0.75}Ga_{0.25}Se_2$ takes a max of 3 at 722 nm and decreases after that, and finally stabilizes at a value of 2.9 as observed in **Fig III.7**.

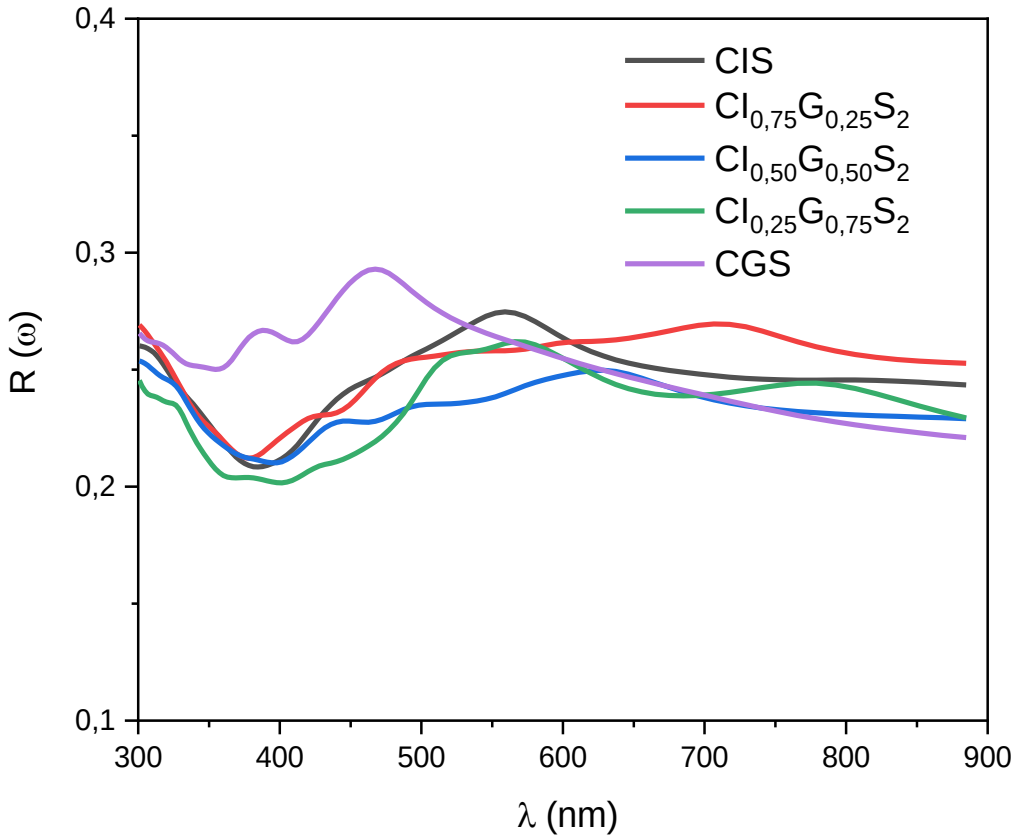

Figure III. 6: The reflectivity as a function of wavelength.

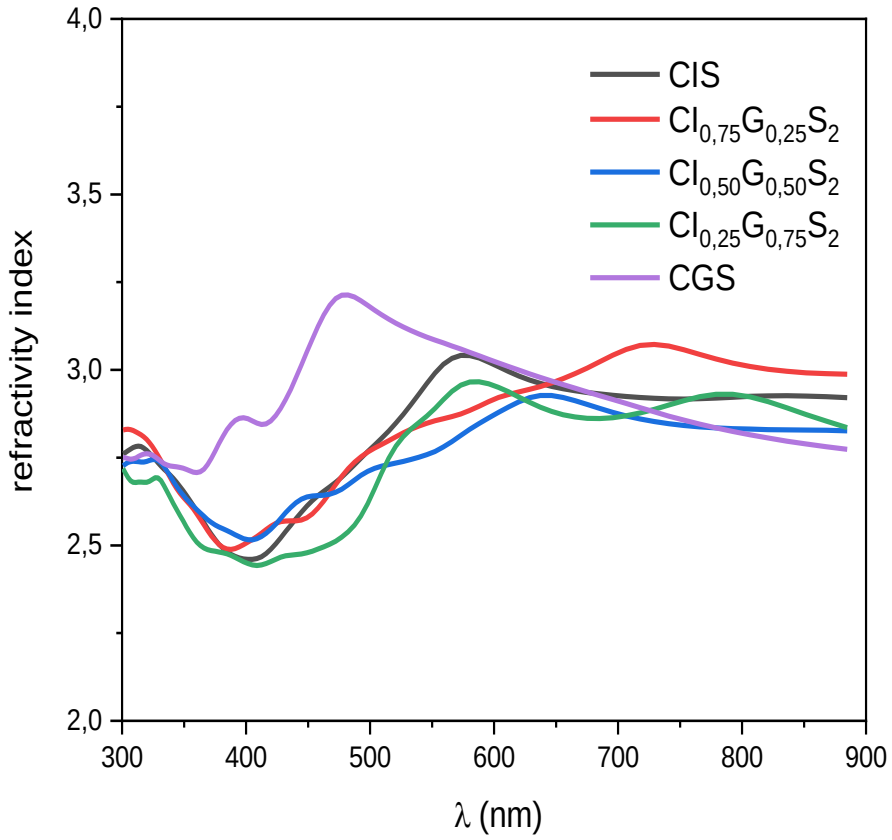

Figure III. 7: The refractivity index as a function of wavelength.

The **Fig III. 8** represent the optical conductivity depending on the wavelength between 300 nm and 900 nm, we can see a high conductivity for the CGS which far exceeds the others compound until 468 nm, where the CIS takes over with a value that varies between 1578-1187 $Ohm^{-1}cm^{-1}$ at 487-570 nm respectively, for λ>570 nm $CuIn_{0.75}Ga_{0.25}Se_2$ is the most conductive. This allows it to be a good candidate for photovoltaic application.

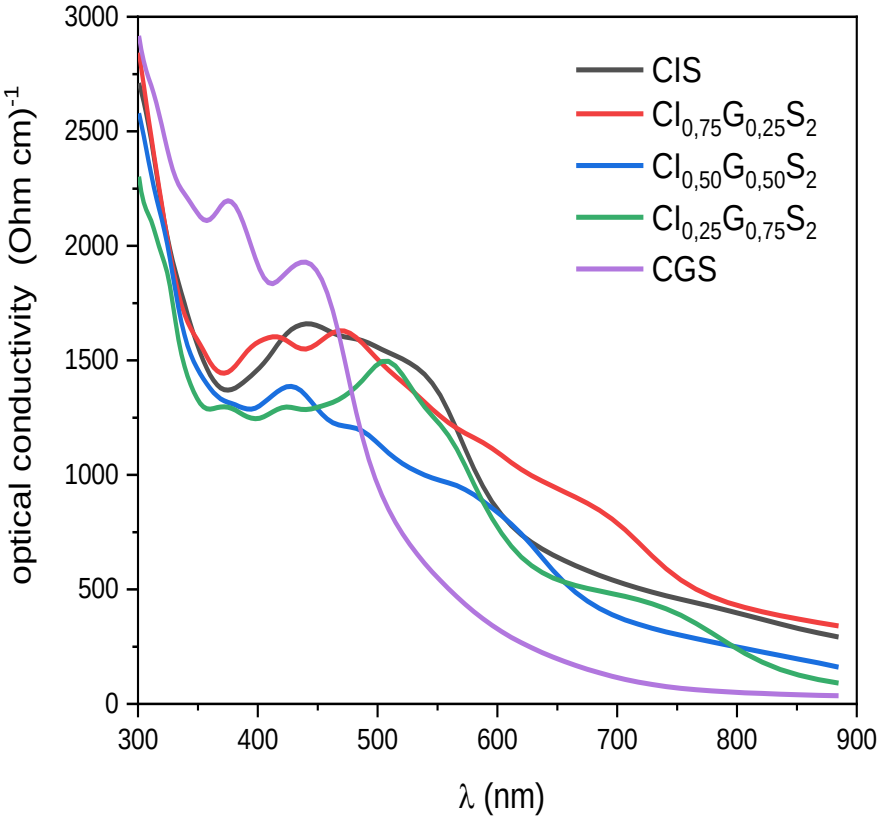

Figure III. 8: Represent the optical conductivity as a function of wavelength.

The optical gap energies were evaluated by plotting $(\alpha h\nu)^n$, where α is the absorption coefficient, hν is the energy and n is 1/2 for an indirect transition and 2 for a direct transition. From the intercept of the extrapolated linear portion, the band gap values of CIS, $CuIn_{0.75}Ga_{0.25}Se_2$, $CuIn_{0.50}Ga_{0.50}Se_2$, $CuIn_{0.25}Ga_{0.75}Se_2$ and CGS is 1.002, 1.070, 1.265, 1.421 and 1.671 eV respectively, is shown in **Fig III.9**. These values are in good agreement with experimental [108]. The optical band gap increased with increasing Ga content. Therefore, it was concluded that CIGS nanostructures are an appropriate candidate for light absorber material for thin film solar cells.

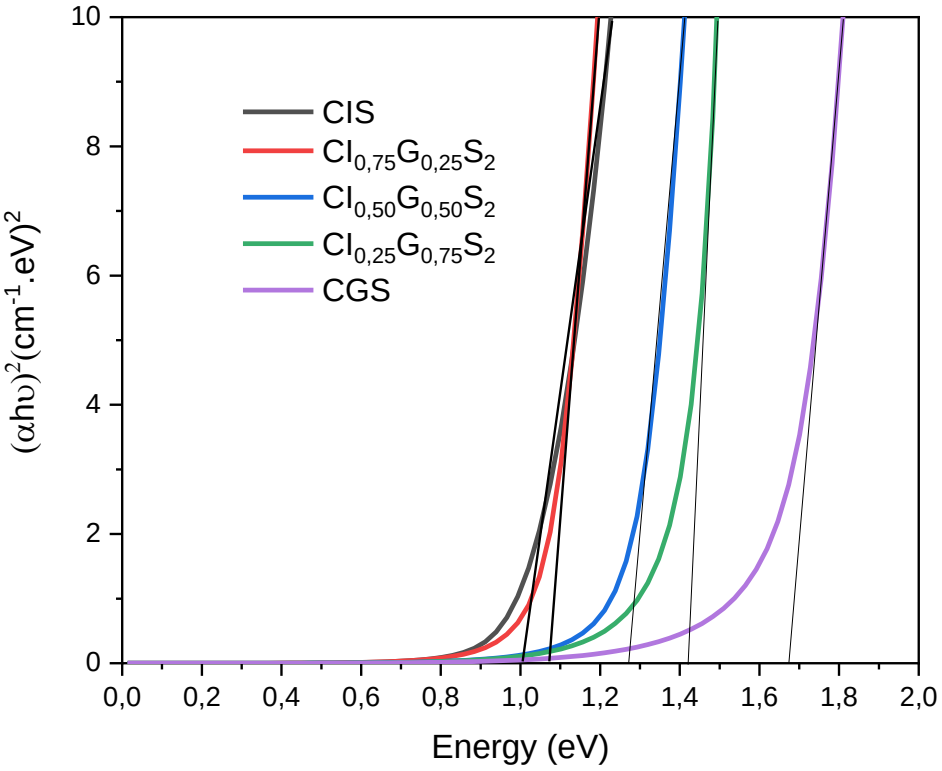

Figure III. 9: Represent the optical band gap versus photon energy.

The Seebeck coefficient and the electronic thermal conductivity were performed for the CIGS compound using BoltzTraP code [98]. The **Fig III.10**, shows the seebeck coefficient variation, all values are positive. Which means that the hole is the dominant. For CIS, it begins from 0 µV/K for 0°K and increase proportionally to the temperature, and stabilizes at 230 µV/K at 200°K, once introduction Ga, the behavior of the coefficient changes, and it starts to decrease with the increase of temperature. the maximum value is 3404 µV/K for $CuIn_{0.75}Ga_{0.25}Se_2$ at 10°K and decrease until stabilization at 243 µV/K at 298 °K, same look for $CuIn_{0.50}Ga_{0.50}Se_2$, $CuIn_{0.25}Ga_{0.75}Se_2$ and CGS, decrease up to 276 µV/K at 278 °K. For the Thermal conductivity **Fig III.11**, it increases with increasing the temperature, starting from 0(W/m s K) at 0 K to reaching 10^{14} (W/m s K) at high temperature. We can also remark that for the same temperature the value of the conductivity decreases when the percentage of Ga increases.

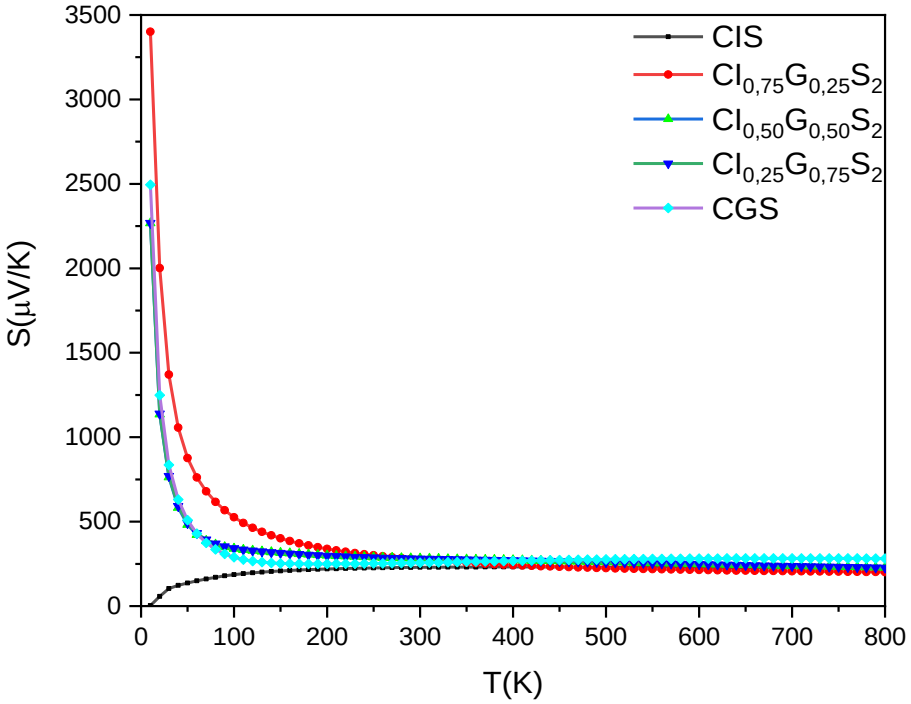

Figure III. 10: The Seebeck coefficient versus temperature.

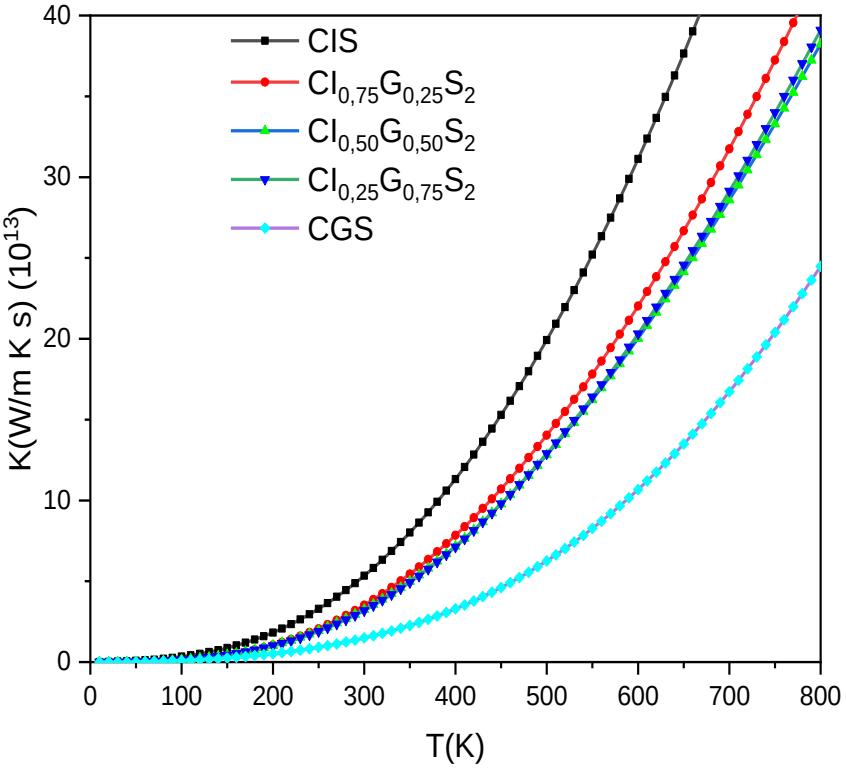

Figure III. 11: The thermal conductivity versus temperature.

III.4 Conclusion

In summary, we carried out a theoretical study using the DFT method to compare electronic and optical properties of the CIGS compound with different values of concentration (x), from CIS to CGS keeping the chalcopyrite structure. For this we used the FP-LAPW method with GGA+mBJ functional, which seems to be an apt methodology to optimize structural and optical parameters. The theoretical values of energy gaps are in good agreement to the experimental values. We find that $CuIn_{0.75}Ga_{0.25}Se_2$ is more absorbent compared to other compounds, with reflectivity and refractive index quite remarkable for a photovoltaic application. All values of the seebeck coefficient are positive, which means that the hole is the dominant. The values of the optical properties revealed that the CIGS chalcopyrite material is an interesting compound for solar cell applications. With a thermal conductivity reach the 10^{14} (W/m s K) and an optical absorption that surrounds 10^4 in visible range. The $CuIn_{0.75}Ga_{0.25}Se_2$ is more attractive and can be more productive for photovoltaic applications.

Chapter IV: Study of the electronic, optical properties and the strain effect on the perovskite KBX_3 compound with (B = Sn, Ge and X = Cl, Br, I).

IV.1 Introduction

With the growing concerns for the deficiency of the world's natural resources and global environmental pollution, it has become necessary to shift away from fossil fuel usage and invest in clean renewable energy resources [109]. In this light, scientists started to develop renewable energy technologies. Among these different renewable resources, solar energy is surely considered as one of the most promising technologies to meet future energy demands [110,111]. Over the last decades, perovskites have become one of the most promising materials for solar cells. Known for their low-cost fabrication, abundance in nature, easy manufacturing process, attractive photovoltaic, and optoelectronic properties [112,113]. The common formula for organic-inorganic hybrid halide perovskite compounds iswell known as ABX_3, where A-site and B-site are inhabited respectively by inorganic or organic cation and a divalent metal cation, while halogens are on the X-site [114-116]. The inorganic perovskite, especially the halide perovskite, have redrawn great attention as solar cell materials for their distinguished physical properties like adaptable bandgap, wide optical absorption coefficient, small effective masses, high charge carrier mobility, and long electron-hole diffusion lengths [117,119]. Nonetheless, these perovskites materials encounter many challenges such as the stability issue [120, 121]. Correspondingly, the development of stable and efficient perovskite materials has grown into an active research topic in the field of photovoltaics. So far, there are a number of theoretical publications available that investigate the potential of the halide perovskite in terms of their energy band gaps using density functional theory calculations (DFT) [122-127]. Recently, M. Kar and T. Körzdörfer [128] have replaced the organic cation in the hybrid perovskites by inorganic cations, looking for perovskite materials that proved to be suitable for application in tandem solar cells.

In this chapter, firstly we have investigated the physical properties of perovskite KBX_3 compounds (B = Sn, Ge and X = Br, Cl, I) in the cubic structure, as reflectivity, absorption coefficient and refractive index in order to study their properties using the first principles calculation through the

Generalized Gradient Approximation (GGA) executed with the Wien2k code. We take in account the spin-orbit interaction in the calculation. In this chapiter, we inspected the strain effect on the electronic evolution of $KGeI_3$ in the cubic structure applying first-principles calculations.

IV.2 Computational Methods

The calculations on the compounds are done using the full potential linearized augmented plane wave method (FP-LAPW) based on the Density Functional Theory (DFT) method used on the Wien2K code [68]. It enables us to calculate several properties including the bandgap, density of state, absorption and reflectivity of the compounds at T = 0 K. we started with the Optimization step **figure IV.1.** The atoms on the cubic halides perovskites KBX_3 with (B: Sn, Ge) and (X: Br, Cl, I) have position as follow [129], the B atoms occupy the body centered position $(\frac{1}{2};\frac{1}{2};\frac{1}{2})$ fractional coordinates, the X atoms occupy the face centered positions $(\frac{1}{2};\frac{1}{2};0)$, $(0;\frac{1}{2};\frac{1}{2})$ and $(\frac{1}{2};0;\frac{1}{2})$ respective fractional coordinates and the K atoms occupy the corner positions (0, 0, 0) fractional coordinates as shown in **Fig IV.2**. All the calculations take into account spin-orbit coupling (SOC) with a 4×4×4 k-point in the irreducible wedge of the Brillouin zone. The convergence criterion was fixed at 10^{-4} Ry. All parameters have been tested for convergence and all the calculations are done using the generalized gradient approximation (GGA) [130]. The strain has been simulated by changing the lattice parameter a, which is determined by the formula $a = a_0 (1+\varepsilon)$. In the formula, a_0 is the lattice parameter without strain, and the range of ε values varies from 1% to5%.

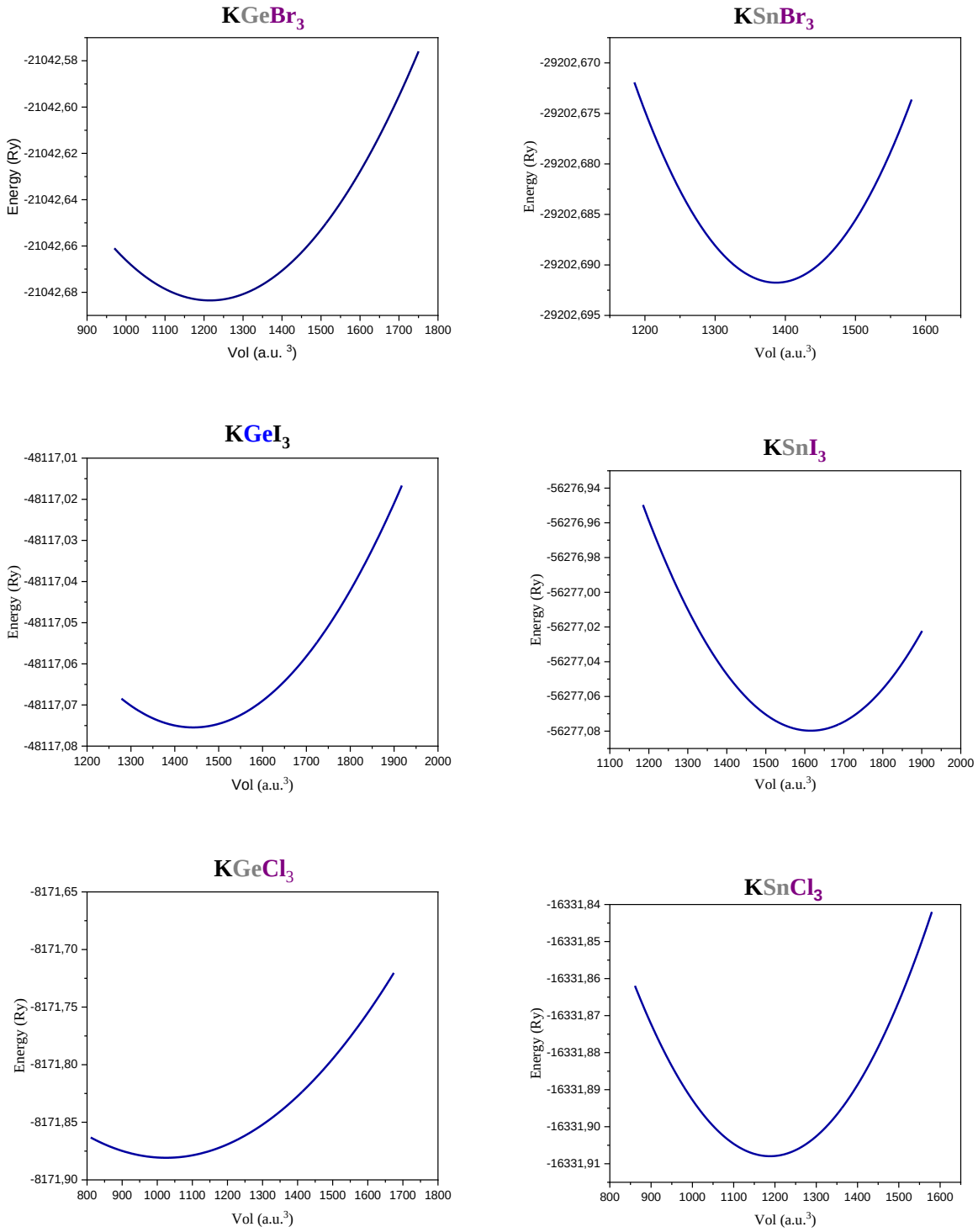

Figure IV. 1: Optimization of the cubic halide perovskites KBX_3 (B = Sn, Ge and X = Br, Cl and I).

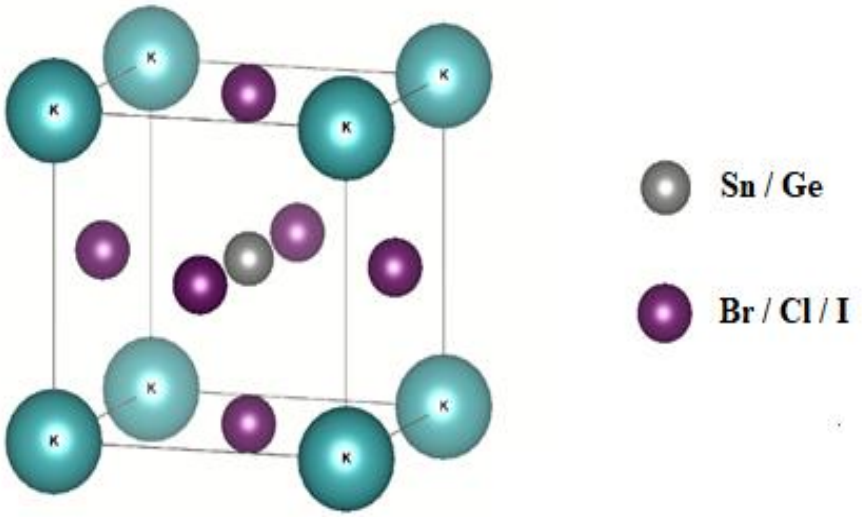

.

Figure IV. 2: Crystal structure of cubic halide perovskites KBX_3 (B = Sn, Ge and X = Br, Cl and I).

IV.3 Results and discussion

IV.3.1 KBX_3 compounds without strain effect

IV.3.1. 1 The electronic properties of the KBX_3 compound.

The electronic properties of the halide perovskites have been studied in cubic structure KBX_3 to determine the band gap energy for these compounds. The results affirm a semiconductor behavior with direct bandgap for perovskite KBX_3 compounds investigated in cubic phase. The minimum of the valence band (CBM) and the maximum of the valence band (VBM) are located at the R point as shown in **Fig IV.3**. When the B cation changes from Germanium (Ge) to Tin (Sn), the bandgap increases. But, when the halogen X changes from Chlorine (Cl) to Iodine(I), we notice a decrease in the bandgap. Band Gap energy values are listed in **Table IV. 1**. The width of the bandgap variation from 0.502eVto 1.067eV gives us a high level of tenability and it makes the compounds promising candidates for photovoltaic devices.

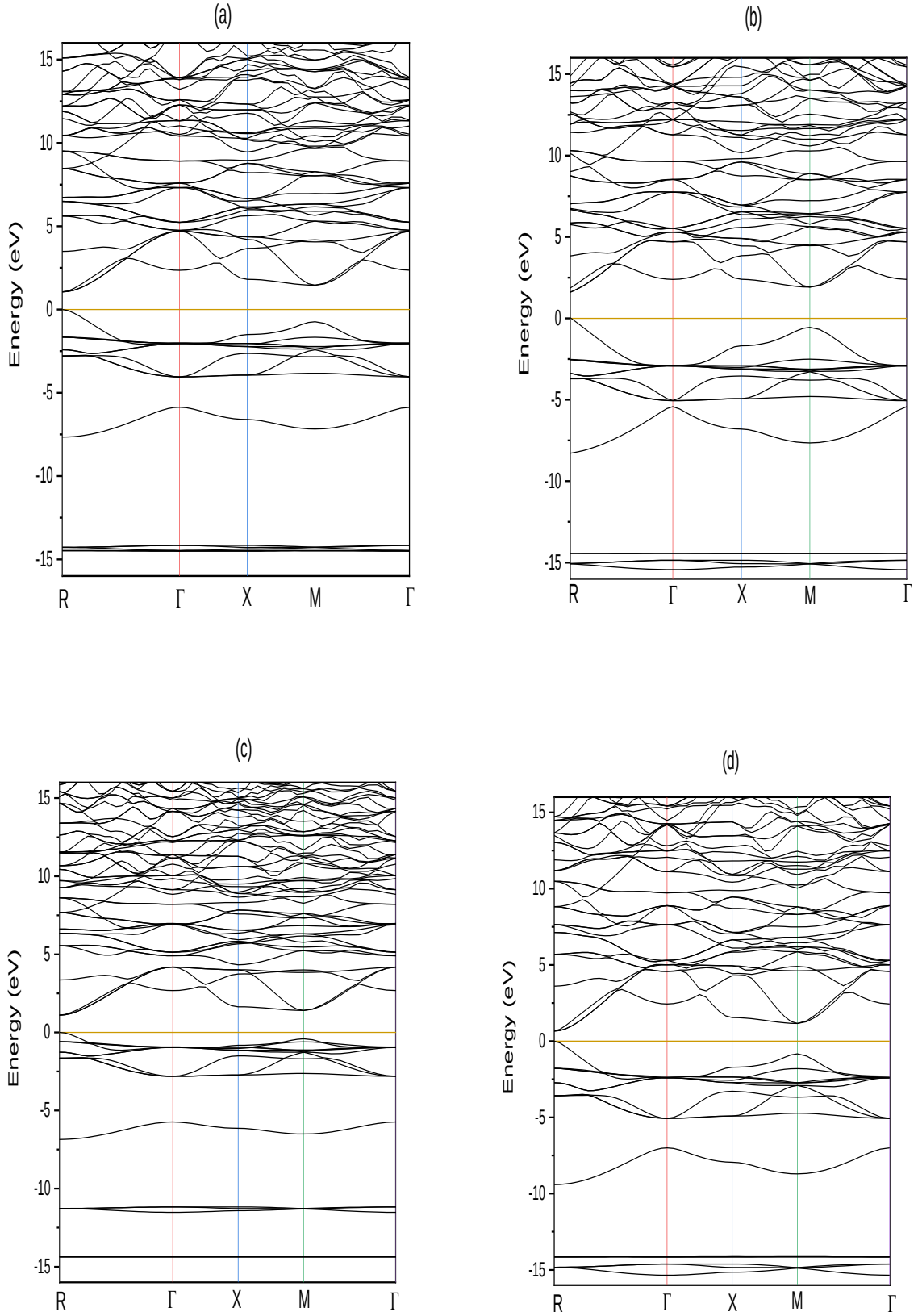
(a)
(b)
(c)
(d)
Energy (eV)
15
10
5
0
-5
-10
-15
R
Γ
X
M
Γ

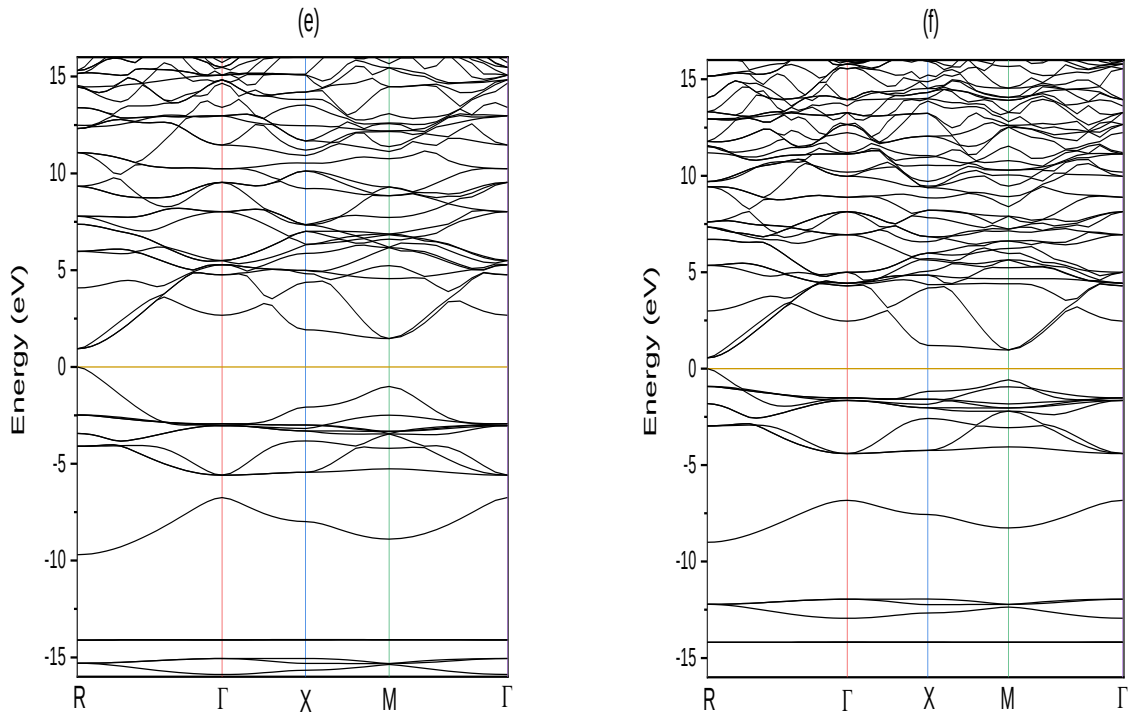

Figure IV. 3: Band structure of perovskite KBX_3 compound: (a) $KSnBr_3$, (b) $KSnCl_3$, (c) $KSnI_3$, (d) $KGeBr_3$, (e) $KGeCl_3$and (f) $KGeI_3$.

Table IV. 1: Optimized lattice parameters a (Å) and band gap values for perovskite KBX_3 compounds (B = Sn and Ge; X = Br, Cl and I).

	a (Å)		**Eg (eV)**		
	Present work	**Other works**	**Present work**		**Other works**
			Calculation without Spin-Orbit	**Calculation with Spin-Orbit**	
$KSnCl_3$	5.59	---	1.629	1.550	---
$KSnBr_3$	6.08	---	1.177	1.070	---
$KSnI_3$	6.73	---	1.134	1.130	---
$KGeCl_3$	5.29	5.27[129]	0.958	0.950	0.90 [129]
$KGeBr_3$	5.57	5.55 [129]	0.689	0.670	0.61 [129]
$KGeI_3$	5.96	5.81[130] 5.94 [123]	0.502	0.500	0.26[130] 0.53 [123]

To know the atom resolved contribution to the density of states (DOS) and the bonding nature for these compounds. The total and partial densities of states were calculated using the GGA

approximation for KBX_3 halide perovskites (B = Sn and Ge; X = Br, Cl and I) compounds and plotted in the **Figs IV.4-9**. It shows that the density of states of $KSnX_3$ has three distinct regions. The first region is located between -8 eV and -6 eV formed by s-states of tin atom and halogen atom Cl, Br and I respectively. Above this region, the valence band is mainly dominated by p-state on each halide with a light presence of p-state of the tin atom. However, the conduction band is formed by p-Sn and each halide. For these compounds, we see that there is hybridization between p-Sn and p-X (X = Br, Cl and I) which confirms the covalent nature of their chemical bond. For the $KGeX_3$, the conduction band is formed by the p-Ge and each halide, while the valence band is influenced by the p-state of halides. It's practically the same reasoning for Sn compounds since there is hybridization between p-Ge and p-X (X = Br, Cl and I).

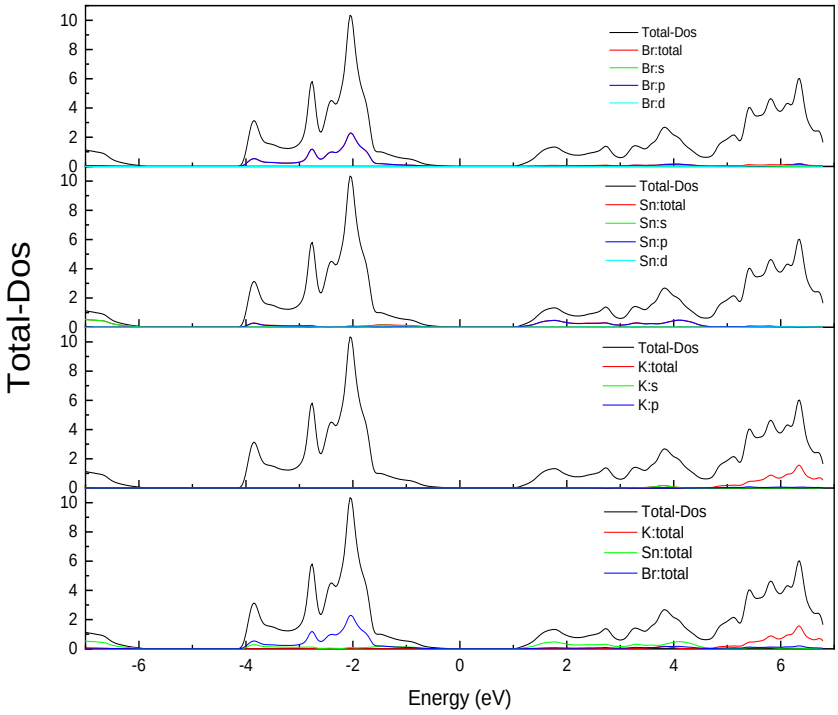

Figure IV. 4: Total and partial densities of states for perovskite $KSnBr_3$ compound.

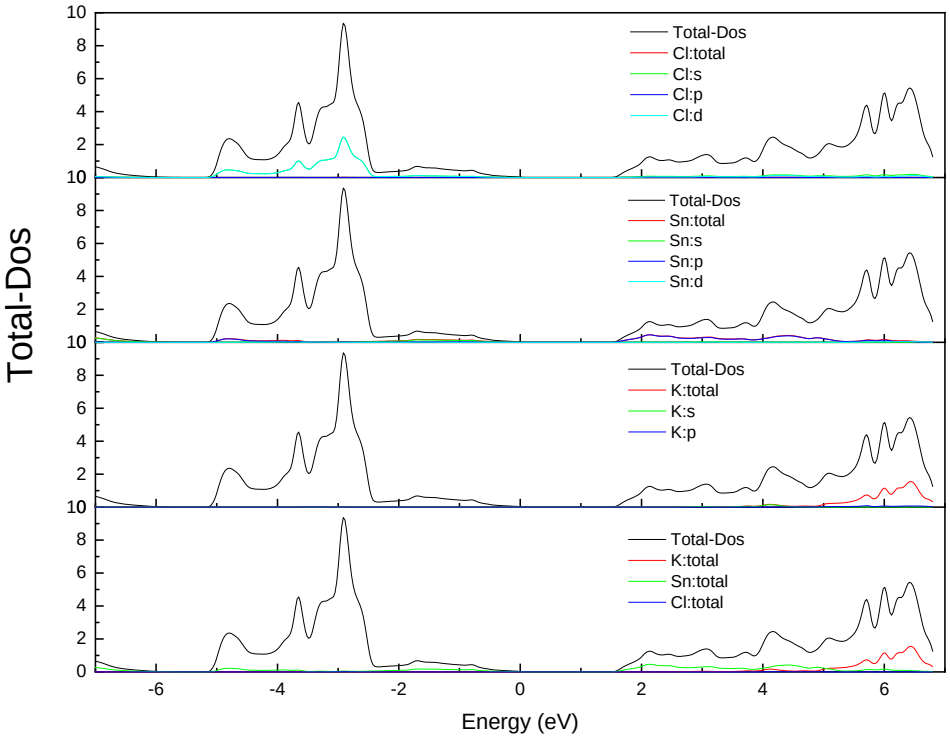

Figure IV. 5: Total and partial densities of states for perovskite $KSnCl_3$ compound.

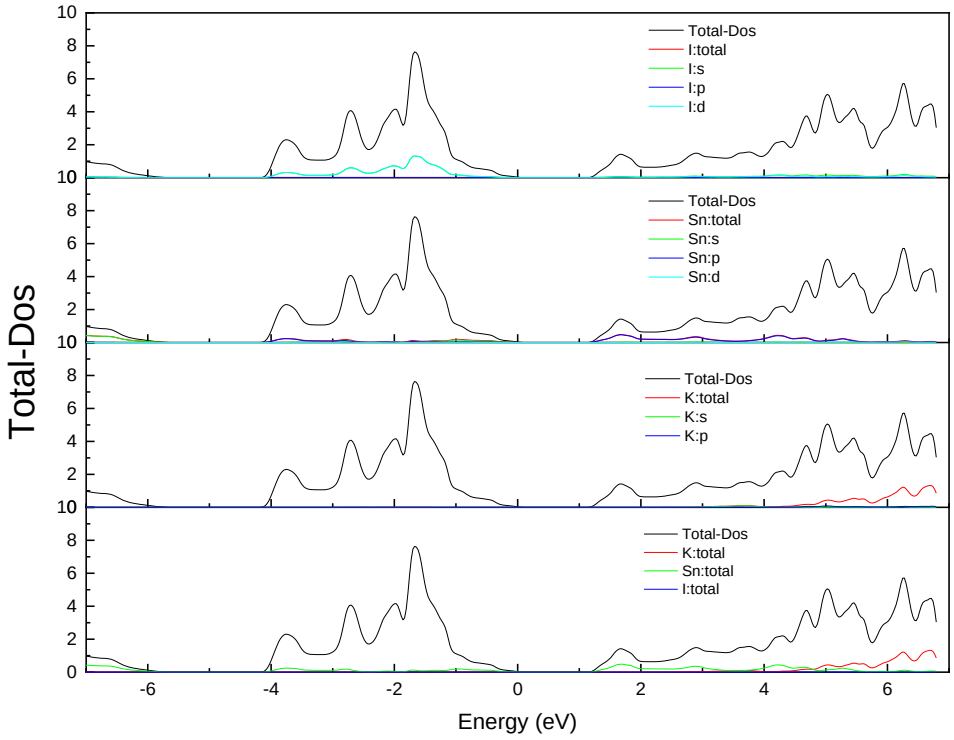

Figure IV. 6: Total and partial densities of states for perovskite $KSnI_3$ compound.

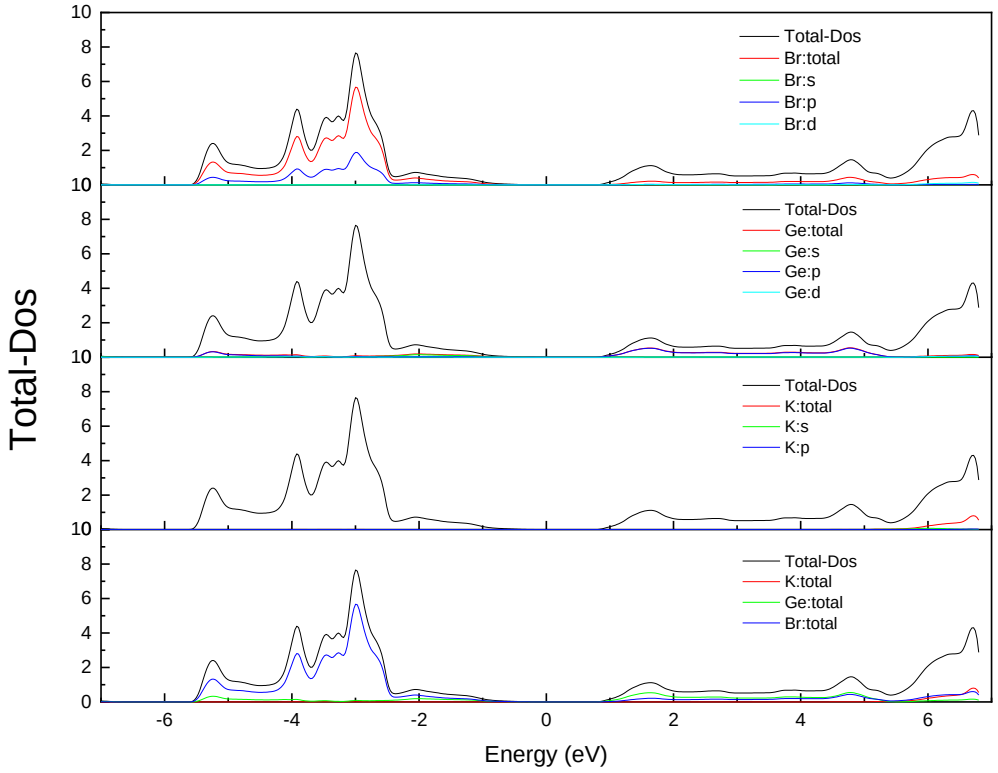

Figure IV. 7: Total and partial densities of states for perovskite $KGeBr_3$ compound.

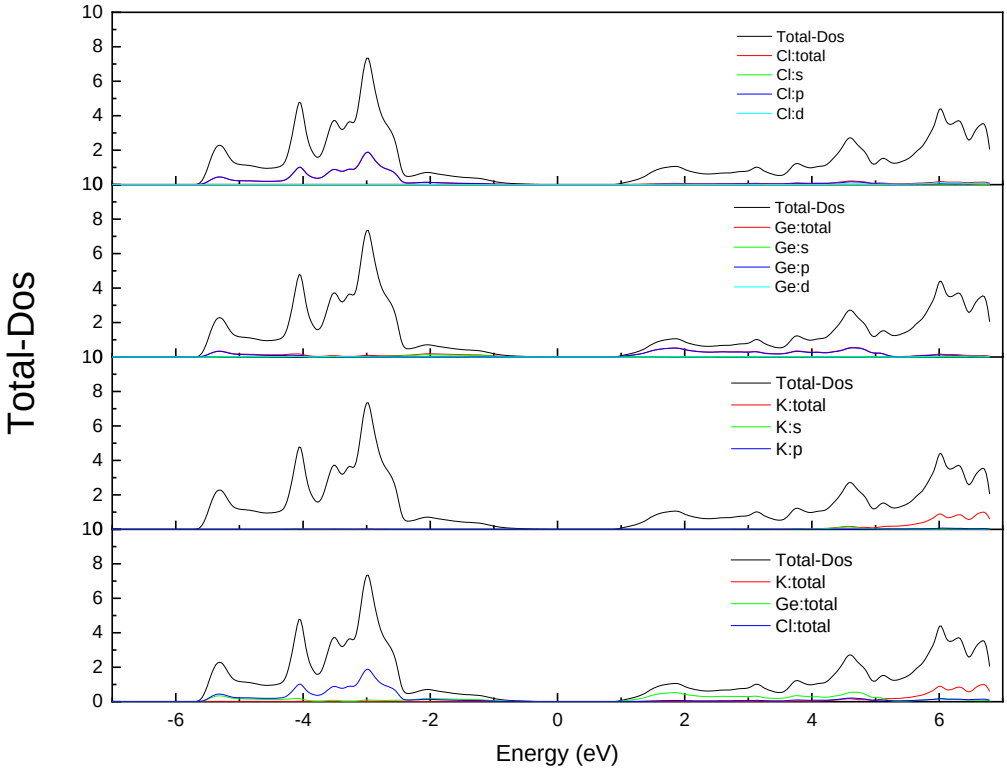

Figure IV. 8: Total and partial densities of states for perovskite $KGeCl_3$ compound.

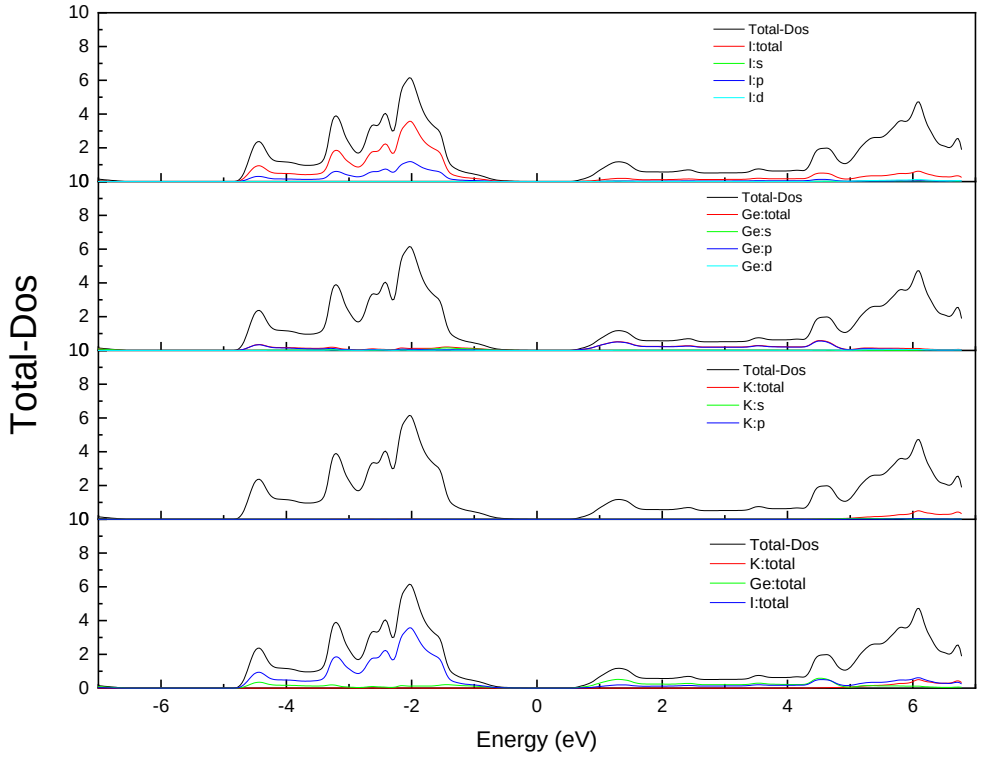

Figure IV. 9: Total and partial densities of states for perovskite $KGeI_3$ compound.

IV.3.1. 2 The Optical properties of the KBX_3 compound.

Looking for the behavior of the light-exposed material and its interaction with it, the optical properties such the reflectance R(ω), refractive index n(ω) and absorption coefficient α(ω) are calculated for KBX_3 halide perovskites (B = Sn and Ge; X = Br, Cl and I) which can be extracted by using the following relations [131,132]:

$$\alpha(\omega) = \sqrt{2}\omega\left[\sqrt{\varepsilon_1^2(\omega) + \varepsilon_2^2(\omega)} - \varepsilon_1(\omega)\right]^{1/2} \quad (4.1)$$

$$R(\omega) = \left|\frac{\sqrt{\varepsilon(\omega)}-1}{\sqrt{\varepsilon(\omega)}+1}\right|^2 \quad (4.2)$$

where $\varepsilon(\omega) = \varepsilon_1(\omega) + i\varepsilon_2(\omega)$

$$n(\omega) = \frac{1}{\sqrt{2}}\left[\sqrt{\varepsilon_1^2(\omega) + \varepsilon_2^2(\omega)} + \varepsilon_1(\omega)\right]^{1/2} \quad (4.3)$$

where, $\varepsilon_1(\omega)$ and $\varepsilon_2(\omega)$ are real and imaginary parts of the dielectric function.

The absorption coefficient for perovskite KBX_3 compounds were plotted as a function of wavelength as shown in **Fig IV.10.** Changing the B cation from Sn to Ge, the shape of the curve is the same but the value of the absorption coefficient increases when it comes to Ge. Considering the visible range is around 380 nm, the Cl halogen compounds present the lowest value compared to the Br, but changing to Iodine, it shows peaks for both compounds with Sn and Ge atoms. The value reached the 5×10^5 and 5.6×10^5 at 430 nm for the KSnI3 and $KGeI_3$ compounds respectively. After that, the absorption decreases with the increase of the wavelength. The iodine compounds also show very important results also for the reflectivity R(ω) illustrated in **Fig IV.11** with a peak of 0.4 at 516 nm and an average of 3.4 in the visible range. For the $KSnI_3$, the reflectivity decreases from 0.34 at 460 nm to 0.25 at 800 nm which is a good value. However, the $KSnCl_3$ has the lowest coefficient of reflectivity because the peak doesn't exceed 0.2 as well as $KGeCl_3$ and $KSnBr_3$. And nowadays, the reflected part can be used to increase the performance of cells. The **Fig IV.12** represents the refractivity index, in the range between 300 and 900 nm, for KBX_3 with (B = Sn and Ge; X = Br, Cl and I) whenλ < 500 nm the $KSnI_3$ and $KGeI_3$ have an index of 1.1 and 1.3 respectively, when λ > 500 nm it increased up till 3 $KSnI_3$ for and 3.5 for KGeI3. For $KSnBr_3$, $KGeBr_3$, $KSnCl_3$ and$KGeCl_3$ the refractivity index increases from 1.5 up to 2.5 with the increase of the wavelength.

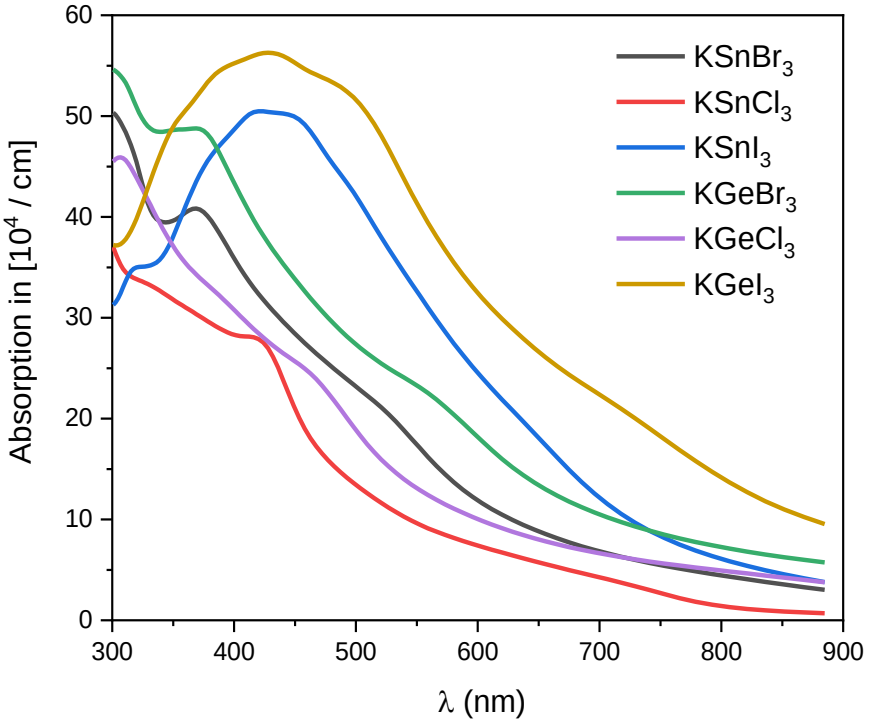

Figure IV. 10: Behavior of the optical absorption spectrums of perovskite KBX_3 compounds (B = Sn and Ge; X = Br, Cl and I) as a function of wavelength.

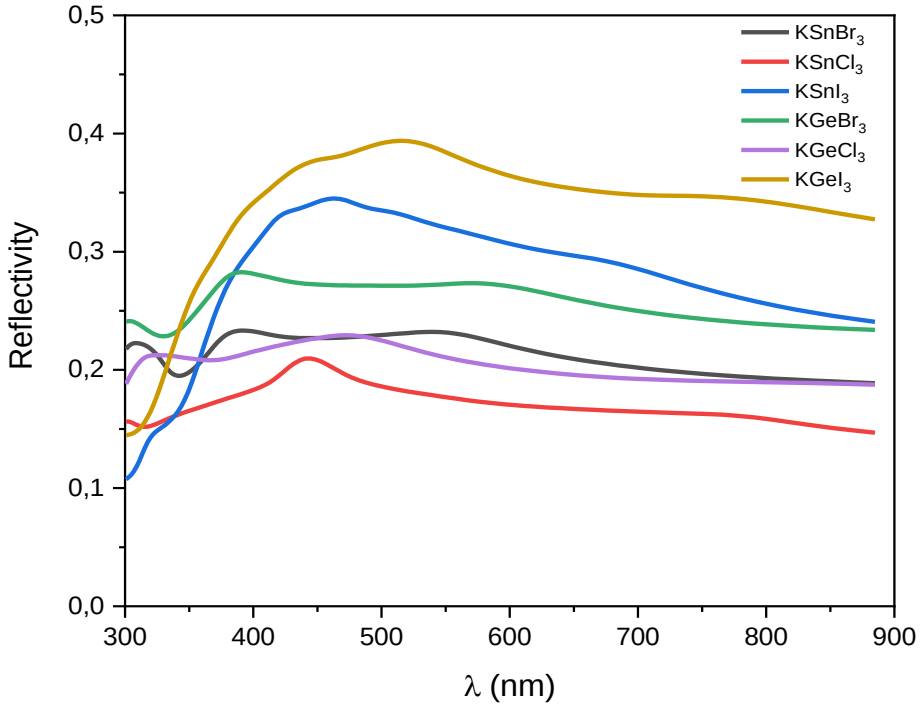

Figure IV. 11:Reflectivity spectrums of perovskite KBX_3 compounds (B = Sn and Ge; X = Br, Cl and I) as a function of wavelength.

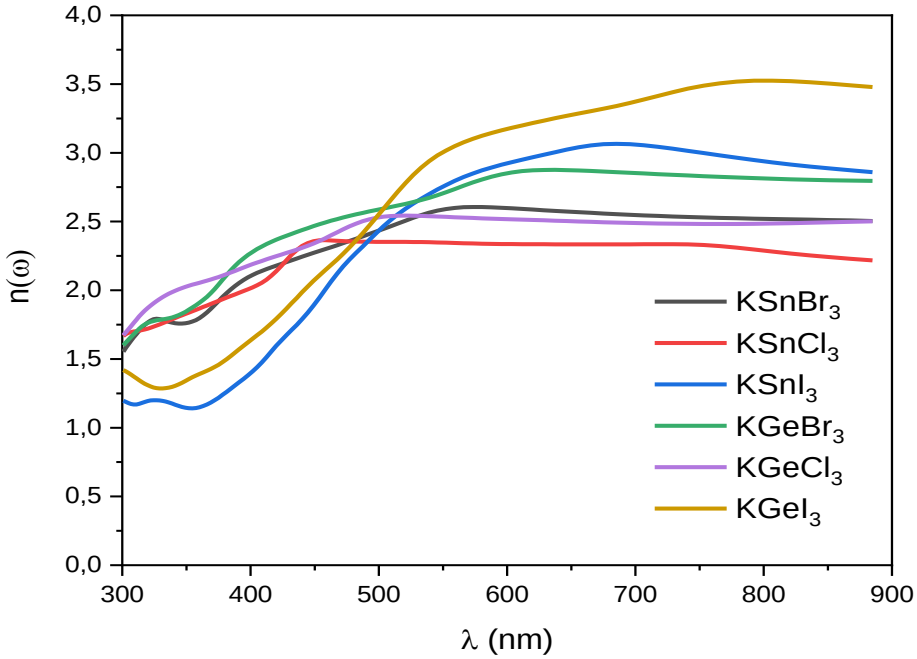

Figure IV. 12: Refractivity index of perovskite KBX_3 compounds (B = Sn and Ge; X = Br, Cl and I) as a function of wavelength.

IV.3.2 $KGeI_3$ compound with strain effect

The aim of our study is to find suitable candidates' material for the absorbent layer for solar cells. And one of the important characteristic features to look at is the absorption coefficient and the energy bandgap of the studied perovskite material. The results show two potentially interesting compounds, the$KSnI_3$ with suitable band gap with a good absorption coefficient and $KGeI_3$ which shows the highest capacity of absorption but the value of the band gap doesn't allow it to be used for PV application. That's why we targeted on the part of raising the band gap value of the $KGeI_3$ by trying different strain values from 1% to 5%. **Fig IV.13** indicates that the bandgap value is affected, and increased with increasing the percentage of strain. Fig **IV.14** shows the effect of strain on the bandgap for the compound. It is found that the valence band is practically not affected contrary to the conduction band, the minimum increase when applying the strains. $KGeI_3$ still remains a direct-bandgap semiconductor over the whole strain range. Strain effects, the structural, electronic and optical properties of the compound which were also investigated.

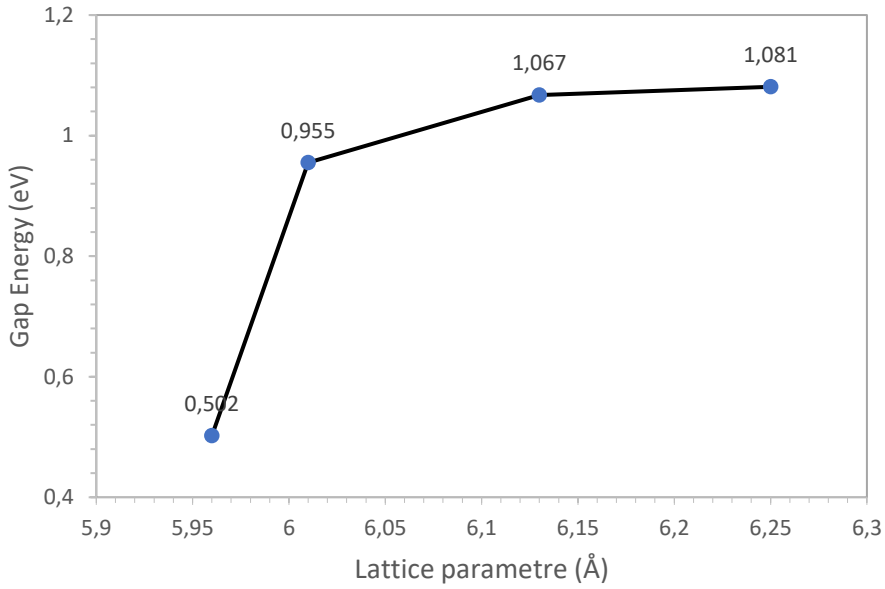

Figure IV. 13: Lattice parameters a (Å) and band gap values for $KGeI_3$ compound under strain effect.

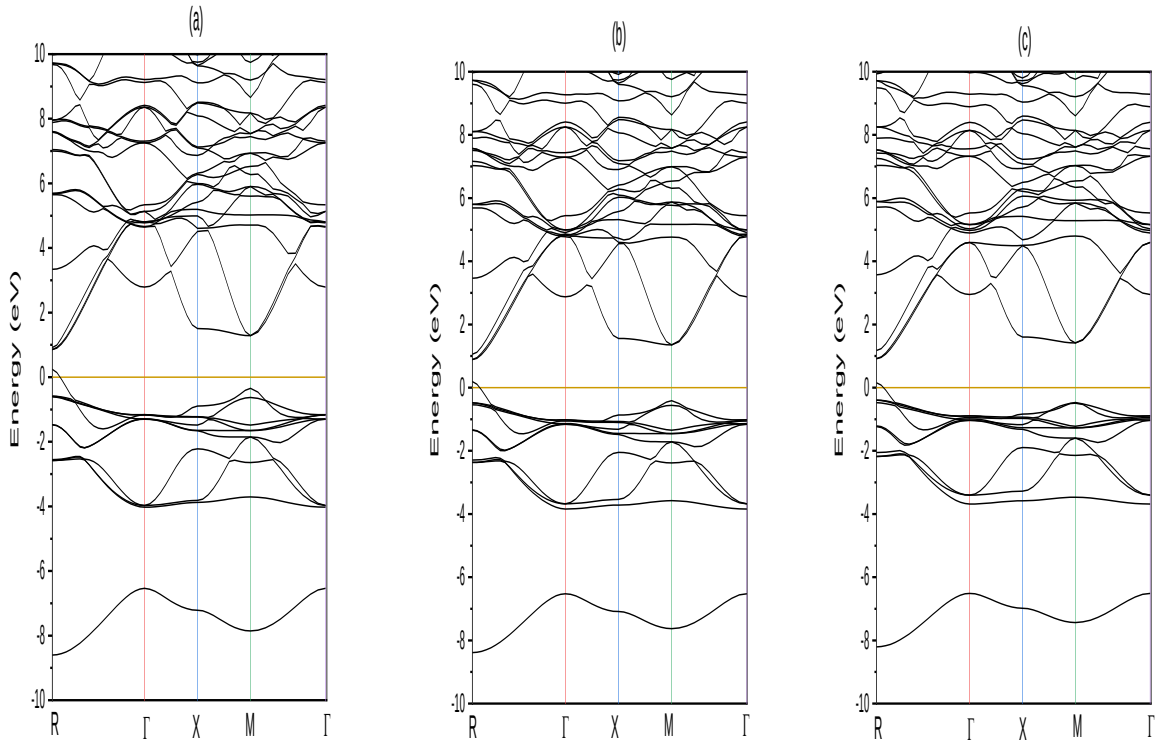

Figure IV. 14: Band structure of perovskite $KGeI_3$ compound under strain effect: (a) 1% (b) 3%and (c) 5%.

We clearly notice that when increasing the strain, the width of the bandgap increases, see **Fig IV.14.** Also, the absorption coefficient increases to reach 6×10^5 for the 3% strain. Regarding the 5% of strain, the value doesn't increase, but the thickness of the peak does, see **Fig IV.15**.

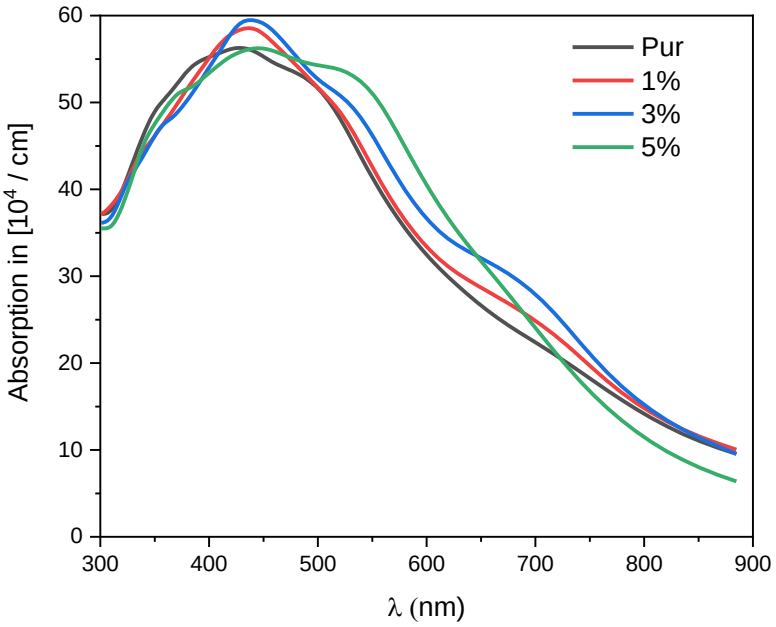

Figure IV. 15: Optical absorption spectrums of $KGeI_3$compound as a function of wavelength under strain effect.

IV.5 Conclusion

In this study, we have performed a detailed investigation on the structural, optical and electronic properties of cubic halide perovskites KBX_3compounds (B = Sn and Ge; X = Br, Cl and I) using DFT based on FP-LAPW method. The results show some good compounds with an appropriate direct band gap semiconductor, and a very interesting absorption coefficient in visible range. Moreover, by applying the strain effect on the $KGeI_3$, the gap energy increases. It is concluded that $KGeI_3$ and $KSnI_3$ perovskites are really interesting compounds. Up to now, no experimental evidence of the synthesis of Potassium based halide perovskites has been found. But it can be seen from the DFT studies done in this work, that these perovskites show very promising band gaps as well to be used in photovoltaic devices.

CHAPTER V: Study of the electronic, optical and thermal properties of the perovskite halides mixte $ABI_{3-x}Br_x$ with (A = Cs, K and B = Pb, Sn, Ge)

V.1 Introduction

In recent years, the halide perovskite has attracted great attention from the scientific community because of its high performance in a very short time frame, due to its outstanding physical properties such as: adjustable band gap, large optical absorption coefficient, small effective masses, high charge carrier mobility, and long electron-hole diffusion lengths. In addition, they have been considered to be a wonderful and practical matter for studying. The development of the mixed-halide $ABI_{3-x}Br_x$ perovskites are particularly suitable for investigating the influence of perovskite preparation on properties of perovskite solar cells (PSC). A large body of computational investigations of the mixed halide were reported, since 2013, Edoardo Mosconi and al, perform periodic DFT calculations on the mixed halide $CH_3NH_3PbI_2X$ perovskites [133]. Onetheless, Waqaas Rehman and al confirmed that the mixed halide $CsPb(Br_xI_{(1-x)})_3$ materials show significantly better resistance under heat stress and enhanced photo-stability compared to their MA+ and FA+ based counterparts [134]. Furthermore, McMeekin et al [135]. demonstrated a mixed cation $Cs_{0.17}FA_{0.83}$ Pb $(Br_{0.4}I_{0.6})_3$ perovskite with 1.74 eV bandgap that allowed for 17% PCE in a single-junction device and exhibited low disorder, long charge-carrier lifetimes and high mobilities. Due to our previous studies, the germanium-based compounds have gained our attention due to their high optical absorption. And what made us observe that the gap energy can be tuned by changing the halide composition in mixed I/ Br perovskite. That's why we were so excited to perform the gap energy tuning in AGeI3 by the substitution of the iodine atom for bromine. Here we examine a wide parameter space in the mixed-halide perovskite $ABI_{3-x}Br_x$, in general our investigation highlights the electronic structure, optical, and thermoelectric properties. These thesis calculations are based on the full-potential linearized augmented plane wave. In this chapter, we discuss the result found while studying the halide compounds.

V.2. Computational Methods

The calculations are performed using the full-potential linearized augmented plane wave method (FP-LAPW) based on density functional theory (DFT) as implemented in the Wien2k code [68]. This method allows us to calculate the optical and electronic properties, band gaps, and densities of states, counting the absorption coefficient, and the reflectivity of our compounds at T= 0.0 K. In the cubic halide perovskite $ABI_{3-x}Br_x$ (x = 0; 1; 2; 3), the A atoms occupy the corner positions (0, 0, 0) fractional coordinates, the B atoms occupy the body-centered position $(\frac{1}{2};\frac{1}{2};\frac{1}{2})$ fractional coordinates, and the I and Br atoms occupy the face-centered positions $(\frac{1}{2};\frac{1}{2};0)$, $(0;\frac{1}{2};\frac{1}{2})$ and $(\frac{1}{2};0;\frac{1}{2})$ respective fractional coordinates. We started by the optimization step showed in the **figure V.1.** The generalized gradient approximation (GGA) [136] and the modified Becke-Johnson with Generalized Gradient Approximation (GGA+mBJ) [137] are used for exchange and correlation calculations. We fixed the convergence criterion at 10^{-4} Ry and the convergence force to 1 mRy/a.u. We also use the Boltzmann theory embedded in BoltzTraP code [98] to calculate the thermoelectric properties as the Seebeck coefficient, the electrical, and the thermal conductivity.

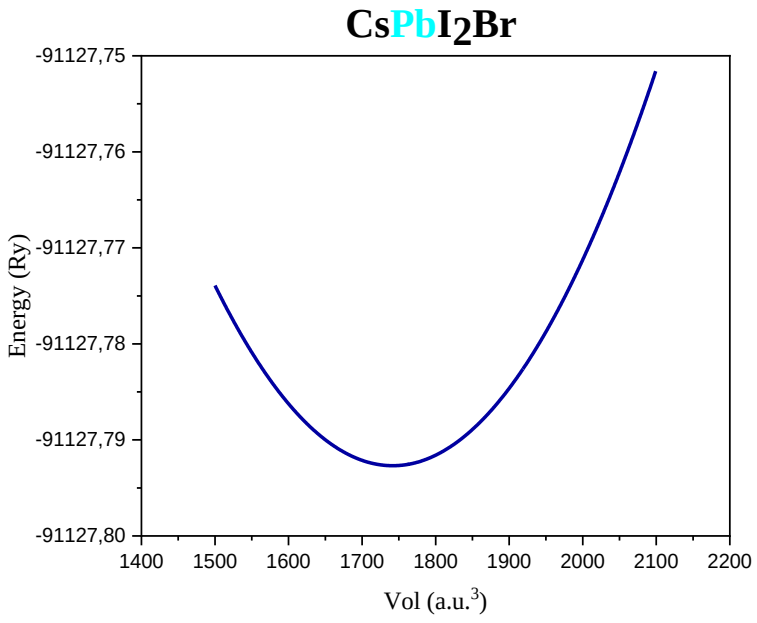

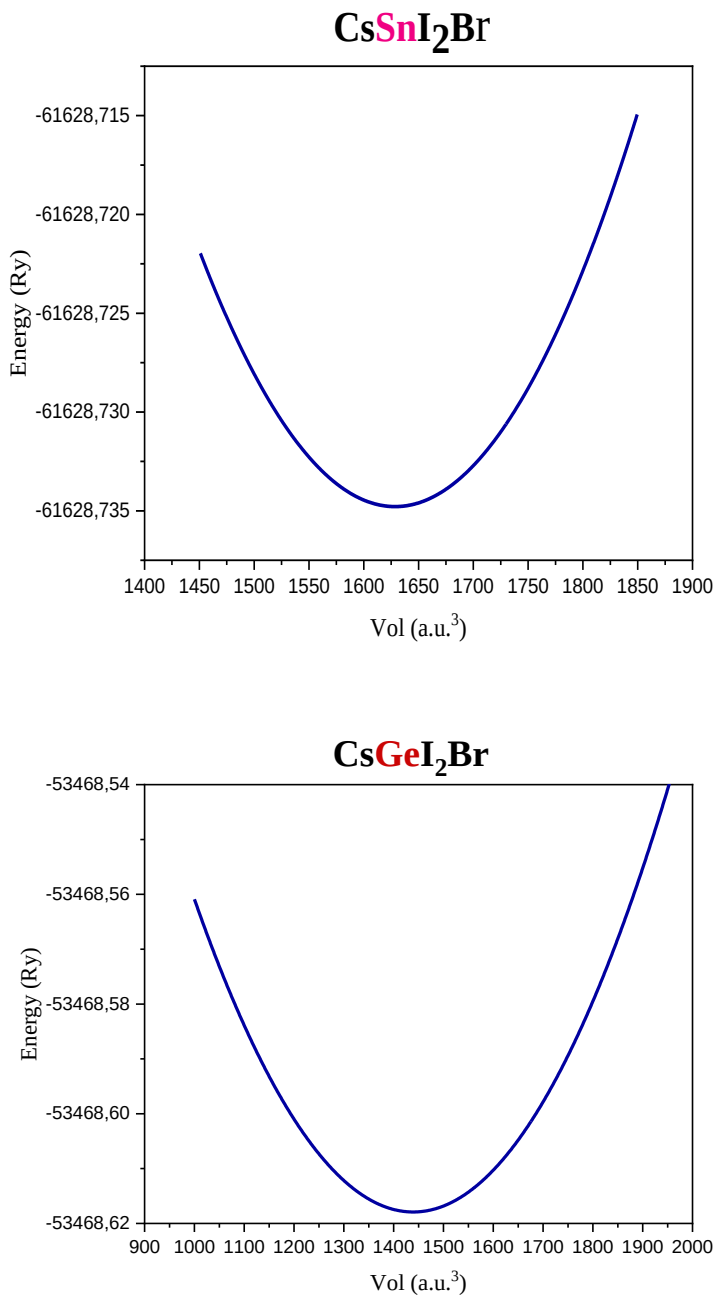

Figure V. 1: Optimization of the of CsBI2Br compounds as a function of volume.

V.3 Results and discussion

V.3.1 $CsBI_2Br$ Compound.

In this part, we methodically investigated the electronic and optical properties of $CsBI_2Br$ (B = Pb, Ge, Sn) in the cubic structure applying first-principles calculations, through Generalized Gradient Approximation (GGA), in order to compare, upgrade, predict, and complete other studies announced on $CsBI_2Br$ (B = Pb, Sn, Ge) compounds for optoelectronics applications. The

calculated results have shown that both electronic and optical properties have been affected by the change of the metal ion. The effect on the bandgap is considerable when we replace the Lead with Germanium or Tin. We found out 1.913 eV for $CsPbI_2Br$, 1.358 for $CsGeI_2Br$ and 1.192 eV for $CsSnI_2Br$, the three values are adjustable bandgap for PV applications. Moreover, the optical results, notably the absorption, show a peak for each compound that goes up to 10^5 in the visible range, yet, the $CsGeI_2Br$ presents the highest absorption which allows it to be more productive, hence better performance than Lead and Tin for PV panels.

V.3.1.1 Electronic properties

As result, the compounds are presenting a semiconducting behavior with a direct band gap, the **Fig. V.2** represents the total and partial densities of states of $CsBI_2Br$ (B = Sn, Ge, Pb) compounds using GGA approximation. We can distinguish between three different regions; for $CsPbI_2Br$ the first region is located between -7.63 eV and -6.58 eV dominated by Pb. Above this region, there is another one between -3.27 eV and Fermi level dominated by Br and I. Finally, for the conductive region which starts at 1.912 eV, that means it's an element with a good band gap energy, which is firstly leaded by the Pb, and exceeding 4.5; we have a dominance of Cs. For $CsGeI_2Br$ and $CsSnI_2Br$ it's practically the same reasoning; we just replace the domination of Pb by Ge or Sn. There is also a change in the value of the band gap because by replacing Pb with Ge, we find a gap of 1.358 eV and a gap of 1.192eV in case we replace it with Sn. **Table V.1** shows the obtained results in band and optical gap compared with some other theoretical and experimental studies; we can clearly say that the three compounds are good candidates for solar cell's application because they fit into the range of photovoltaic.

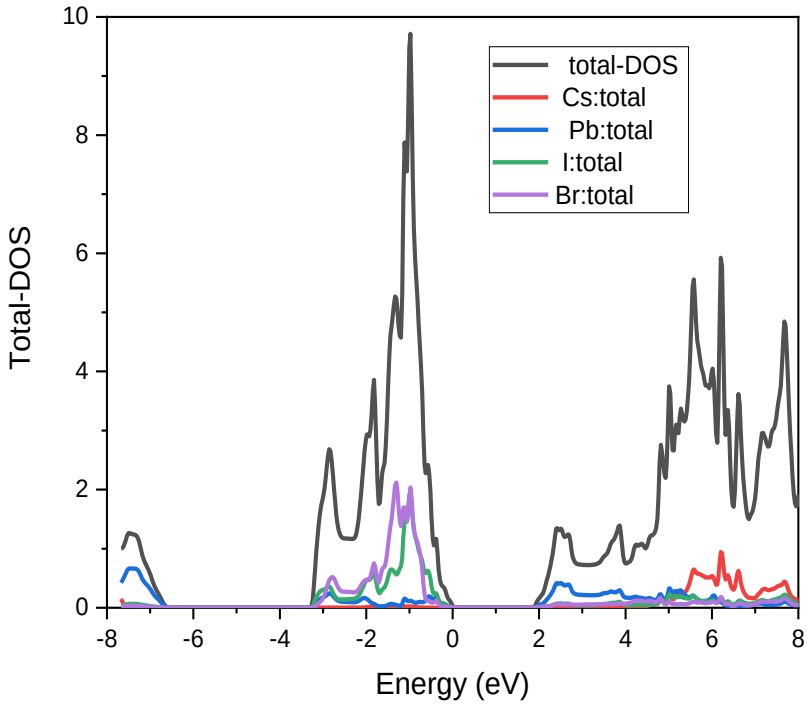
total-DOS
Cs:total
Pb:total
I:total
Br:total
Total-DOS
Energy (eV)
10
8
6
4
2
0
-8
-6
-4
-2
0
2
4
6
8

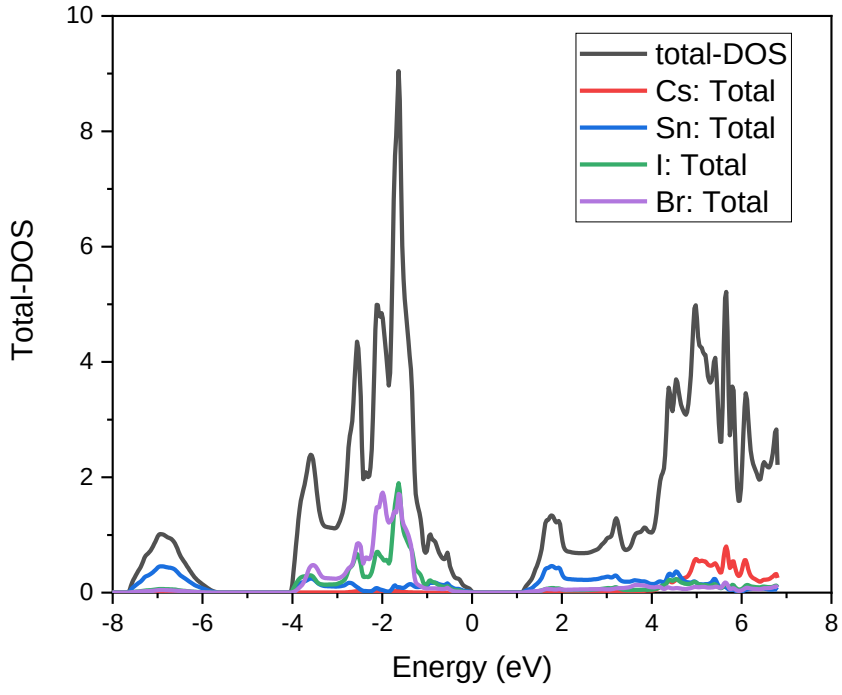
total-DOS
Cs: Total
Sn: Total
I: Total
Br: Total
Total-DOS
Energy (eV)
10
8
6
4
2
0
-8
-6
-4
-2
0
2
4
6
8

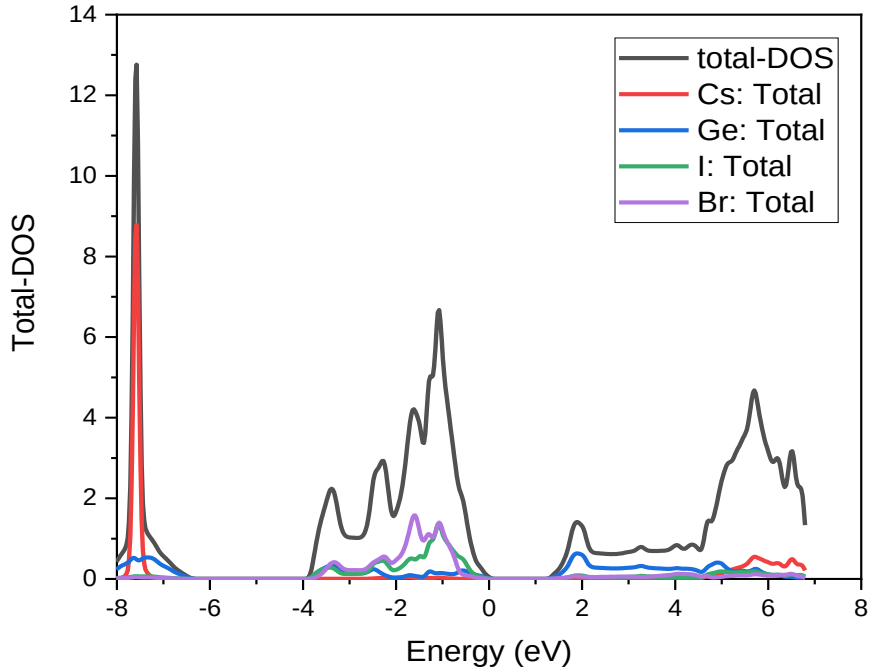

Figure V. 2 : Total and partial density of states of $CsBI_2Br$ compounds as a function of incident photon energies: (a) CsPbI2Br, (b) CsSnI2Br and (c) CsGeI2Br.

Table V. 1: Band and optical gap for $CsPbI_2Br$, $CsGeI_2Br$ and $CsSnI_2Br$.

Compounds	Present work				Other theoretical work	Experimental studies
	Gap energy (eV) with GGA	Gap energy (eV) with GGA + mBJ	Gap energy (eV) with GGA-HSE	Gap energy (eV) with GGA + HSE and SOC		
$CsPbI_2Br$	1.39	1.85	1.74	1.41	-	1.92 [138]
$CsGeI_2Br$	0.99	1.18	0.99	0.44	1.58 [139]	-
$CsSnI_2Br$	0.37	1.07	0.52	0.31	0.75 [140]	1.37 [141]

V.3.1.2 Optical properties

Reflectivity R(ω), refractive index n(ω) and absorption spectra α(ω) are investigated for our considered compounds in a range between 350 and 800 nm. The **Fig. V.3** represents the optical absorption spectrum which is the penetration of light at specific wavelength into the material before it gets absorbed which is very fundamental to determine the solar energy conversion efficiency of a material for solar cell application. The absorption spectra present two main peaks in visible range. We can also notice the replacement of Pb by Ge or Sn affects the spectra, and the position of the peak shifts from 375 nm to 425 nm for $CsSnI_2Br$, and to 460 nm for $CsGeI_2Br$. In addition to that, the studied compounds show high absorption capacity in the visible range, and it is something that we are looking for in solar cell application. A maximum absorption is observed with Ge based compounds compared to Sn and Pb based counterparts. Therefore, $CsGeI_2Br$ would be a better applicant and successor to $CsPbI_2Br$ for application in solar cells.

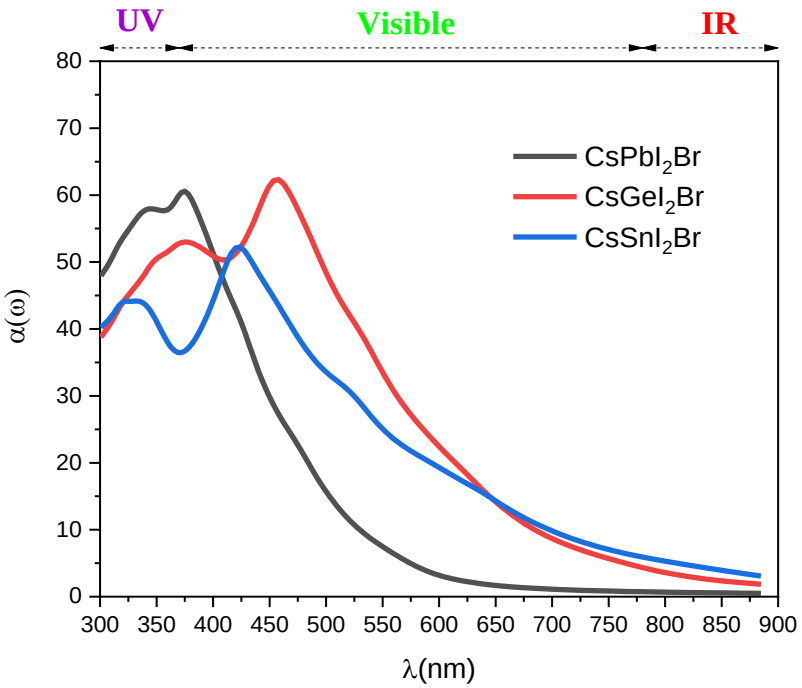

Figure V. 3: The behavior of optical absorption spectrums of the $CsBI_2Br$ (B = Pb, Sn, Ge) compounds as a function of wavelength.

Among the important properties for photovoltaic application, we found reflectivity and the capacity of reflection of a sample surface to the incident radiation flux.

Fig.V.4 shows the reflectivity of the compounds in the visible region of the spectra, we can note that the $CsPbI_2Br$ has a peak of reflectivity at 378 nm not exceeding 0.34 and for $\lambda > 378$ the reflectivity decreases. For $CsSnI_2Br$, we have a very low coefficient of reflectivity that increases between 370 nm and 425 nm to reach 0.33 and decreases, however, it remains above the $CsPbI_2Br$ one. Furthermore, CsGeI2Br has the highest reflectivity up to 0.42 at 457 nm, and it decreases as the wavelength increases. Anyhow, it's still a very low coefficient compared to its high absorption. And nowadays, the reflected part may also be collected to increase the performance of panels. The **Fig.V.5** represents the refractivity index, in the range between 350 and 800 nm, for $CsPbI_2Br$ it clearly noted a coefficient increasing till 3.09 after the peak, the curve starts decreasing, for $CsGeI_2Br$ it is started with very low refractivity index less than 1.5, after it increased up to 3.5 at 640 nm. For $CsSnI_2Br$, it started increasing from 400 nm until it reached 2.8. As we can see, for $\lambda < 500$ nm $CsPbI_2Br$ has the highest refractivity index, $CsGeI_2Br$ takes the lead for $\lambda > 500$ nm.

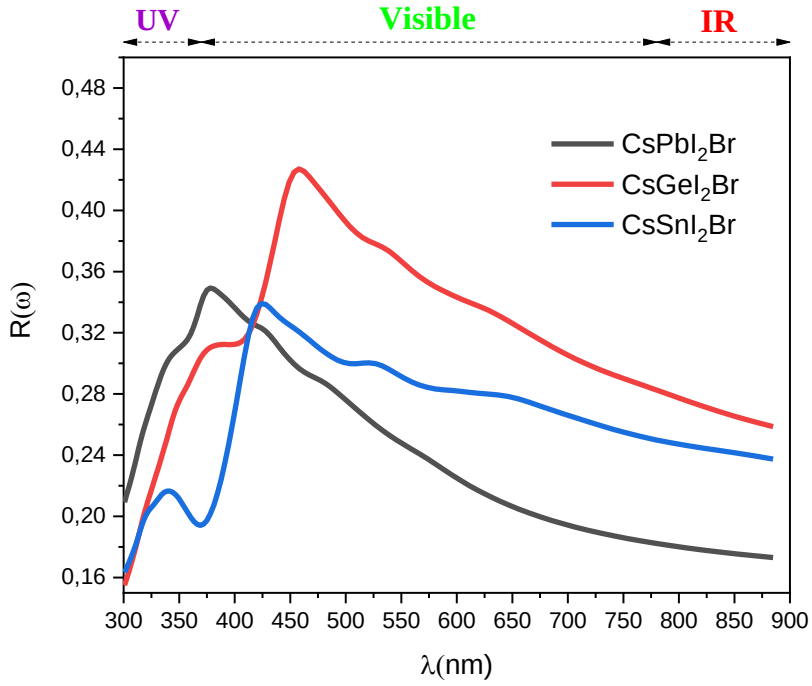

Figure V. 4: Reflectivity of the $CsBI_2Br$ (B = Pb, Sn, Ge) as a function of wavelength.

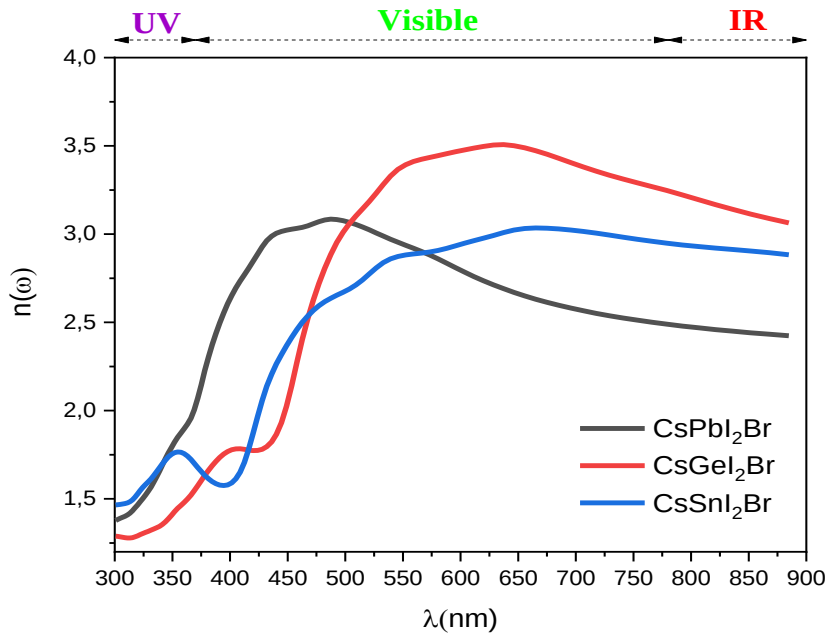

Figure V. 5: Refractivity index of the $CsBI_2Br$ (B = Pb, Sn, Ge) as a function of wavelength.

V.3.1.3 Thermoelectrical properties

The Seebeck coefficient and the thermal conductivity were performed for the $CsBI_2Br$ (B = Pb, Sn, Ge) compound using BoltzTraP code [141]. The **Fig.V.6 (a)** shows the Seebeck coefficient variation as a function of temperature in kelvin (°K), for the three compounds it begins from 0 µV/K for 0°K, and it decreases, for $CsPbI_2Br$, it decreases to -200 µV/K at 5°k and it increases with the increase of temperature, for $CsSnI_2Br$ it decreases up till -1200 µV/K at 4.3°K and like the previous compound it starts increasing up to positive values. One replacing Pb by Ge, we can note a slight decrease, and for T >33°K it begins increasing. For T > 120°K the value of the Seebeck coefficient is positive for all compounds and it has the same appearance and the same value. For the Thermal conductivity **Fig.V.5 (b)** it increases with increasing the temperature, starting from 0(W/m s K) at 0°K, to reach the 10^{14} (W/m s K) at higher temperatures for $CsPbI_2Br$, $CsGeI_2Br$ and $CsSnI_2Br$. So we can note that the replacing of the Pb by Sn and Ge does not affect their thermal conductivity, but it clearly affects their Seebeck coefficient.

(a)

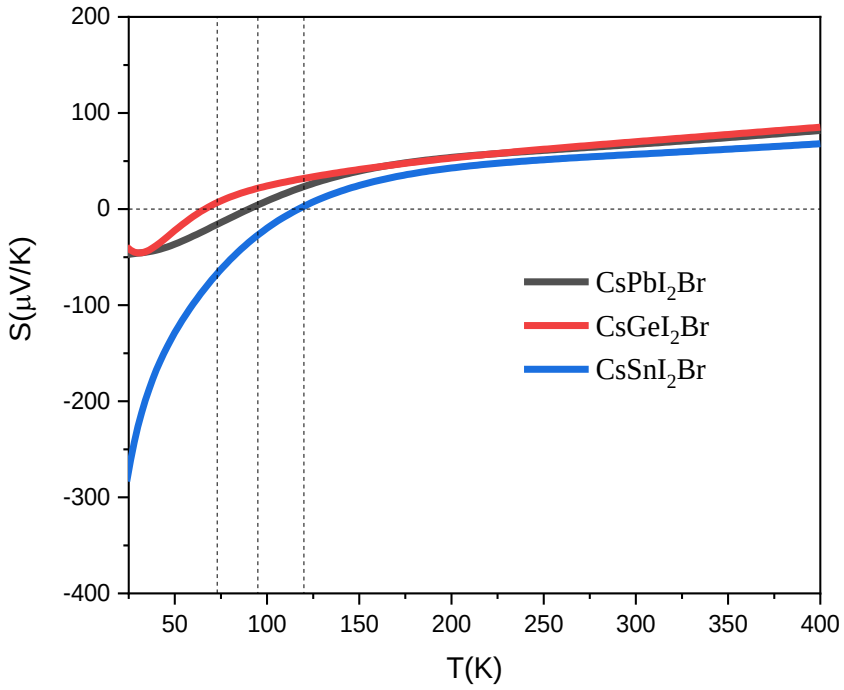

(b)

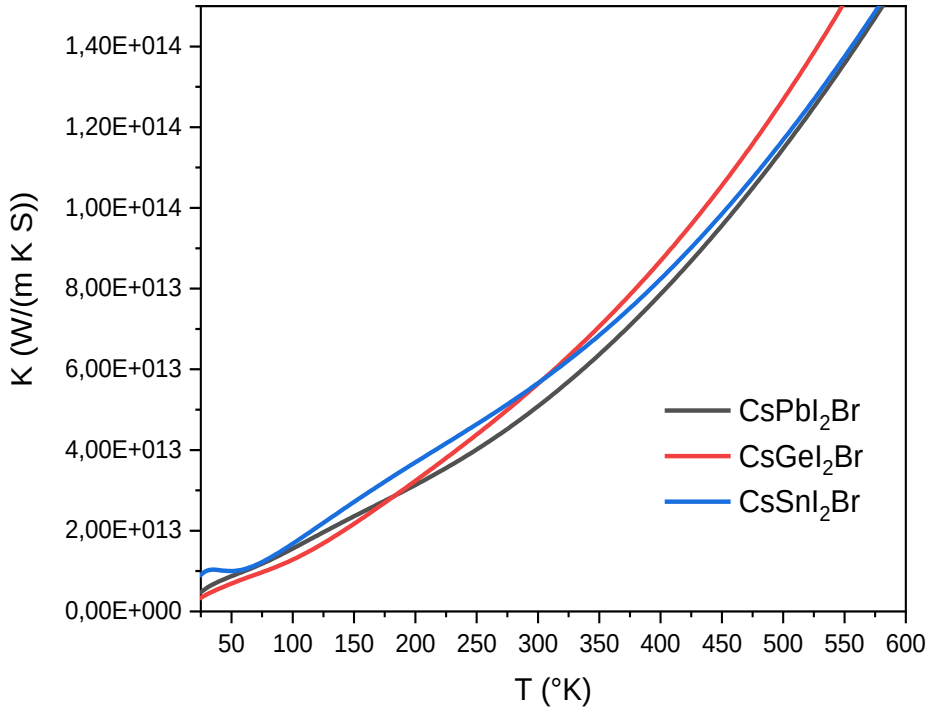

Figure V. 6: (a) Seebeck coefficient and (b) The thermal conductivity of the $CsBI_2Br$ (B = Pb, Sn, Ge) as a function of temperature

V.3.2 $KGeI_{3-x}Br_x$ ($KGeI_2Br$, $KGeIBr_2$)

Due to our previous studies, the germanium-based compounds have gained our attention due to their high optical absorption. And what made us observe that the gap energy can be tuned by changing the halide composition in mixed I/Br perovskite. That's why we were so excited to perform the gap energy tuning in $KGeI_3$ by the substitution of the iodine atom for bromine. In this work, we investigate the electronic structure, optical, and thermoelectric properties of $KGeI_{3-x}Br_x$ (x = 1; 2) compounds that are not yet studied theoretically or experimentally. Calculations on the properties were achieved adopting the full potential Linearized augmented plane wave (FP-LAPW) method in the framework of density functional theory with GGA and the modified Becke–Johnson (mBJ) approximations to define the electronic and optical properties to look for new and useful properties for different applications.

V.3.2.1 Electronic properties

The electronic structure of the perovskite $KGeI_2Br$ and $KGeIBr_2$ compound are analyzed by computing the band gap and the total density of states (T-DOS) at normal pressure, and the plots are depicted in **Fig.V.7** The compounds are direct band gaps with a clear semiconducting behavior, see **Fig V.8** We can notice the maximum of the valence band (VB) and the minimum of the conduction band (CB) are located at the same point with a value of 0.894 eV and 1.126 eV for the $KGeI_2Br$, $KGeIBr_2$, compounds respectively as mentioned in **Table V.2**.

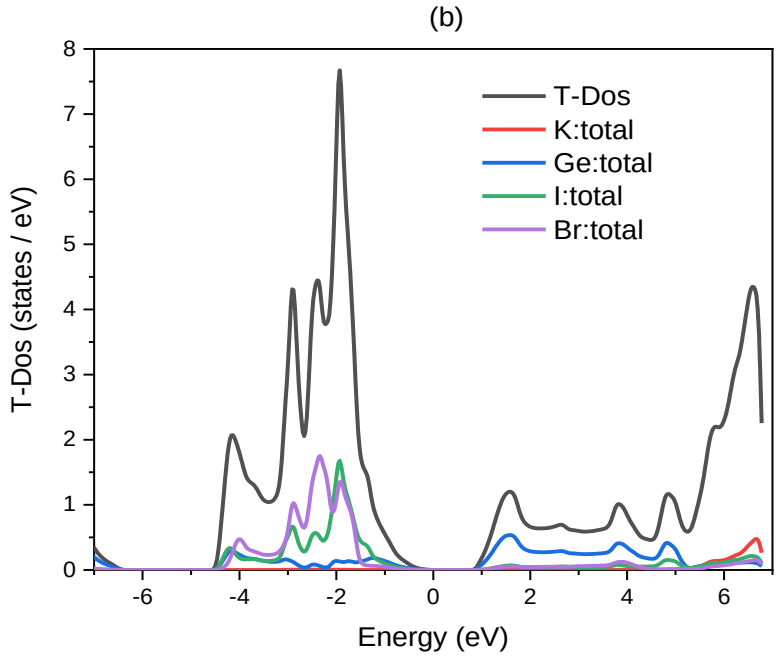

Figure V. 7: Total densities of states of the (a) $KGeI_2Br$ and (b) $KGeIBr_2$ as a function of the incident photon energies.

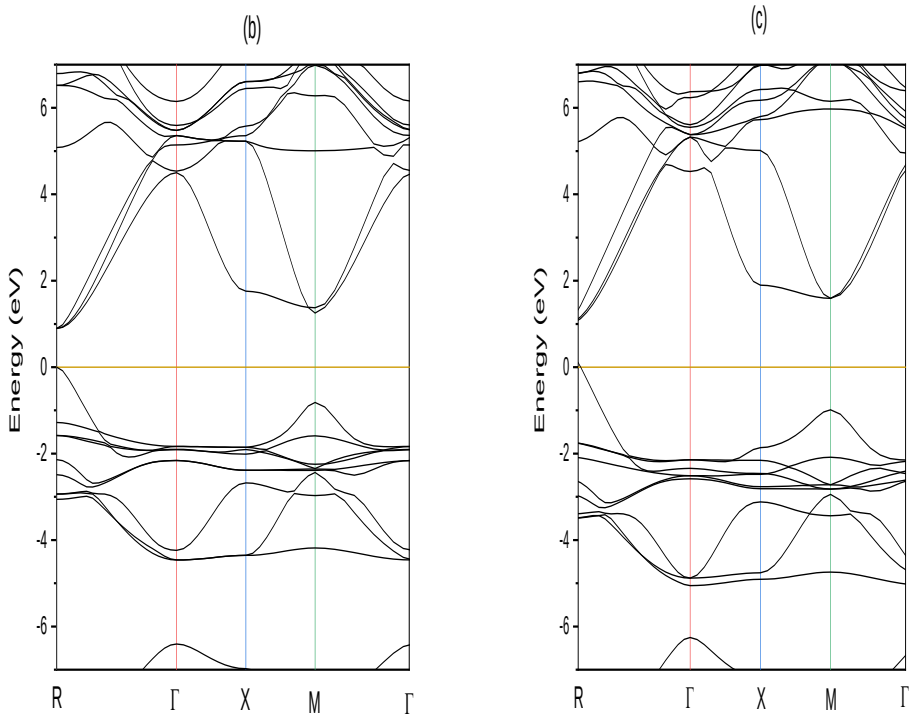

Figure V. 8: Band-gaps of the: (b) $KGeI_2Br$, (c) $KGeIBr_2$ compounds.

Table V. 2: Bandgap values of the $KGeI_{3-x}Br_x$ (x = 0; 1; 2; 3) compounds.

Compounds	a(Å)	Eg (eV)		
		GGA	GGA+mBJ	GGA+mBJ with SO
$KGeI_2Br$	5.82	0.685	0.894	0.777
$KGeIBr_2$	5.70	0.983	1.126	1.075

V.3.2.2 Optical properties

The optical properties of the $KGeI_{3-x}Br_x$ compounds are studied by figuring out the complex dielectric function. The imaginary part illustrates the absorptive behavior and the real part of the dielectric function $\varepsilon_r(\omega)$, can be obtained from the imaginary part. The absorption spectra $\alpha(\omega)$ of $KGeI_2Br$ and $KGeIBr_2$ are plotted against wavelength in the range of 300-900 nm in **Fig V.9** The optical absorption spectrums have as definition, the penetration of light at a specific wavelength into the material before it gets absorbed. Determining the solar energy conversion efficiency of material for solar cell application is very fundamental. The spectra show two peaks, we noticed that the substitution of iodine atom to bromine atom allows the increase of the absorption peak value, it goes from 54×10^4/cm at 428 nm for $KGeI_2Br$, 67×10^4/cm at 447 nm for $KGeIBr_2$. We notice high absorption capacity in the visible range for the examined compounds and it is something that we are looking for in solar cell applications. The highest absorption value is clearly shown by the $KGeIBr_2$ compound compared to others. Therefore, $KGeIBr_2$ would be a better applicant for solar cell applications.

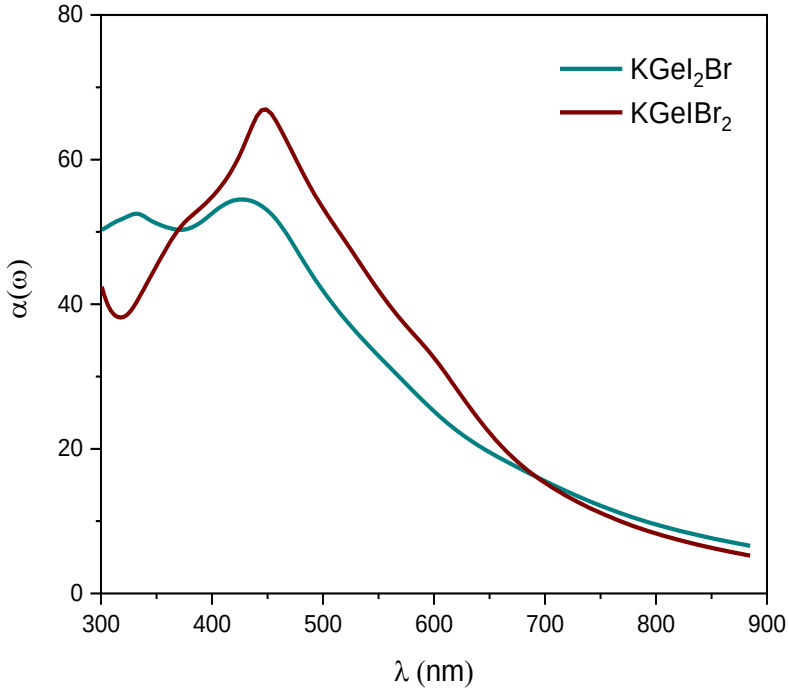

Figure V. 9: Absorption spectrums of the $KGeI_2Br$ and $KGeIBr_2$ compounds as a function of the wavelength.

Among the relevant properties for photovoltaic application, reflectivity is the capacity of reflecting a sample surface to the incident radiation flux. **Fig.V.9** shows the reflectivity of the compounds in the visible region of the spectra. We clearly see that the reflectivity of the $KGeI_2Br$ has a value of 0.29 at 320 nm and suddenly decreases to 0.17. The $KGeIBr_2$ have an average value of 0.19 which is a low value which is great for the PV application.

Fig V.11 represents the refractivity index, in the range between 300 and 900 nm calculated by the expression (3). Clearly, it distinguishes the increase of the refractive index for the compounds, crossing on the value 2.4. For $\lambda > 450\ nm$, we find a value of 2.39 and 2.44, for $KGeI_2Br$ and $KGeIBr_2$, compounds, respectively.

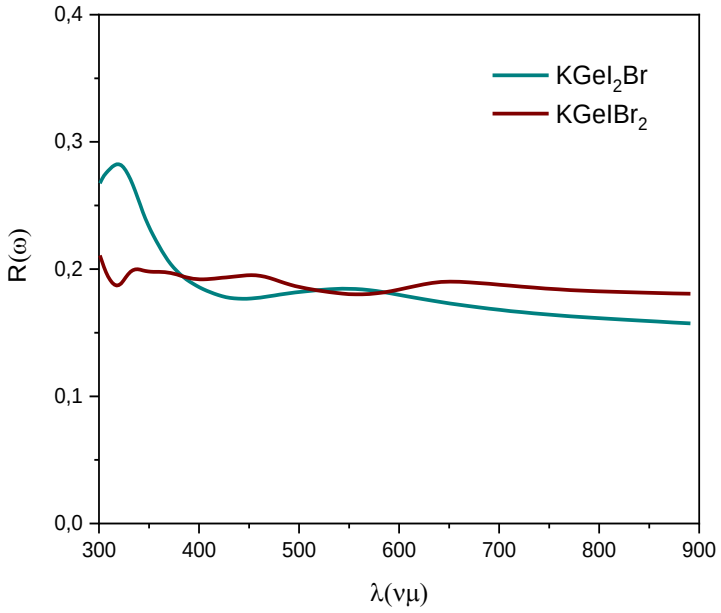

Figure V. 10: Reflectivity behavior of the $KeI_{3-x}Br_x$ (x = 1; 2) as a function of the wavelength.

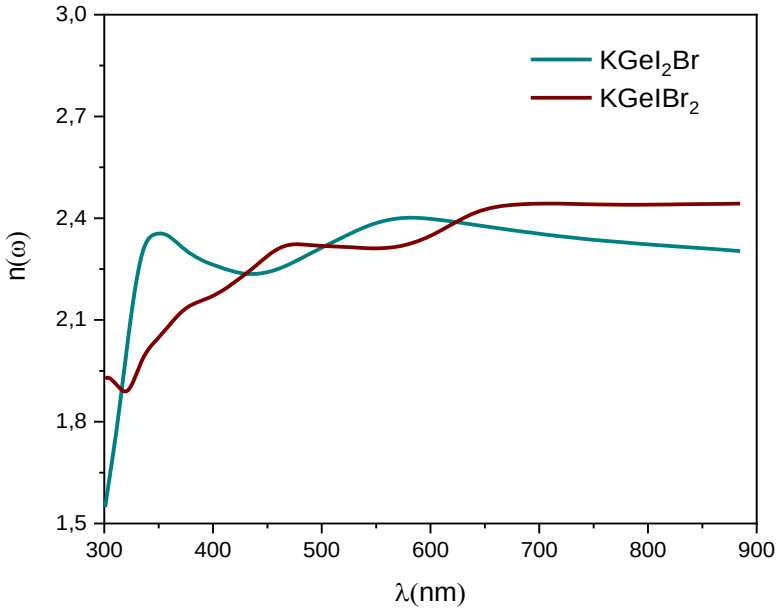

Figure V. 11: Refractivity index of the $KGeI_{3-x}Br_x$ (x = 1; 2) as a function of the wavelength.

V.3.2.3 Formation energy

The calculation of the formation energy for $KGeI_{3-x}Br_x$ (x = 1; 2) compounds gives an idea of the stability phase and the possibility of synthesizing the compounds under investigation. The formation energy is given by the expression (5.1) [24], where x, y, and z are the numbers of the atoms K, Ge and, X in the unit cell, respectively. $E_{total}^{KGeX3}, E_{solid}^{K}, E_{solid}^{Ge}$ and, E_{solid}^{X} are the calculated total energies of $KGeX_3$ compounds, K, Ge, and X, respectively. We find -2.431 and -2.552 for $KGeI_2Br$ and $KGeIBr_2$ respectively. The energy values are negatives. This implies that these phases are energetically favorable, and chemically stable structures and most likely to be synthesis experimentally. Also, the Goldschmidt tolerance factor (t) of all compounds is around ~0.86 ; this confirmed that the compounds are stable.

$$E_{form}^{KGeX3} = \frac{1}{x+y+z}\left[E_{total}^{KGeX3} - \left(xE_{solid}^{K} + yE_{solid}^{Ge} + zE_{solid}^{X}\right)\right] \qquad (5.1)$$

V.3.2.4 Thermoelectric properties

To calculate the thermoelectric properties as the Seebeck coefficient, the electrical and the thermal conductivity using the Boltzmann theory embedded in BoltzTraP code. **Fig V.12 (a)** shows the Seebeck coefficient variation as a function in temperature. This coefficient allows us to know if we have an abomination of charge carrier, if the results show a negative sign; it represents n-type material, so if its positive sign means that it's a p-type material. According to our results, for the compounds, it's clearly positive. Concluding that, these compounds are p-type materials.

Figs. V.12 (b) and **(c)** represent the electrical conductivity (σ) and thermal conductivity (k_0) of the $KGeI_2Br$ and $KGeIBr_2$ respectively. We see an increase in both electrical (σ) and thermal conductivity (k_0) by increasing temperature to reach $10^{17}$and 10^{12}, respectively. The thermal conductivity depends on the molecular vibrations of the free electrons. So, we can say that the molecular vibration increases in our compounds with the increase of temperature.

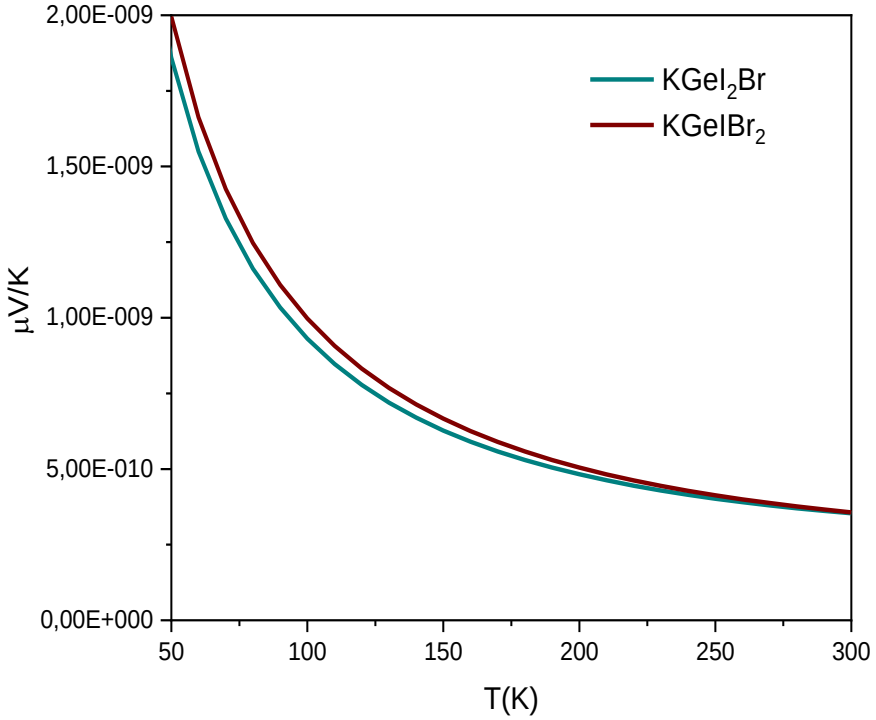
2,00E-009
1,50E-009
1,00E-009
5,00E-010
0,00E+000
µV/K
50
100
150
200
250
300
T(K)
KGeI2Br
KGeIBr2

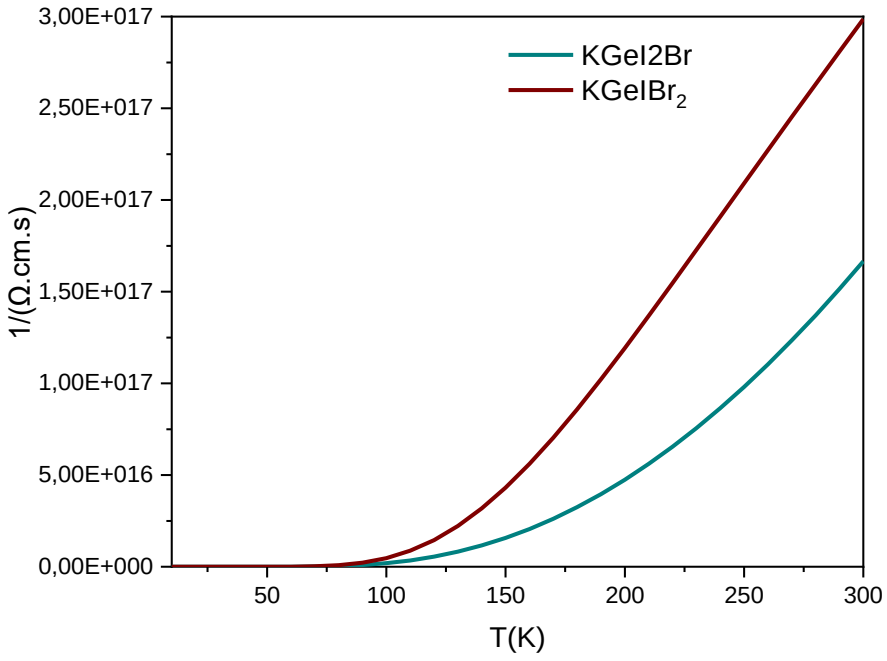
3,00E+017
2,50E+017
2,00E+017
1,50E+017
1,00E+017
5,00E+016
0,00E+000
1/(Ω.cm.s)
50
100
150
200
250
300
T(K)
KGeI2Br
KGeIBr2

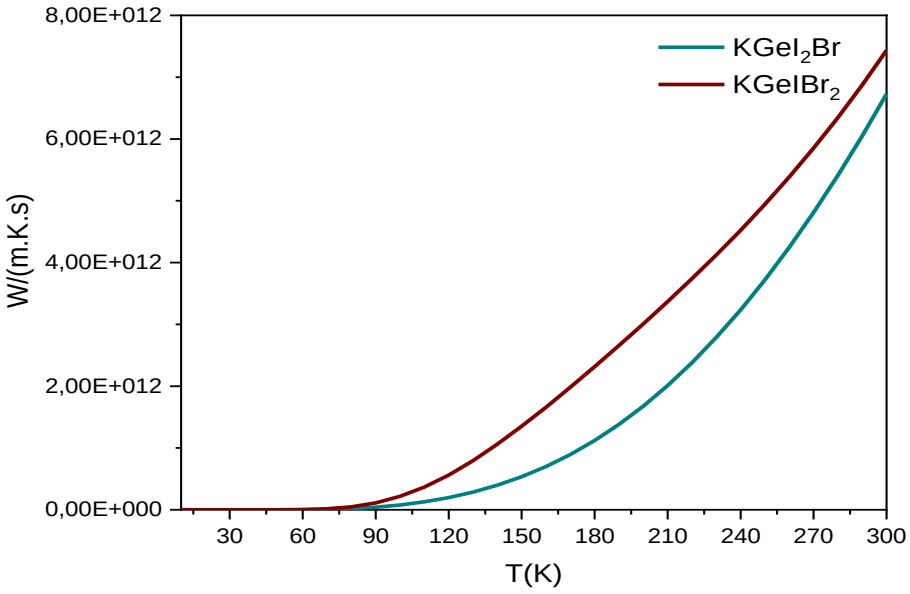

Figure V. 12: (a) Seebeck coefficient, (b) the electrical conductivity, and (c) the thermal conductivity of the $KGeI_{3-x}Br_x$ (x = 1; 2) as a function of the temperature.

Conclusion

As a conclusion, the modified Becke–Johnson with generalized gradient approximation has been used in order to study the electronic structure, optical, and thermoelectric properties of the perovskite $KGeI_{3-x}Br_x$ and $CsBI_2Br$ compounds using the FP-LAPW with Generalized Gradient Approximation (GGA + mBJ) implemented in Wien2k code. Based on the result, we can clearly see the effect of the change of the metal ion on the electronic as well as the optical properties. By analyzing the results, it is evident that the Germanium is more attractive compound because of its high optical absorption up to 6.3 × 105 cm-1 in the visible range and very favorable band gap of 1.18 which allows them to be more productive. This means that there is better performance than Lead and Tin for PV panels. In addition, The $KGeIBr_2$ shows a very interesting absorption value up to 6,7 $.10^5$ in the visible range what allows it to be more productive is attractive for solar cell application. Moreover, we have investigated the effect of adding the spin–orbit correction on the bandgap energy of the perovskite. Such results have been compared with those of the GGA + mBJ values without the spin–orbit correction.

CHAPTER VI : Study of the electronic, optical and thermal properties of the perovskite halides mixte $AGeI_2Br$ with (A = Cs, K, Rb)

VI.1 Introduction

Investigating the $CsBI_2Br$ (B = Pb, Ge, Sn) and the $KGeI_{3-x}Br_x$ (x = 0; 1; 2; 3) lead me to explore the potential of $AGeI_2Br$ with (A= K, Cs, Rb) compounds, trying to find new improvement for PV application. In this part, we investigate the electronic structure, optical, and thermoelectric properties of $AGeI_2Br$ with (A= K, Cs, Rb) compounds. Calculations on the properties were achieved adopting the full-potential linearized augmented plane wave (FP-LAPW) method in the framework of density functional theory with GGA and the modified Becke–Johnson (mBJ) approximations to define the electronic and optical properties to look for new and useful properties of these compounds for different applications.

VI.2 Computational Methods

The calculations are performed using the full-potential linearized augmented plane wave method (FP-LAPW) based on density functional theory (DFT) as implemented in the Wien2k code [68]. This method allows us to calculate the optical and electronic properties, band gaps, and densities of states, counting the absorption coefficient, and the reflectivity of our compounds at T=0.0K. In the cubic halide perovskite $AGeI_2Br$ (A = Cs, K, Rb), the A atoms occupy the corner positions (0, 0, 0) fractional coordinates, the B atoms occupy the body-centered position $(\frac{1}{2};\frac{1}{2};\frac{1}{2})$ fractional coordinates, and the I and Br atoms occupy the face-centered positions $(\frac{1}{2};\frac{1}{2};0)$, $(0;\frac{1}{2};\frac{1}{2})$ and $(\frac{1}{2};0;\frac{1}{2})$ respective fractional coordinates. We started by the optimization step **figure VI.1** for the determination of the lattice parameters. The generalized gradient approximation (GGA) [136] and the modified Becke-Johnson with Generalized Gradient Approximation (GGA+mBJ) are used for exchange and correlation calculations. We fixed the convergence criterion at 10^{-4} Ry and the convergence force to 1 mRy/a.u. We also use the Boltzmann theory embedded in BoltzTraP code to calculate the thermoelectric properties as the Seebeck coefficient, the electrical, and the thermal conductivity.

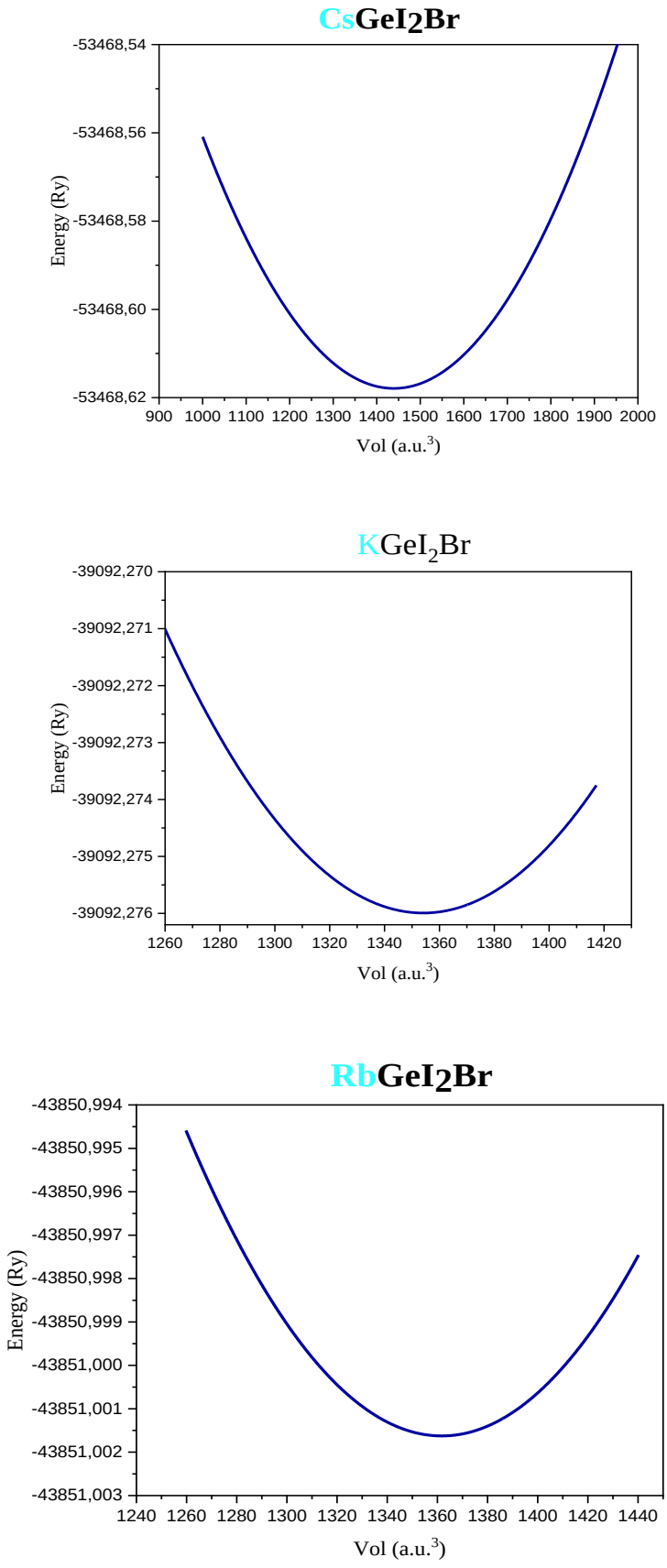

Figure VI. 1: Optimization of the of the AGeI2Br compounds

VI.3 Result and discussion

VI.3.1 Electronic properties

The studied compounds display direct band gaps with a clear semiconducting behavior, as shown in **Fig VI.2**. The calculated total density of state without strain effect was plotted in **Fig VI.3**. From **Fig VI.2. (a, b, and c),** It's clearly shows that the maximum of the valence band (VB) and the minimum of the conduction band (CB) are located at R axe which confirmed the direct bandgap, with bandgap values of 0.894 eV, 0.913 eV, and 1.18 eV for the $KGeI_2Br$, $RbGeI_2Br$ and $CsGeI_2Br$ compounds, respectively, calculated using GGA + mBJ approximation as seen in the **table VI.1**. One of the most important factors of our study is the calculation of the formation energy of the $AGeI_2Br$ compounds.

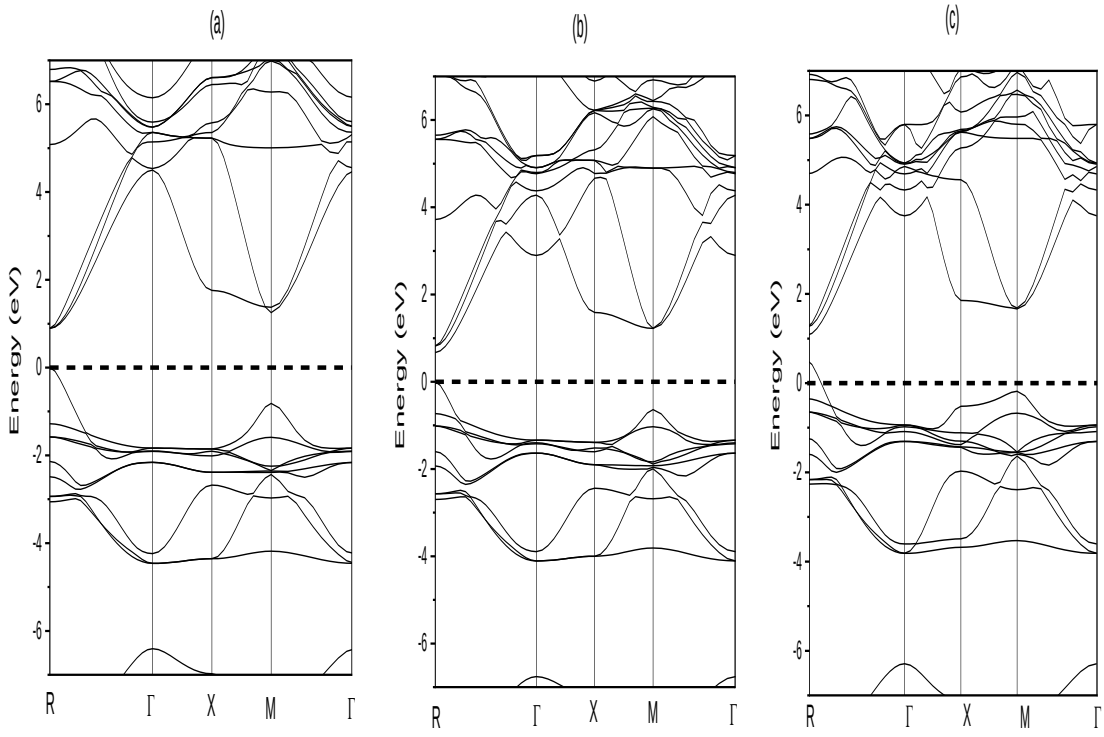

Figure VI. 2: Band structure of the $AGeI_2Br$ compounds calculated via GGA + mBJ approximation: (a) KGeI2Br, (b) RbGeI2Br, (c) CsGeI2Br.

Table VI. 1 : Lattice parameters a, Formation energy E_f, and Band Gap energy values E_g of the $AGeI_2Br$ (A= K, Rb, Cs) compounds calculated via PBE-GGA, and GGA + mBJ approximations.

	a (Å)	V (Å^3)	E_f	Energy Gap (eV)	
				PBE-GGA	GGA + mBJ
$KGeI_2Br$	5.82	197.14	-2.431	0.685	0.894
$RbGeI_2Br$	5.87	202.26	-2.441	0.702	0.913
$CsGeI_2Br$	5.89	204.34	-2.471	0.989	1.180

The total density of state is represented in **Fig VI.3.** of the $AGeI_2Br$ (A = K, Rb, Cs), two distinguished regions are asserted. The first region in the valence band is located between -4 and the fermi level which is dominated by the halide atoms Bromine and the Iodine. For the conductive region, it starts from 0.894 eV, 0.913 eV and 1.18 eV for the $KGeI_2Br$, $RbGeI_2Br$ and $CsGeI_2Br$ compounds respectively. With a dominance of the germanium (Ge) in large part, exceeding 4.5 eV we have a dominance of the alkali metal A.

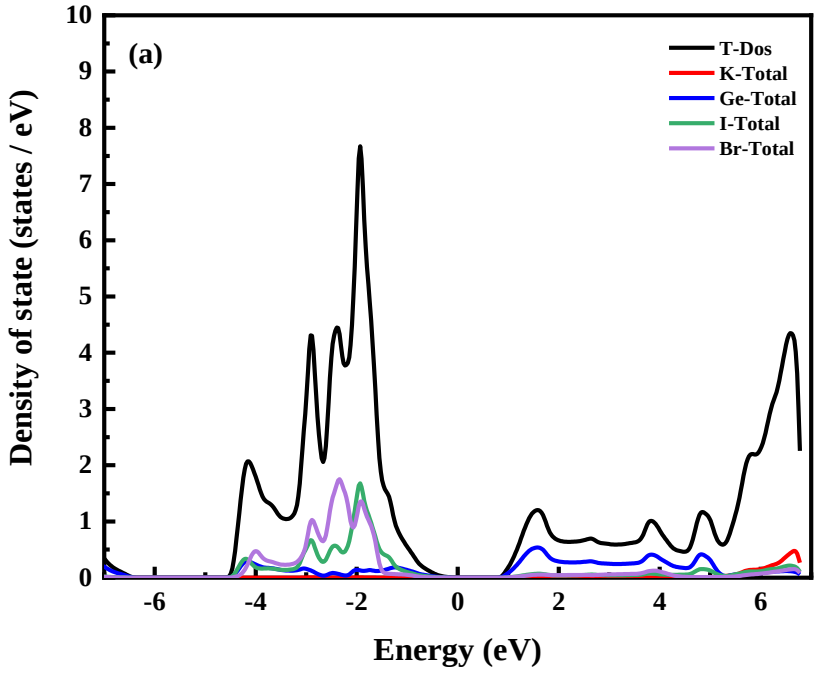

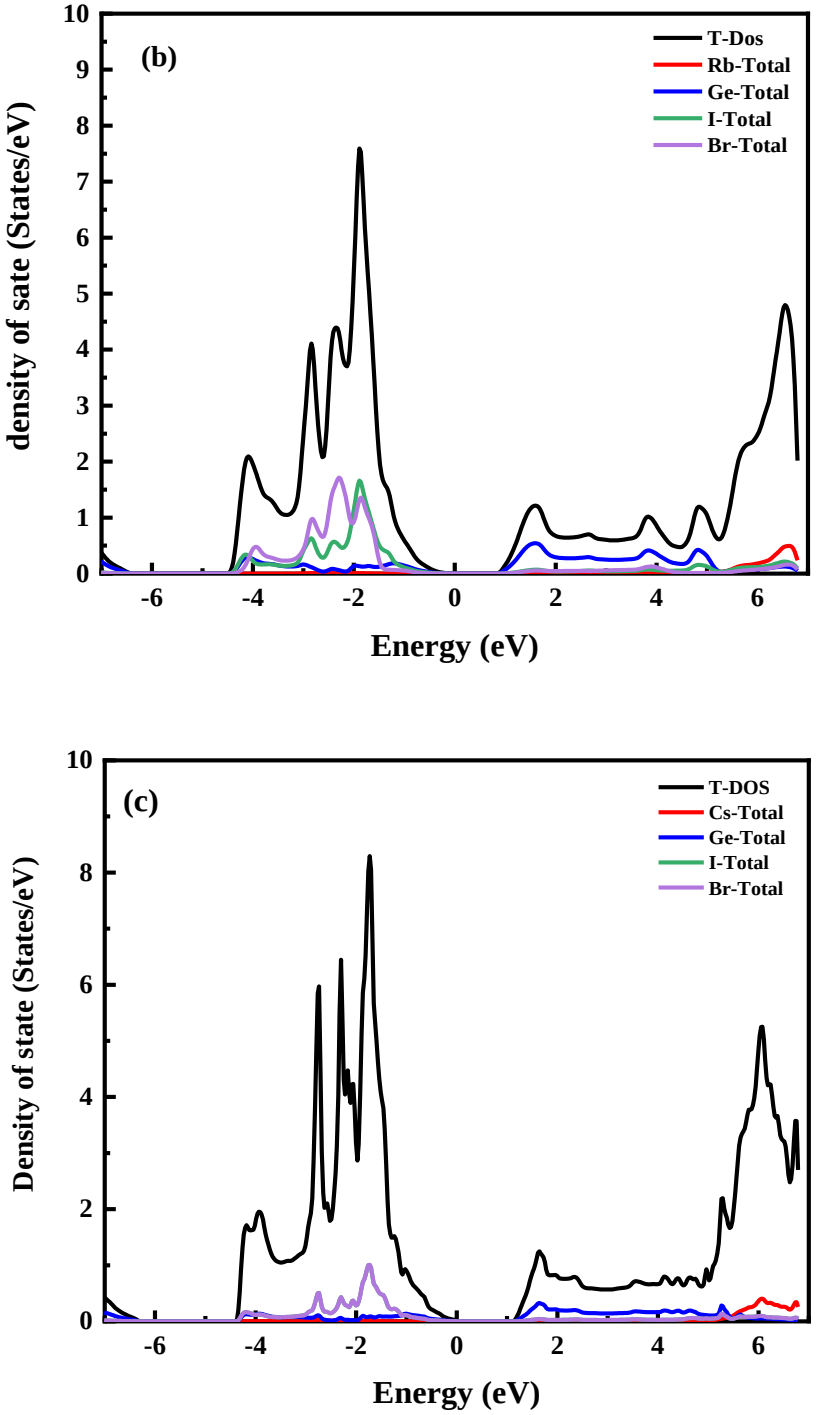

Figure VI. 3 : Total Density of charge of the $AGeI_2Br$ compounds calculated via GGA + mBJ approximation: (**a)** $KGeI_2Br$, (**b)** $RbGeI_2Br$, (**c)** $CsGeI_2Br$.

As a second part of our study, we applied the strain to the cubic structure of $AGeI_2Br$ compounds along the axis z, and we determined the volume of the stretch in percentage (%) to determine the effect on the $AGeI_2Br$ properties. **Table VI.2**, shows the results obtained by applying the strain with 1%, 2%, and 3% with GGA and GGA + mBJ approximations. The value of the gap energy

increases when the percentage of strain. As we can see, the gap increases from 0.685 eV (0%) to 1.206 eV (3%) for the $KGeI_2Br$, from 0.702 eV (0%) to 1.208 eV (3%) for $RbGeI_2Br$, and from 0.989 eV (0%) to 1.319 eV (3%) for $CsGeI_2Br$.

Table VI. 2 *:* Band gap with strain effect simulated via PBE-GGA and GGA + mBJ.

	PBE-GGA				**GGA + mBJ**			
	0%	**+1%**	**+2%**	**+3%**	**0%**	**+1%**	**+2%**	**+3%**
$KGeI_2Br$	0.685	0.909	0.934	0.969	0.894	1.124	1.167	1.206
$RbGeI_2Br$	0.702	0.904	0.945	0.981	0.702	1.123	1.168	1.208
$CsGeI_2Br$	0.989	1.123	1.164	1.199	0.989	1.289	1.317	1.319

VI.3.2 Optical properties

On the other hand, the optical properties of the $AGeI_2Br$ with (A = K, Rb, Cs) compounds are studied by figuring out the complex dielectric function, which includes a real and an imaginary part. Reflectivity R(ω), refractive index n(ω) and absorption spectra α(ω) are investigated for our considered compounds in a range between 300 nm and 900 nm**. Fig.VI.4** represents the optical absorption spectrum, we can notice that the absorption spectra present peaks for each compound in the visible range. A peak that reaches 62×10^4 at 455 nm for $CsGeI_2Br$, 58×10^4 at 434 nm for $RbGeI_2Br$ and 54×10^4 at 428 nm for $KGeI_2Br$. For solar cell application, we are always looking for high absorption capacity in visible range. A maximum absorption is observed with Cs based compounds compared to K and Rb based counterparts. We also investigate the reflectivity and the capacity of the compounds to reflect the incident radiation flux. **Fig VI.5** represents the reflectivity of the compounds in the visible region of the spectra. We notice for the $CsGeI_2Br$ a peak at 460 nm, but it has an average of 30% of reflectivity. The $RbGeI_2Br$ compound also has a peak of 34%

at 376 nm but the average is about 25%. $KGeI_2Br$ has the least value of the reflectivity at the visible spectra with 20%. However, this reflective part can be used to increase the solar cell efficiency. Further, the refractive index is plotted in **Fig.VI.6**. in the range between 300 nm and 900 nm. It's increased to 3.4, for both Cs and Rb compounds respectively, and to 2.3 for the $KGeI_2Br$. **The figure VI.7** resumes the result of the optical properties in percentage.

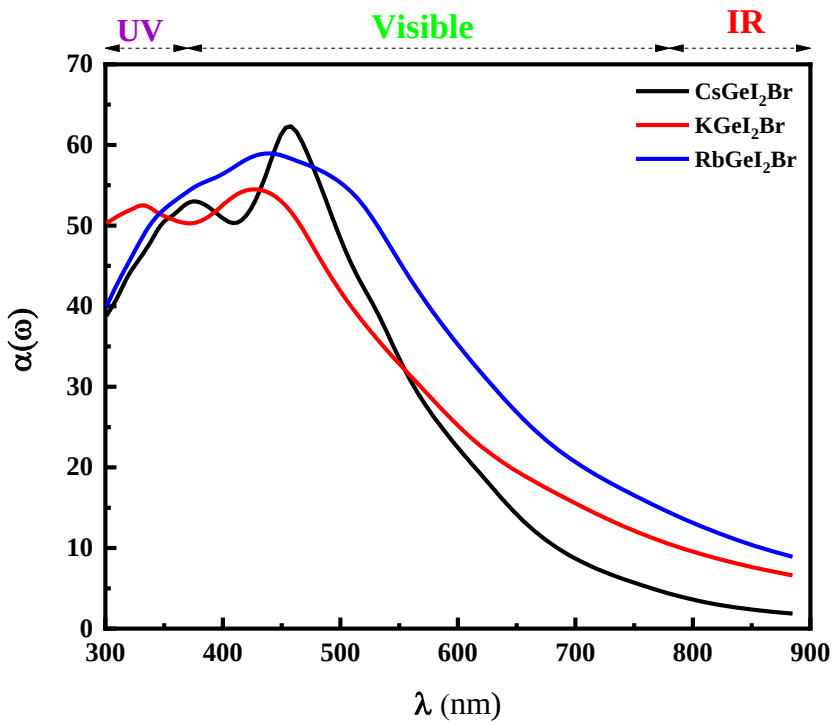

Figure VI. 4: Absorption spectrums of the $AGeI_2Br$ (A = K, Rb, Cs) compounds as a function of wavelength.

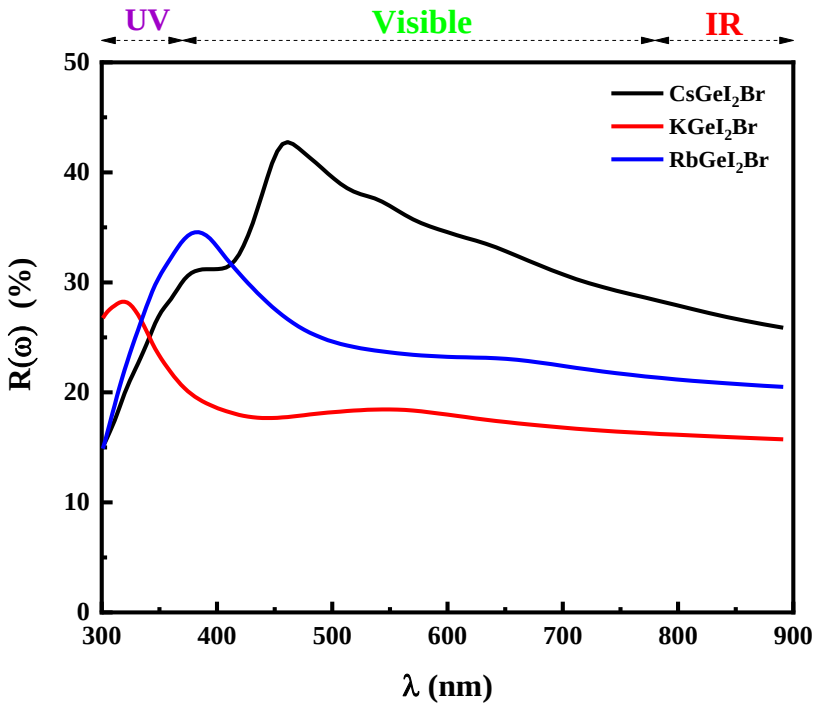

Figure VI. 5 : Reflectivity of the $AGeI_2Br$ (A = K, Rb, Cs) compounds as a function of wavelength.

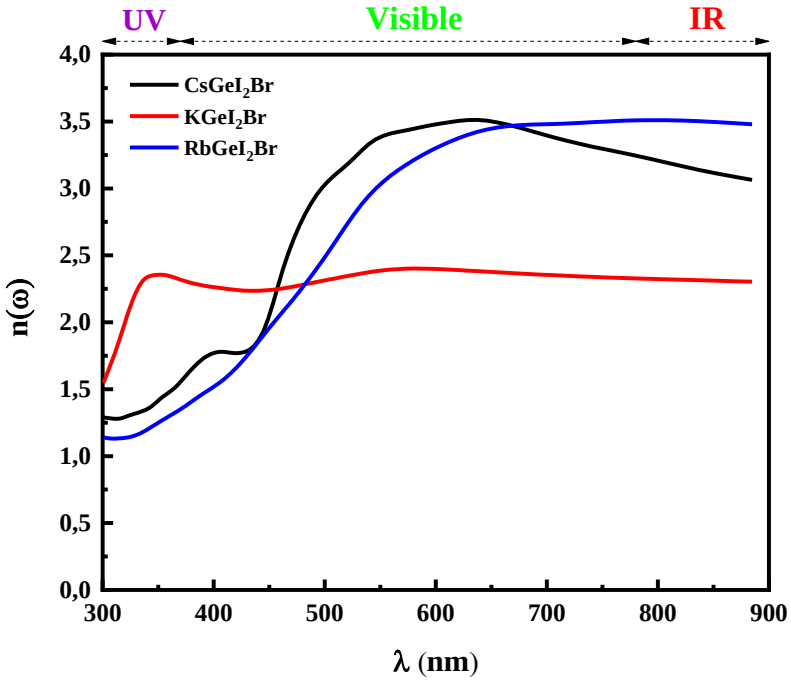

Figure VI. 6: Refractivity index of the $AGeI_2Br$ (A = K, Rb, Cs) compounds as a function of wavelength.

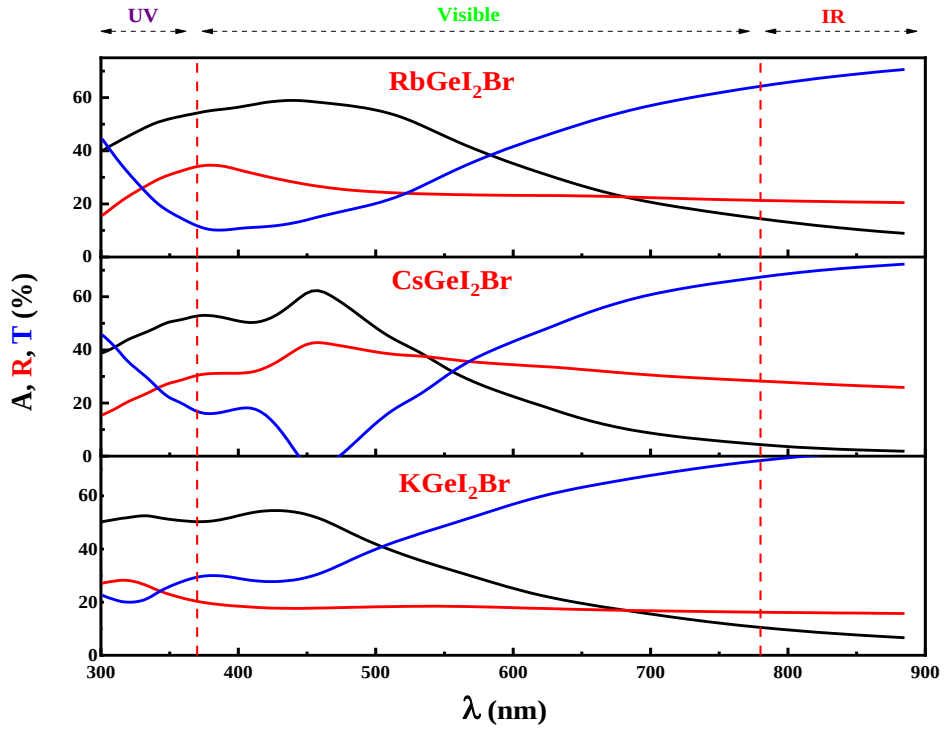

Figure VI. 7: Absorption coefficient (A), Reflectivity (R) and Transmittance (T) evolution of the $AGeI_2Br$ (A = K, Rb, Cs) compounds as a function of wavelength.

VI.3.3 Optical properties under the strain effect

Furthermore, we investigate the optical properties under the strain effect on the compounds, to examine the effect of strain on absorption coefficient, reflectivity and refractive index for different strain values from 1% to 3%. **The figures VI.8; VI.9; VI.10** show the difference between the 0% strain which means no strain effect and the 1%, 2% and 3% strain. For the absorption coefficient we can note a slight difference for the K and Cs compounds, for the Rb the width of the peak shrunk, but the maximum is the same value. The strain effect is negligible for the reflectivity in $KGeI_2Br$ compound, a slight for the $CsGeI_2Br$, but we can see a decrease of the value and it goes from 35% to 25% at the peak and from 30% to 20% for the average for the $RbGeI_2Br$, and the same goes for the refractive index.

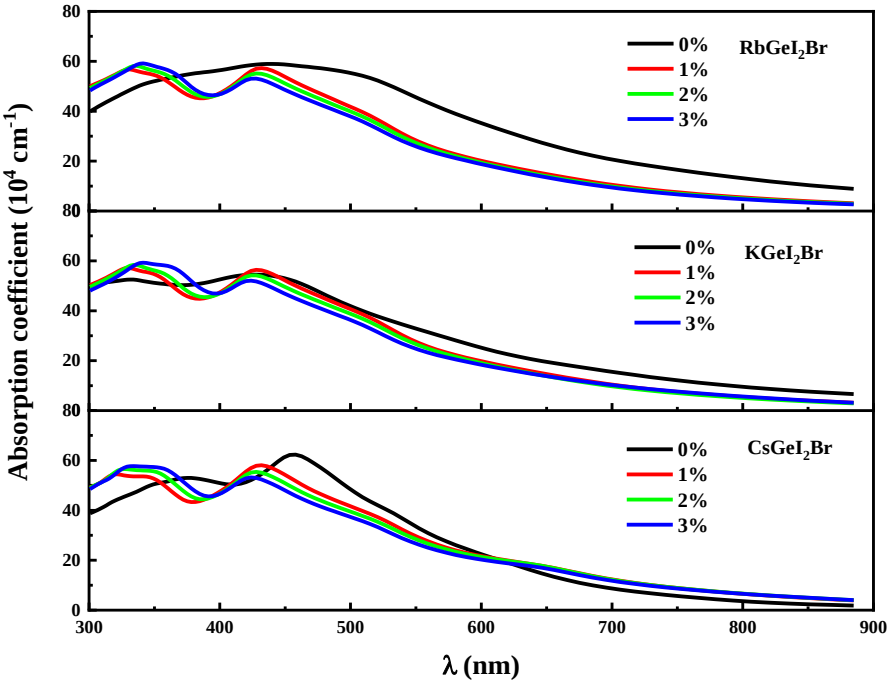

Figure VI. 8 : Absorption coefficient of the $AGeI_2Br$ (A = K, Rb, Cs) compounds as a function of wavelength under strain effect.

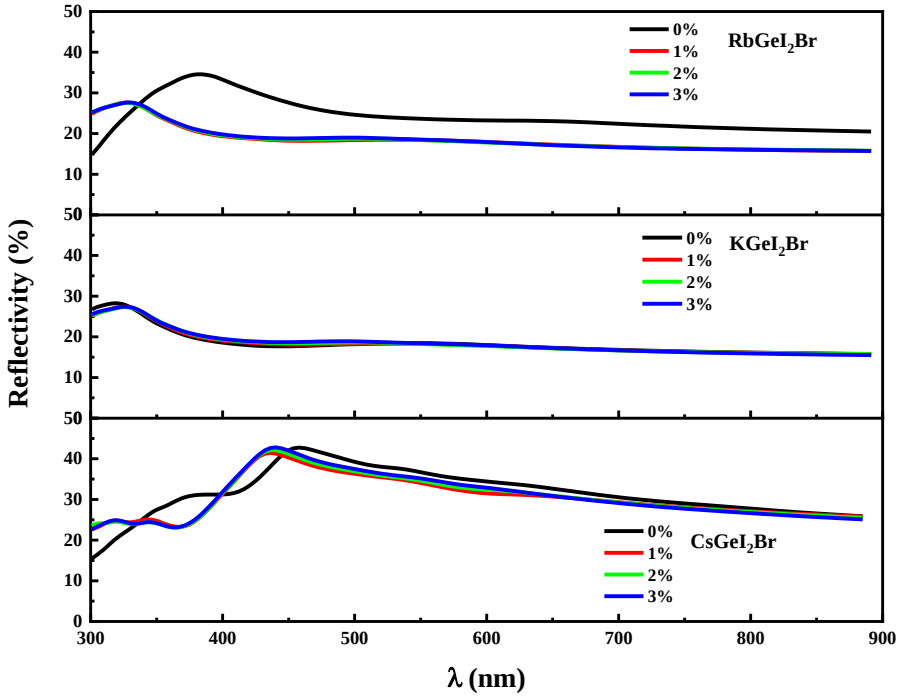

Figure VI. 9: Reflectivity of the $AGeI_2Br$ (A = K, Rb, Cs) compounds as a function of wavelength under strain effect.

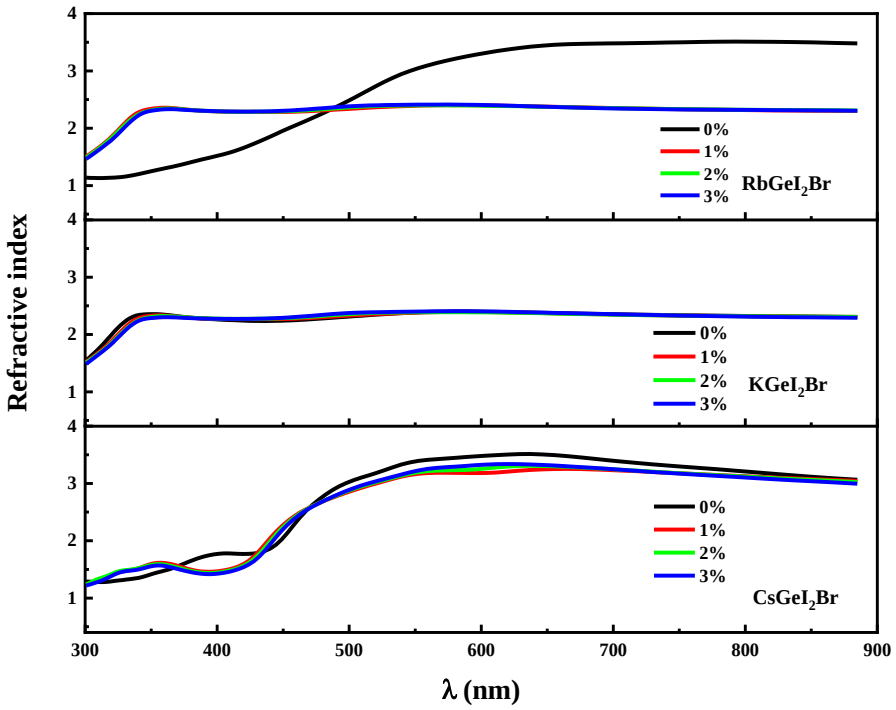

Figure VI. 10: Refraction index of the $AGeI_2Br$ (A = K, Rb, Cs) compounds as a function of wavelength under starin effect.

VI.3.4 Photocatalytic properties

The photocatalysis for water-splitting process prerequisite semiconductors possess wide bandgap to achieve a strong redox potential, by the reason of the intrinsic chemical inertness for both H_2 and H_2O molecules. Though, these demands will bring on a decrease in the photocatalysis light response area. For this purpose, the new research will be of interest on the development of photocatalysis with a combination between a slight band gap and high charge separation efficiency. The halide perovskite semiconductors characterized by their wide band gap, redshift absorption, as well as appropriate positions of the CB edge over the water reduction level (H^+/H_2) and the VB edge under the water oxidation level (O_2/H_2O) [142] as described by the following equations:

$$H_2O + 2h^+ \rightarrow 2H^+ + \frac{1}{2}O_2 \qquad (6.1)$$

$$2H^+ + 2\,e^- \rightarrow H_2 \qquad (6.2)$$

Despite the excellent photocatalysis performance of lead halide perovskite semiconductors for water splitting H_2 production and/or CO_2 reduction, there are some drawbacks [143-145]. To ascertain the above conditions, we will investigate the water splitting photocatalytic properties of $AGeI_2Br$ (A = K, Rb and Cs) with and without strain effect. The mechanism of photocatalytic water-splitting is based on merging the photocatalyst in water, when it is excited with a photo-induced light energy equal to or larger than its band gap energy, the electrons in the VB migrate to the CB, then start the reduction of H^+ to H_2. Whereas, the holes remain in the VB and start the oxidation of H_2O to H^+ and O_2. A schematic photocatalytic water-splitting diagram is presented in **Fig VI.10**. The band-edge potential levels of $AGeI_2Br$ (A = K, Rb and Cs) photocatalysis are calculated using the well-known Mulliken electronegativity theory [146] as follow:

$$E_{VB} = \chi - E_0 + 0.5E_g \tag{6.3}$$

$$E_{CB} = E_{VB} - E_g \tag{6.4}$$

where, E_g, E_{VB} and E_{CB} are the band gap energy, valence band and the conduction band edge potential, respectively, E_0 is the energy of free electrons on the hydrogen scale (E_0 = 4.5 eV) [147], and χ is the absolute electronegativity of the simulated systems (4.26, 4.62, and 4.34 for $AGeI_2Br$ (A = Cs, K, and Rb) respectively) calculated by the following formula:

$$\chi\,(AGeI_2Br) = (\chi(A)\,\chi(Ge)\,\chi(I)^2\,\chi(Br)\,)^{1/5} \tag{6.5}$$

where; χ(A), χ(Ge), χ(I), and χ(Br) are the absolute electronegativity of A with (A = K, Rb and Cs), Ge, I, and Br elements, respectively. The absolute electronegativity of $AGeI_2Br$ (A = K, Rb and Cs) systems elements equal to; 1.29, 1.92, 1.41, 4.10, 6.04, and 7.29 for Cs, K, Rb, Ge, I, and Br, respectively [148].

The band gap energy (E_g) of the studied compounds was found to be 1.18 eV [144], 0.91 eV, and 0.89 eV for $AGeI_2Br$ (A = K, Rb and Cs) systems, respectively. The effective mass values calculated of photo-induced electrons and holes are presented in Table 1. In addition to the calculation of band edges, the relative effective mass ratio (D) of photo-induced electrons and

holes (Table 3) was calculated to evaluate the charge separation efficiency [142]. The relative ratios of effective mass were calculated via the following formula:

$$D = m_h^*(m_0) / m_e^*(m_0) \quad (6.6)$$

Overall, a photocatalyst possessing a higher D value allows the higher probability of photogeneration electron-hole pairs separation, by consequence a lower recombination rate improving the photocatalytic activity [149]. The calculated value of relative ratios of effective mass were 1.20, 0.72, and 0.76 for $AGeI_2Br$ (A = K, Rb and Cs) halide perovskite, respectively. According to the NHE (normal hydrogen electrode), the CB edge potentials of simulated halide perovskite $AGeI_2Br$ (A = K, Rb and Cs) were, -0.83 eV, -0.33 eV, and -0.62 eV, respectively, while the VB ones are found to be 0.35 eV, 0.57 eV and 0.30 eV. The calculated relative ratio D of $CsGeI_2Br$ is higher than those of $KGeI_2Br$ and $RbGeI_2Br$, and greater than one, highlighting on the more rapid diffusion rates of the both latest halide perovskite, signifying the easier separation of electron-hole pairs in $CsGeI_2Br$ [150]. To enhance the performance of the studied halide perovskites $AGeI_2Br$ (A = K, Rb and Cs), the strain effect was evaluated (Table VI.3). The $AGeI_2Br$ (A = Cs, K, and Rb) semiconductor undergoes a tensile effect following the proportions 0%, 1%, 2%, and 3%. For $CsGeI_2Br$ and $RbGeI_2Br$, the relative ratio D were improved under a tensile effect of 1% reaching a maximum value of 1.99 and 1.34 for $CsGeI_2Br$ and $RbGeI_2Br$, respectively, then start decreasing until a value still greater than the unmodified compound. Whereas, for $KGeI_2Br$, the relative ratio D is also enhanced under a stretching effect of 1%, hence decreasing to arrive at a minimum value which is slighter than the pure one.

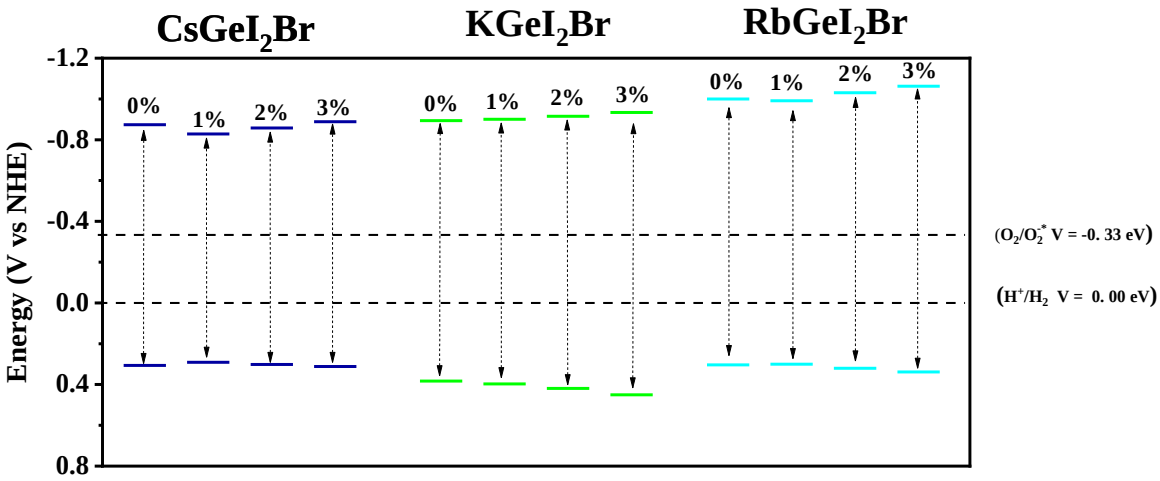

Figure VI. 11: Schematic illustration for the calculated energy band diagram of $AGeI_2Br$ (A = K, Rb and Cs) with and without strain effect.

From the calculated relative ratio D (Table VI.3) and the band edges (Figure VI.11), one can conclude the improvement of the photo-induced ability of all studied semiconductors under strain effect of 1% due to the increasing values of D (1.99, 1.10, and 1.34 for $AGeI_2Br$ (A = K, Rb and Cs) respectively), allowing them to be promising candidate for photocatalysis water-splitting.

V.3.5 Thermoelectric properties

Among the sources for conversion of the waste heat into electricity, thermoelectric materials are considered the promising one for this area. Hence, the efficiency of this application is evaluated through the calculation of the figure of merit (*ZT*) and power factor (*PF*). The electrical conductivity, thermal conductivity, seebeck coefficient, carrier mobility, and carrier's concentration of the studied compounds, have been investigated at room temperature via the BoltzTraP package, and recapitulated in Table VI.4. The variation of figure of merit ZT as function of temperature has been examined used the following equation [151]:

$$ZT = \frac{\sigma S^2 T}{\kappa} \qquad (6.7)$$

where, σ, S, $\boldsymbol{\kappa}$, and T are the electrical conductivity, thermal conductivity, seebeck coefficient, and the temperature, respectively. And the variation of power factor as function of temperature is calculated as follow:

$$PF = \sigma S^2 \tag{6.8}$$

From Table V.6, one can notice the high electrical conductivity, high thermal conductivity, low seebeck coefficient of $AGeI_2Br$ (A = Cs, K, and Rb) halide perovskites. $KGeI_2Br$ and $RbGeI_2Br$ possess values of figure of merit around a unit. While, CsGeI2Br has a negligible figure of merit value due to the low seebeck coefficient and the high thermal conductivity compared to $KGeI_2Br$ and $RbGeI_2Br$. Whereas, $CsGeI_2Br$ has a power factor value greater than $KGeI_2Br$ and $RbGeI_2Br$ due to their higher value of electrical conductivity compared to others. From the results presented on the Table VI.4, one can conclude that results obtained with strain effect have no effect on the thermoelectric properties and/or electrical properties. While for $CsGeI_2Br$, the figure of merit and the power factor were slightly improved under tensile effect of 1%, then started decreasing until reaching minimum values. In spite of this, among the three compositions we found that $KGeI_2Br$ and $RbGeI_2Br$ can be considered as promising candidates for thermoelectric potential.

Table VI. 3 : Carrier effective masses, the relative ratio (D) of the effective masses, and the band-edge potential levels of $AGeI_2Br$ (A = Cs, K, and Rb).

	Compound	**0%**	**+1%**	**+2%**	**+3%**
m_h^***(m₀)**	$CsGeI_2Br$ $KGeI_2Br$ $RbGeI_2Br$	12.47 5.88 7.96	16.23 9.70 10.29	8.20 2.74 6.84	9.55 2.86 6.62
m_e^***(m₀)**	$CsGeI_2Br$ $KGeI_2Br$ $RbGeI_2Br$	10.23 8.24 10.52	8.15 8.81 7.68	5.66 5.73 10.57	6.73 6.97 7.65
D	$CsGeI_2Br$ $KGeI_2Br$ $RbGeI_2Br$	1.22 0.72 0.76	1.99 1.10 1.34	1.45 0.48 0.65	1.42 0.41 0.87
E_{VB}	$CsGeI_2Br$ $KGeI_2Br$ $RbGeI_2Br$	0.35 0.57 0.30	0.29 0.56 0.31	0.30 0.58 0.32	0.31 0.60 0.33
E_{CB}	$CsGeI_2Br$ $KGeI_2Br$ $RbGeI_2Br$	-0.83 -0.33 -0.62	-0.83 -0.35 -0.60	-0.86 -0.36 -0.62	-0.89 -0.37 -0.65

Table VI. 4: Electrical Conductivity, Thermal Conductivity, Seebeck coefficient, Figure of merit, Power factor, Carrier mobility, and Carrier's concentration of $AGeI_2Br$ (A = Cs, K, and Rb) calculated at 300 K for different values of strain using TB-mBJ method

	Compound $AGeI_2Br$		**0%**	**+1%**	**+2%**	**+3%**
σ(S.cm^{-1}.s^{-1})/ τ	A :	Cs	6.59 10^{19}	2.78 10^{19}	6.53 10^{19}	2.82 10^{19}
		K	1.67 10^{17}	1.66 10^{17}	1.66 10^{17}	1.66 10^{17}
		Rb	4.28 10^{15}	4.20 10^{15}	4.19 10^{15}	4.18 10^{15}
K_{el} (W.m^{-1}.K^{-1}.s^{-1})/ τ	A :	Cs	4.40 10^{14}	3.29 10^{14}	4.38 10^{14}	2.21 10^{14}
		K	6.73 10^{12}	6.71 10^{12}	6.71 10^{12}	6.70 10^{12}
		Rb	4.81 10^{11}	4.72 10^{11}	4.71 10^{11}	4.70 10^{11}
S (V.K^{-1})	A :	Cs	3.56 10^{-5}	8.31 10^{-5}	3.54 10^{-5}	1.46 10^{-5}
		K	3.54 10^{-4}	3.54 10^{-4}	3.53 10^{-4}	3.53 10^{-4}
		Rb	5.99 10^{-4}	5.99 10^{-4}	5.99 10^{-4}	5.99 10^{-4}
ZT	A :	Cs	0.06	0.18	0.06	0.01
		K	0.93	0.93	0.93	0.93
		Rb	0.96	0.96	0.96	0.96
PF (W. cm^{-1} K^{-2})	A :	Cs	8.37 10^{10}	1.92 10^{11}	8.20 10^{10}	5.99 10^{9}
		K	2.0810^{10}	2.0810^{10}	2.07 10^{10}	2.07 10^{10}
		Rb	1.54 10^{9}	1.51 10^{9}	1.51 10^{9}	1.50 10^{9}
μ_p (cm^2.V^{-1}.s^{-1})	A :	Cs	3.47 10^{18}	2.39 10^{18}	3.44 10^{18}	1.48 10^{18}
		K	8.77 10^{15}	8.74 10^{15}	8.74 10^{15}	8.71 10^{15}
		Rb	2.25 10^{14}	2.21 10^{14}	2.21 10^{14}	2.20 10^{14}
p (cm^{-3})	A :	Cs	3.6610^{23}	3.19 10^{23}	3.66 10^{23}	3.67 10^{23}
		K	3.07 10^{23}	3.18 10^{23}	3.18 10^{23}	3.18 10^{23}
		Rb	3.06 10^{23}	3.18 10^{23}	3.18 10^{23}	3.18 10^{23}

VI.4 Conclusion

In this part, the first-principles density functional theory (DFT) has been performed to explore the structural, electronic, optical, photocatalytic, and transport properties of Germanium based halide perovskite $AGeI_2Br$ (A= K, Rb, and Cs) compounds using the FP-LAPW method with the modified Becke-Johnson with Generalized Gradient Approximation (GGA+mBJ) implemented in Wien2k code. Moreover, by applying the strain effect, the gap energy increases when increasing the strain from 1% to 3%, whereas the optical properties are not affected by the strain, and we were able to keep a very good absorption coefficient. Furthermore, the photo-generated ability of the studied halide perovskites was improved only under strain effect of 1% due to the increasing values of D (1.99, 1.10, and 1.34 for $AGeI_2Br$ (A = K, Rb, and Cs) respectively), leading them to be a suitable candidate for photocatalysis water-splitting under UV-Visible illumination. In addition to that, among the studied compounds, we found that $KGeI_2Br$ and $RbGeI_2Br$ can be considered promising candidates for thermoelectric potential. Moreover, the technique proposed in this investigation is a good method to increase the gap energy, thus the photocatalytic water-splitting performance. In conclusion, we can consider the three compounds as promising candidates for photovoltaic, photocatalytic applications.

Conclusion

Conclusion

The work presented in this thesis focuses on the theoretical study of potentially promising materials for photovoltaic application. The study undertaken in this thesis aims first to investigate the structural, electronic and optical properties using the FP LAPW method based on the DFT density functional theory with the modified Becke-Johnson corrective approach implemented in the wien2k calculation code. We performed the calculation in a first step for the CIGS compound with different values of doping concentration of Ga, from CIS to CGS keeping the chalcopyrite structure. In a second part, we are interested in the study of another generation of materials called 'perovskites' and more precisely the cubic perovskite halides of type ABX 3 (A = K; B = Ge, Sn; X = Cl, Br, I) with in common the direct character of their band gap in the R-R direction. The electronic charge density shows an ionic (between A and X) and covalent (between Ge and X) bonding of these compounds. The optical properties of these compounds such as real and imaginary parts of dielectric functions, refractive indices, reflectivity and absorption coefficients are also calculated. The direct band gap and high absorption of these compounds in the visible and ultraviolet energy range allow these perovskites to be used in PV and optoelectronic devices operating in this range of the energy spectrum. Moreover, the thermodynamic properties have been investigated by the BoltzTrap software based on the semi-classical Boltzmann model. In the last part, we studied the mixed perovskite halides $ABI_{3-X}Br_x$ (A = K, Rb, Cs; B = Ge, Pb) with the generalized gradient approximation (GGA) as exchange correlation potential. The modified Becke - Johnson (mBJ) potential approximation is also used to calculate the electronic and optical properties of these materials. The results showed a direct band gap, a high absorption, in the visible range very attractive for photovoltaic

applications. For any future experimental or theoretical research, these results could be used as reference results.

Refrences :

[1] Crabtree, G. W., & Lewis, N. S. (2007). Solar energy conversion. Physics today, 60(3), 37-42.

[2] Chamorro, M. V., Blanco, E. E., & Rojas, J. P. (2020). Direct, diffuse and total solar radiation data set in La Guajira, Magdalena and Cesar departments-Colombia. Data in Brief, 33, 106397.

[3] Tan, L., Du, W., Zhang, Y., Tang, L. J., Jiang, J. H., & Yu, R. Q. (2020). Rayleigh scattering correction for fluorescence spectroscopy analysis. Chemometrics and Intelligent Laboratory Systems, 203, 104028.

[4] Julajaturasirarath, S., Jonburom, W., & Pornsuwancharoen, N. (2012). The experiment of double solar energy by reflection light method. Procedia Engineering, 32, 522-530.

[5] Trieb, F., Müller-Steinhagen, H., Kern, J., Scharfe, J., Kabariti, M., & Al Taher, A. (2009). Technologies for large scale seawater desalination using concentrated solar radiation. Desalination, 235(1-3), 33-43.

[6] Green, M. A. (2002). Photovoltaic principles. Physica E: Low-dimensional Systems and Nanostructures, 14(1-2), 11-17.

[7] Goetzberger, A., & Hoffmann, V. U. (2005). Photovoltaic solar energy generation (Vol. 112). Springer Science & Business Media.

[8] Pleskov, Y. V. (1990). Solar energy conversion.

[9] Lançon, R., & Marfaing, Y. (1969). Mécanisme de génération-recombinaison dans les jonctions pn de tellurure de cadmium. Journal de Physique, 30(1), 97-102.

[10] Falama, R. Z., & Doka, S. Y. (2019). A promising concept to push efficiency of pn-junction photovoltaic solar cell beyond Shockley and Queisser limit based on impact ionization due to high electric field. Optik, 187, 39-48.

[11] J.H. Scofield, A. Duda, D. Albin, B.L. Ballard, et P. Predecki. Sputtered molybdenum bilayer back contact for copper indium diselenide-based polycrystalline thin-film solar cells. Thin Solid Films, 260:26-31, 1995.

[12] J. Kessler, K.O. Velthaus, M. Ruckh et al . Chemical bath deposition of CdS on CuInSe2, etching effects and growth kinetics. Dans Proceeding of 6th IPSEC. 1005-1009. New Delhi, India. 1992.

[13] Ortuño-López, M. B., Sotelo-Lerma, M., Mendoza-Galván, A., & Ramirez-Bon, R. (2004). Optical band gap tuning and study of strain in CdS thin films. Vacuum, 76(2-3), 181-184.

[14] Conibeer, G. (2007). Third-generation photovoltaics. Materials today, 10(11), 42-50.

[15] Kim, J. Y., Lee, J. W., Jung, H. S., Shin, H., & Park, N. G. (2020). High-efficiency perovskite solar cells. Chemical Reviews, 120(15), 7867-7918.

[16] E. C. C. d. Souza and R. Muccillo, "Properties and applications of perovskite proton conductors," Materials Research, vol. 13, pp. 385-394, 2010.

[17] J. J. Urban, W. S. Yun, Q. Gu, and H. Park, "Synthesis of single-crystalline perovskite nanorods composed of barium titanate and strontium titanate," Journal of the American Chemical Society, vol. 124, pp. 1186-1187, 2002.

[18] A. Dejneka, "perovskite ferroelectric tuned by thermal strain."

[19] R. Song, Y. Zhao, W. Li, Y. Yu, J. Sheng, Z. Li, et al., "High Temperature Stability and Mechanical Quality Factor of Donor-Acceptor Co-Doped BaTiO 3 Piezoelectrics," Available at SSRN 3406952, 2019.

[20] G. Chen, C. Dai, and C. Ma, "A stable half-metallic ferromagnetic material SrNiO3: a prediction from first principles," in 2014 International Conference on Mechatronics, Electronic, Industrial and Control Engineering (MEIC-14), 2014.
[21] R. Gotardo, E. Silva, R. Alonso, J. Rosso, D. Silva, G. Santos, et al., "Dielectric, magnetic and structural characterizations in Mn doped 0.9 BiFeO3-0.1 BaTiO3 compositions,"
[22] V. M. Goldschmidt and T. Barth, "Skrifter Norske Videnskaps-Akad. Oslo, I. Mat," Nat. Kl, vol. 8, 1926.
[23] L. Pauling, "The nature of the electrostatic bond," ed: Cornell University Press: Ithaca, NY, 1967.
[24] Z. W. Huang, Y. H. Zhao, H. Hou, and P. D. Han, Physica.B: Condensed Matter 407 (2012) 1075.
[25] H. L. Wells, "Über die Cäsium-und Kalium-Bleihalogenide," Zeitschrift für anorganische Chemie, vol. 3, pp. 195-210, 1893.
[26] D. Weber, "CH3NH3PbX3, ein Pb (II)-system mit kubischer perowskitstruktur/CH3NH3PbX3, a Pb (II)-system with cubic perovskite structure," Zeitschrift für Naturforschung B, vol. 33, pp. 1443-1445, 1978.
[27] C. K. MØLLER, "Crystal structure and photoconductivity of caesium plumbohalides," Nature, vol. 182, p. 1436, 1958.
[28] D. Mitzi, S. Wang, C. Feild, C. Chess, and A. Guloy, "Conducting layered organic-inorganic halides containing< 110>-oriented perovskite sheets," Science, vol. 267, pp. 1473-1476, 1995.
[29] A. Kojima, K. Teshima, Y. Shirai, and T. Miyasaka, "Novel photoelectrochemical cell with mesoscopic electrodes sensitized by lead-halide compounds (5)," in Meeting Abstracts, 2007, pp. 352-352.
[30] Jena, A. K., Kulkarni, A., & Miyasaka, T. (2019). Halide perovskite photovoltaics: background, status, and future prospects. Chemical reviews, 119(5), 3036-3103.
[31] Kovalenko, M. V., Protesescu, L., & Bodnarchuk, M. I. (2017). Properties and potential optoelectronic applications of lead halide perovskite nanocrystals. Science, 358(6364), 745-750.
[32] Kim, H., Han, J. S., Choi, J., Kim, S. Y., & Jang, H. W. (2018). Halide perovskites for applications beyond photovoltaics. Small Methods, 2(3), 1700310.
[33] Li, H., Luo, T., Zhang, S., Sun, Z., He, X., Zhang, W., & Chang, H. (2021). Two-dimensional metal-halide perovskite-based optoelectronics: synthesis, structure, properties and applications. Energy & Environmental Materials, 4(1), 46-64.
[34] K. Wang, G. Li, S. Wang, S. Liu, W. Sun, C. Huang, et al., "Dark-Field Sensors based on Organometallic Halide Perovskite Microlasers," Advanced Materials, vol. 30, p. 1801481, 2018.
[35] Xu, Y., Cao, M., & Huang, S. (2021). Recent advances and perspective on the synthesis and photocatalytic application of metal halide perovskite nanocrystals. Nano Research, 1-22.
[36] SHENTOV, Ognjan V., MITRA, Sanjit K., HEUTE, Ulrich, *et al.* Subband DFT—Part I: Definition, interpretation and extensions. *Signal Processing*, 1995, vol. 41, no 3, p. 261-277.
[37] KOHLER, Bernd, WILKE, Steffen, SCHEFFLER, Matthias, et al. Force calculation and atomic-structure optimization for the full-potential linearized augmented plane-wave code WIEN. Computer physics communications, 1996, vol. 94, no 1, p. 31-48.
[38] FADDEEV, L. D. SCHRÖDINGER EQUATION. Nine Papers on Partial Differential Equations and Functional Analysis, 1967, vol. 65, p. 139.

[39] E. Adams, "E. Schrödinger, Mémoires sur la Mécanique Ondulatoire," Bulletin of the American Mathematical Society, vol. 39, pp. 854-854, 1933.
[40] BORN, Max et OPPENHEIMER, Robert. Zur quantentheorie der molekeln. Annalen der physik, 1927, vol. 389, no 20, p. 457-484.
[41] HARTREE, Douglas R. The wave mechanics of an atom with a non-Coulomb central field. Part I. Theory and methods. In : Mathematical Proceedings of the Cambridge Philosophical Society. Cambridge university press, 1928. p. 89-110.
[42] FOCK, Vladimir. Näherungsmethode zur Lösung des quantenmechanischen Mehrkörperproblems. Zeitschrift für Physik, 1930, vol. 61, no 1-2, p. 126-148.
[43] ANDERSEN, O. Krogh. Linear methods in band theory. Physical Review B, 1975, vol. 12, no 8, p. 3060.
[44] OBOT, I. B., MACDONALD, D. D., et GASEM, Z. M. Density functional theory (DFT) as a powerful tool for designing new organic corrosion inhibitors. Part 1: an overview. Corrosion Science, 2015, vol. 99, p. 1-30.
[45] COMBES, Jean-Michel, DUCLOS, Pierre, et SEILER, Ruedi. The born-oppenheimer approximation. In : Rigorous atomic and molecular physics. Springer, Boston, MA, 1981. p. 185-213.
[46] HAINES, Larry K. et ROBERTS, David H. One-dimensional hydrogen atom. American journal of physics, 1969, vol. 37, no 11, p. 1145-1154.
[47] FRANK, N. H. Note on the Hartree and Hartree-Fock Methods. Physical Review, 1937, vol. 51, no 7, p. 577.
[48] W. Kohn, "Electronic structure of matter–wave functions and density functionals," Rev. Mod. Phys, vol. 71, pp. 1253-1266, 1999.
[49] LYKOS, P. et PRATT, G. W. Discussion on the Hartree-Fock approximation. Reviews of Modern Physics, 1963, vol. 35, no 3, p. 496.
[50] MOSHINSKY, M. How good is the Hartree-Fock approximation. American Journal of Physics, 1968, vol. 36, no 1, p. 52-53.
[51] FRISHBERG, C. Slater determinant from atomic form factors. International journal of quantum chemistry, 1986, vol. 30, no 1, p. 1-5.
[52] L. H. Thomas, "The calculation of atomic fields," in Mathematical Proceedings of the Cambridge Philosophical Society, 1927, pp. 542-548.
[53] E. Fermi, "Eine statistische Methode zur Bestimmung einiger Eigenschaften des Atoms und ihre Anwendung auf die Theorie des periodischen Systems der Elemente," Zeitschrift für Physik, vol. 48, pp. 73-79, 1928.
[54] BAGAYOKO, Diola. Understanding density functional theory (DFT) and completing it in practice. AIP Advances, 2014, vol. 4, no 12, p. 127104.
[55] SHOLL, David et STECKEL, Janice A. Density functional theory: a practical introduction. John Wiley & Sons, 2011.
[56] HOHENBERG, P. et KOHN, W. J. P. R. Density functional theory (DFT). Phys. Rev, 1964, vol. 136, p. B864.
[57] KOHN, Walter et SHAM, Lu Jeu. Self-consistent equations including exchange and correlation effects. Physical review, 1965, vol. 140, no 4A, p. A1133.
[58] STUKEL, D. J., COLLINS, T. C., et EUWEMA, R. N. Theoretical Electron Density of States Study of Tetrahedrally Bonded Semiconductors. NBS Special Publication, 1968, no 187-188, p. 93.
[59] J. Singh David, "Planewaves, Pseudopotentials and the LAPW Method," ed: Boston: Kluwer) p6, 1994.
[60] MARCUS, Paul M. Variational methods in the computation of energy bands. International Journal of Quantum Chemistry, 1967, vol. 1, no S1, p. 567-588.

[61] CHAN, M. K. Y. et CEDER, Gerbrand. Efficient band gap prediction for solids. Physical review letters, 2010, vol. 105, no 19, p. 196403.
[62] J. P. Perdew, K. Burke, and M. Ernzerhof, "Generalized gradient approximation made simple," Physical review letters, vol. 77, p. 3865, 1996.
[63] J. P. Perdew, J. Chevary, S. Vosko, K. A. Jackson, M. R. Pederson, D. Singh, et al., "Erratum: Atoms, molecules, solids, and surfaces: Applications of the generalized gradient approximation for exchange and correlation," Physical Review B, vol. 48, p. 4978, 1993.
[64] J. P. Perdew, K. Burke, and M. Ernzerhof, "Phys rev lett 77: 3865," Errata:(1997) Phys Rev Lett, vol. 78, p. 1396, 1996.
[65] E. Engel and S. H. Vosko, "Exact exchange-only potentials and the virial relation as microscopic criteria for generalized gradient approximations," Physical Review B, vol. 47, p. 13164, 1993.
[66] BECKE, Axel D. et JOHNSON, Erin R. A simple effective potential for exchange. The Journal of chemical physics, 2006, vol. 124, no 22, p. 221101.
[67] TRAN, Fabien et BLAHA, Peter. Accurate band gaps of semiconductors and insulators with a semilocal exchange-correlation potential. Physical review letters, 2009, vol. 102, no 22, p. 226401.
[68] BLAHA, Peter, SCHWARZ, Karlheinz, MADSEN, Georg KH, et al. wien2k. An augmented plane wave+ local orbitals program for calculating crystal properties, 2001, vol. 60.
[69] GERBER, Iann C. et ANGYÁN, János G. Hybrid functional with separated range. Chemical physics letters, 2005, vol. 415, no 1-3, p. 100-105.
[70] DRESSELHAUS, Gene. Spin-orbit coupling effects in zinc blende structures. Physical Review, 1955, vol. 100, no 2, p. 580.
[71] MADSEN, Georg KH, CARRETE, Jesús, et VERSTRAETE, Matthieu J. BoltzTraP2, a program for interpolating band structures and calculating semi-classical transport coefficients. Computer Physics Communications, 2018, vol. 231, p. 140-145.
[72] BALOUT, Hilal. BoltzTraP_Tools UserGuide. 2018.
[73] BLAHA, P. WIEN97, Vienna University of Technology 1997. Comput. Phys. Commun., 1990, vol. 59, p. 399.
[74] P. Jackson, R. Wuerz, D. Hariskos, E. Lotter, W. Witte, M. Powalla, Effects of heavy alkali elements in Cu(In,Ga)Se2 solar cells with efficiencies up to 22.6%,Phys. Status Solidi Rapid Res. Lett. 10 (2016) 583-586,.
[75] W.N. Shafarman et L. Stolt. Chapter 13 in Handbook of Photovoltaic Science and Engineering. Ed. by A. Luque and S. Hegedus. John Wiley & Sons. 2003.
[76] L. Kazmerski et al . Appl. Phys. Lett., 29:268–269, 1976.
[77] W. Chen, R. Mickelsen. Dans Proc. 16th IEEE Photovoltaic Specialist Conf. 1982.
[78] W. Chen et al . Dans Proc. 19th IEEE Photovoltaic Specialist Conf. 1987.
[79] M. Wang, K.L. Choy, All-nonvacuum-processed CIGS solar cells using scalable Ag NWs/AZO-based transparent electrodes, ACS Appl. Mater. Interfaces 8 (2016) 16640-16648.
[80] FERNANDEZ, A. M. et BHATTACHARYA, R. N. Electrodeposition of CuIn1−xGaxSe2 precursor films: optimization of film composition and morphology. Thin Solid Films, 2005, vol. 474, no 1-2, p. 10-13.
[81] W. E. Devaney, J.M. Stewart, W.S. Chen, Proceedings of the 21stPhotovoltaic Specialists Conference, Hyatt Orlando, Kissimmee, FL, IEEE, New York, (1990), 535.

[82] MARAI, A. Ben, BELGACEM, J. Ben, AYADI, Z. Ben, et al. Structural and optical properties of CuIn1-xGaxSe2 nanoparticles synthesized by solvothermal route. Journal of Alloys and Compounds, 2016, vol. 658, p. 961-96.
[83] M.A. Contreras, J.R. Tuttle, A.M. Gabor, A.L. Tennant, K.R. Ramanathan, S. Asher,A. Franz, J. Keane, L. Wang, R. Noufi, Sol. Energy Mater. Sol. Cells 41/42 (1996)231.
[84] S.Nakagawa, H.Ishihara, N.Mochizuki, T.Kamiya,K. Toyoda, T.Ikeya,K.Sato, M.Ishida, 14thEuropean Photovoltaic Solar energy conf. Barcelona, 1997, p.1216.
[85] M.Wagner, I.Dirstorfer, M.M.Hofmann, M.D.Lampert, f.Karg, B.K.Meyer, Phys.Status Solidi, A Appl. Res 167 (1998) 131
[86] CHANDRAMOHAN, M., VELUMANI, S., et VENKATACHALAM, T. Experimental and theoretical investigations of structural and optical properties of CIGS thin films. Materials Science and Engineering: B, 2010, vol. 174, no 1-3, p. 205-208.
[87] K. Zweibel, H.S. Ullal, B.V. Roedern, Proceedings of the 25th Photovoltalic Specialists Conference, Washinton DC, USA, 1996, pp. 745–750.
[88] W. Wettling, R.P. Mertens, W.C. Sinke, H.W. Schock, Proceedings of the Eurosun '96' Freiburg Germany, 1996, pp. 43– 55.
[89] HADJAB, Moufdi, IBRIR, Miloud, BERRAH, Smail, et al. Structural, electronic and optical properties for chalcopyrite semiconducting materials: ab-initio computational study. Optik, 2018, vol. 169, p. 69-76.
[90] FU-LING, Tang, RAN, Liu, HONG-TAO, Xue, et al. Lattice structures and electronic properties of CIGS/CdS interface: First-principles calculations. Chinese Physics B, 2014, vol. 23, no 7, p. 077301.
[91] WAN, Fu Cheng, TANG, Fu Ling, ZHU, Zheng Xin, et al. First-principles investigation of the optical properties of CuIn (SxSe1–x) 2. Materials Science in Semiconductor Processing, 2013, vol. 16, no 6, p. 1422-1427.
[92] HOHENBERG, P. et KOHN, W. Density Functional Theory (DFT). Phys. Rev, 1964, vol. 136, p. B864.
[93] P. Blaha, K. Schwarz, G.H. Madsen, D. Kvasnicka, J. Luitz, FP-L/APW+lo Program for Calculating Crystal Properties, Vienna University of Technology, Vienna,Austria, 2001.
[94] Koller, David, Fabien Tran, and Peter Blaha. Merits and limits of the modified Becke-Johnson exchange potential. Physical Review B 83.19 (2011): 195134.
[95].SAJID, A., ULLAH, S., MURTAZA, G., et al. Electronic structure and optical properties of chalcopyrite CuYZ 2 (Y= Al Ga In; Z= S Se): an ab initio study. J. Opto. and Adv. Mat., vol. 16, no 1–2, (2014) 76-81.
[96] JAFFE, J. E. et ZUNGER, Alex. Electronic structure of the ternary chalcopyrite semiconductors CuAlS2, CuGaS2, CuInS2, CuAlSe2, CuGaSe2, and CuInSe2. Physical Review B, , vol. 28, no 10, (1983) 5822.
[97] SURI, D. K., NAGPAL, K. C., et CHADHA, G. K. X-ray study of CuGaxIn1− xSe2 solid solutions. Journal of Applied Crystallography, 1989, vol. 22, no 6, p. 578-583.
[98] Madsen, Georg KH, and David J. Singh. BoltzTraP. A code for calculating band structure dependent quantities. Computer Physics Communications 175.1 (2006): 67-71.
[99] CHEN, Xu-Dong, CHEN, Lin, SUN, Qing-Qing, et al. Hybrid density functional theory study of Cu (In1− xGax) Se2 band structure for solar cell application. AIP Advances, vol. 4, no 8, (2014), 087118.
[100] S. Shirakata, S. Chichibu, and S. Isomura, Jpn J Appl Phys 1 36 (12A), (1997) 7160–7161.

[101] J. L. Shay, B. Tell, H. M. Kasper, and Schiavon. Lm, Physical Review B 7(10), 4485–4490 (1973).
[102] Shouxincui, Journal of Alloys and Componds 484 (2009) 597.
[103] D. Eimer, J. Marion, E. K. Graham, H. A. McKinstry, and S. Haussühl, IEEE J. Quantum Electron. QE-27, (1991) 142.
[104] E. Francisco, J K. M.Recio, M.A. Blanco and A. Martin Pend_s, J.Phys.Chem. 102, (1998) 1595.
[105] M. Hadjab, S. Berrah, H. Abid, M.I. Ziane, H. Bennacer, B.G. Yalcin, Optik 127 (2016) 9280–9294.
[106] Jian Sun, et al., Ab initio investigations of optical properties of the high pressure phases of ZnO, Phys. Rev. B 71 (12) (2005) 125132.
[107] Shunji Ozaki, Sadao Adachi, Optical constants of ZnS xSe1- x ternaryalloys, J. Appl. Phys. 75 (11) (1994) 7470e7475.
[108] MARAI, A. Ben, BELGACEM, J. Ben, AYADI, Z. Ben, et al. Structural and optical properties of CuIn1-xGaxSe2 nanoparticles synthesized by solvothermal route. Journal of Alloys and Compounds, 2016, vol. 658, p. 961-966.
[109] ADEDOYIN, Festus Fatai, BEKUN, Festus Victor, et ALOLA, Andrew Adewale. Growth impact of transition from non-renewable to renewable energy in the EU: the role of research and development expenditure. Renewable Energy, 2020, vol. 159, p. 1139-1145.
[110] ZHANG, Yuhu, REN, Jing, PU, Yanru, et al. Solar energy potential assessment: A framework to integrate geographic, technological, and economic indices for a potential analysis. Renewable Energy, 2020, vol. 149, p. 577-586.
[111] GAD, S., EL-SHAZLY, M. A., WASFY, Kamal I., et al. Utilization of solar energy and climate control systems for enhancing poultry houses productivity. Renewable Energy, 2020, vol. 154, p. 278-289.
[112] BURSCHKA, Julian, PELLET, Norman, MOON, Soo-Jin, et al. Sequential deposition as a route to high-performance perovskite-sensitized solar cells. Nature, 2013, vol. 499, no 7458, p. 316-319.
[113] YANG, Woon Seok, PARK, Byung-Wook, JUNG, Eui Hyuk, et al. Iodide management in formamidinium-lead-halide–based perovskite layers for efficient solar cells. Science, 2017, vol. 356, no 6345, p. 1376-1379.
[114] EPERON, Giles E., PATERNÒ, Giuseppe M., SUTTON, Rebecca J., et al. Inorganic caesium lead iodide perovskite solar cells. Journal of Materials Chemistry A, 2015, vol. 3, no 39, p. 19688-19695.
[115] AKBULATOV, Azat F., LUCHKIN, Sergey Yu, FROLOVA, Lyubov A., et al. Probing the intrinsic thermal and photochemical stability of hybrid and inorganic lead halide perovskites. The journal of physical chemistry letters, 2017, vol. 8, no 6, p. 1211-1218.
[116] ZHOU, Wenke, ZHAO, Yicheng, ZHOU, Xu, et al. Light-independent ionic transport in inorganic perovskite and ultrastable Cs-based perovskite solar cells. The journal of physical chemistry letters, 2017, vol. 8, no 17, p. 4122-4128.
[117] ZHOU, Yuanyuan, ZHOU, Hua, DENG, Junjing, et al. Decisive structural and functional characterization of halide perovskites with synchrotron. Matter, 2020, vol. 2, no 2, p. 360-377.
[118] JAHANDAR, Muhammad, KHAN, Nasir, JAHANKHAN, Muhammad, et al. Performance data of CH3NH3PbI3 inverted planar perovskite solar cells via ammonium halide additives. Data in brief, 2019, vol. 27, p. 104817.

[119] KRISHNAMOORTHY, Thirumal, DING, Hong, YAN, Chen, et al. Lead-free germanium iodide perovskite materials for photovoltaic applications. Journal of Materials Chemistry A, 2015, vol. 3, no 47, p. 23829-23832.
[120] ZHOU, Yuanyuan et ZHAO, Yixin. Chemical stability and instability of inorganic halide perovskites. Energy & Environmental Science, 2019, vol. 12, no 5, p. 1495-1511.
[121] TAI, Qidong, TANG, Kai-Chi, et YAN, Feng. Recent progress of inorganic perovskite solar cells. Energy & Environmental Science, 2019, vol. 12, no 8, p. 2375-2405.
[122] TANG, Li-Chuan, CHANG, Chen-Shiung, et HUANG, Jung Y. Electronic structure and optical properties of rhombohedral CsGeI3 crystal. Journal of Physics: Condensed Matter, 2000, vol. 12, no 43, p. 9129.
[123] HOUARI, M., BOUADJEMI, B., MATOUGUI, M., et al. Optoelectronic properties of germanium iodide perovskites AGeI 3 (A= K, Rb and Cs): first principles investigations. Optical and Quantum Electronics, 2019, vol. 51, no 7, p. 1-14.
[124] ORNELAS-CRUZ, I., TREJO, A., OVIEDO-ROA, R., et al. DFT-based study of the bulk tin mixed-halide CsSnI3-xBrx perovskite. Computational Materials Science, 2020, vol. 178, p. 109619.
[125] ZHANG, Qiaoqiao, MUSHAHALI, Hahaer, DUAN, Haiming, et al. The linear and nonlinear optical response of CsGeX3 (X= Cl, Br, and I): The finite field and first-principles investigation. Optik, 2019, vol. 179, p. 89-98..
[126] BRGOCH, Jakoah, LEHNER, Anna J., CHABINYC, Michael, et al. Ab initio calculations of band gaps and absolute band positions of polymorphs of RbPbI3 and CsPbI3: implications for main-group halide perovskite photovoltaics. The Journal of Physical Chemistry C, 2014, vol. 118, no 48, p. 27721-27727.
[127] ROKNUZZAMAN, Md, OSTRIKOV, Kostya Ken, WANG, Hongxia, et al. Towards lead-free perovskite photovoltaics and optoelectronics by ab-initio simulations. Scientific reports, 2017, vol. 7, no 1, p. 1-8. [129] Kar M, Körzdörfer T. Mat. Res. Exp. 2020; 7 (5): 055502.
[128] KAR, M. et KÖRZDÖRFER, T. Computational high throughput screening of inorganic cation based halide perovskites for perovskite only tandem solar cells. Materials Research Express, 2020, vol. 7, no 5, p. 055502.
[129] HOUARI, Mohammed, BOUADJEMI, Bouabdellah, HAID, Slimane, et al. Semiconductor behavior of halide perovskites AGeX3 (A= K, Rb and Cs; X= F, Cl and Br): first-principles calculations. Indian Journal of Physics, 2020, vol. 94, no 4, p. 455-467.
[130] MAHMOOD, Q., NOOR, N. A., RASHID, Muhammad, et al. Physical properties of alkali metals-based iodides via Ab-initio calculations. Journal of Physics and Chemistry of Solids, 2019, vol. 132, p. 68-75..
[131] CUI, Shouxin, FENG, Wenxia, HU, Haiquan, et al. High-pressure structural, electronic and optical properties of KMgF3: A first-principles study. Journal of Alloys and Compounds, 2009, vol. 484, no 1-2, p. 597-600.
[132] D. Eimer, J. Marion, E.K. Graham, H.A. McKinstry, S. Haussühl, IEEE J. Quantum Electron. QE-27 (1991) 142.
[133] MOSCONI, Edoardo, AMAT, Anna, NAZEERUDDIN, Md K., *et al.* First-principles modeling of mixed halide organometal perovskites for photovoltaic applications. *The Journal of Physical Chemistry C*, 2013, vol. 117, no 27, p. 13902-13913.
[134] Rehman, W., McMeekin, D. P., Patel, J. B., Milot, R. L., Johnston, M. B., Snaith, H. J., & Herz, L. M. (2017). Photovoltaic mixed-cation lead mixed-halide perovskites:

links between crystallinity, photo-stability and electronic properties. Energy & Environmental Science, 10(1), 361-369.
[135] McMeekin, D. P., Sadoughi, G., Rehman, W., Eperon, G. E., Saliba, M., Hörantner, M. T., ... & Snaith, H. J. (2016). A mixed-cation lead mixed-halide perovskite absorber for tandem solar cells. Science, 351(6269), 151-155.
[136] Francisco E, Recio JM, Blanco MA, et al. J. Phys. Chem. A. 1998; 102: 1595-1601.
[137] Camargo-Martínez, J. A., & Baquero, R. (2012). Performance of the modified Becke-Johnson potential for semiconductors. Physical Review B, 86(19), 195106.
[138] Jingjing Tian, Qifan Xue, Xiaofeng Tang, Yuxuan Chen, Li Ning, Zhicheng Hu, Tingting Shi, Xin Wang, Fei Huang, Christoph J. Brabec, Hin-Lap Yip and Yong Cao, Dual interfacial design for efficient CsPbI2Br perovskite solar cells with improved photostability, Adv. Mater. 31 (2019), 1901152.
[139] Shuaihua Lu, Qionghua Zhou, Ma Liang, Yilv Guo, Jinlan Wang, Rapid discovery of ferroelectric photovoltaic perovskites and material descriptors via machine learning, Small Methods 11 (2019), 1900360.
[140] R. Padmavathy, A. Amudhavalli, R. Rajeswarapalanichamy, K. Iyakutti, Electronic structure and optical properties of CsSnI3 yBry (y=0,1,2,3) perovskites, Int. J. Mod. Phys. B 33 (2019), 1950003.
[141] D. Sabba, H.K. Mulmudi, R.R. Prabhakar, T. Krishnamoorthy, T. Baikie, P.P. Boix, N. Mathews, Impact of anionic Br–substitution on open circuit voltage in lead free perovskite (CsSnI3-xBr x) solar cells, J. Phys. Chem. C 119 (2015) 1763–1767.
[142] F. Opoku, K. K. Govender, C. G. C. E. van Sittert, et P. P. Govender, « Enhancing Charge Separation and Photocatalytic Activity of Cubic $SrTiO_3$ with Perovskite-Type Materials $MTaO_3$ (M=Na, K) for Environmental Remediation: A First-Principles Study », *ChemistrySelect*, vol. 2, nº 22, p. 6304-6316, juill. 2017, doi: 10.1002/slct.201700886.
[143] J. Cheng *et al.*, « Acetate-assistant efficient cation-exchange of halide perovskite nanocrystals to boost the photocatalytic CO2 reduction », *Nano Res.*, août 2021, doi: 10.1007/s12274-021-3775-3.
[144] X. Zhu, Y. Lin, Y. Sun, M. C. Beard, et Y. Yan, « Lead-Halide Perovskites for Photocatalytic α-Alkylation of Aldehydes », *J. Am. Chem. Soc.*, vol. 141, nº 2, p. 733-738, janv. 2019, doi: 10.1021/jacs.8b08720.
[145] Y. Xu, M. Cao, et S. Huang, « Recent advances and perspective on the synthesis and photocatalytic application of metal halide perovskite nanocrystals », *Nano Res.*, mars 2021, doi: 10.1007/s12274-021-3362-7.
[146] G. Wang *et al.*, « Enhanced visible-light responsive photocatalytic activity of Bi25FeO40/Bi2Fe4O9 composites and mechanism investigation », *J. Mater. Sci. Mater. Electron.*, vol. 30, nº 11, p. 10923-10933, juin 2019, doi: 10.1007/s10854-019-01436-4.
[147] M. A. Basith, R. Ahsan, I. Zarin, et M. A. Jalil, « Enhanced photocatalytic dye degradation and hydrogen production ability of Bi25FeO40-rGO nanocomposite and mechanism insight », *Sci. Rep.*, vol. 8, nº 1, p. 11090, déc. 2018, doi: 10.1038/s41598-018-29402-w.
[148] C. Tantardini et A. R. Oganov, « Thermochemical electronegativities of the elements », *Nat. Commun.*, vol. 12, nº 1, p. 2087, déc. 2021, doi: 10.1038/s41467-021-22429-0.
[149] P. Arunachalam, K. Nagai, M. S. Amer, M. A. Ghanem, R. J. Ramalingam, et A. M. Al-Mayouf, « Recent Developments in the Use of Heterogeneous Semiconductor Photocatalyst Based Materials for a Visible-Light-Induced Water-Splitting System—A

Brief Review », *Catalysts*, vol. 11, n° 2, p. 160, janv. 2021, doi: 10.3390/catal11020160.
[150] L. Ren *et al.*, « Enhanced degradation of organic pollutants using Bi 25 FeO 40 microcrystals as an efficient reusable heterogeneous photo-Fenton like catalyst », *Catal. Today*, vol. 281, p. 656-661, mars 2017, doi: 10.1016/j.cattod.2016.06.028.
[151] N. Gupta et R. Verma, « First-principles study of thermoelectric transport properties in low-buckled monolayer silicene », *Phys. B Condens. Matter*, vol. 606, p. 412715, avr. 2021, doi: 10.1016/j.physb.2020.412715.

Publications :

- **Hamideddine.I,Tahiri.N, ElBounagui.O, Ez-Zahraouy.H**. Theoretical investigation of electronic and optical properties of the CuIn1-xGaxSe2: Ab-initio calculation. Optik, (2020), 163881.
- **Hamideddine, I., Tahiri, N., El Bounagui, O., Ez-Zahraouy, H**. First-principles calculations of electronic, optical and transport properties of the inorganic metal halide perovskite CsBI2Br (B= Sn, Ge, Pb) compounds. Materials Science in Semiconductor Processing, 2021, vol.126, 105657.
- **Hamideddine, I., Zitouni, H., Tahiri, N., El Bounagui, O., Ez-Zahraouy, H** A DFT study of the electronic structure, optical, and thermoelectric properties of halide perovskite KGeI 3-x Br x materials: photovoltaic applications. Applied Physics A, 2021, vol. 127, no 6, p.
- **Hamideddine.I,Tahiri.N, ElBounagui.O, Ez-Zahraouy.H.** Ab initio study of structural and optical properties of the halide perovskite KBX3 compound. Journal of the Korean Ceramic Society, 2022.
- **I. Hamideddine, H. Jebari, N. Tahiri, O. El Bounagui, and H. Ez-Zahraouy.** Theoretical study of the electronic, optical, and thermoelectric properties of the inorganic metal halide perovskite AGeI2Br (A = K, Rb, Cs) compound: Ab initio calculation. (Submitted)
- **A.Ouasri, I. Hamideddine, H. Jebari, N. Tahiri, O. El Bounagui, and H. Ez-Zahraouy.** Structural characterisation and theoretical investigation of electronic and optical properties of hydrazinium (1+) hexafluorosilicate (N2H5)2SiF6. (submistted)

Conferences / Communications :

- JMCON 21
- IRSEC’20
- NANOSMAT Mediterranean 2019
- The Second Annual Inter-lab-LaMCScI-LERMA-Meeting-2019